University of Bremen

Fachbereich 2: Biologie/Chemie

Dissertation

To obtain the academic degree

Doctor Rerum Naturalium (Dr. rer. Nat.)

Electron-induced chemistry in simple molecular ices: Fundamental reaction principles revisited

Submitted by

Fabian Schmidt

Bremen, 2021

The published version of this thesis does not contain the published articles due to copyright reasons. Furthermore, several typos in the reviewed version were corrected.

Reviewers:

Dr. Jan H. Bredehöft

Prof. Dr. Anne Lafosse

Prof. Dr. Christopher R. Arumainayagam

Date of the oral examination:

September 21, 2021

Versicherung an Eides Statt

Ich, Fabian Schmidt, versichere an Eides Statt durch meine Unterschrift, dass ich die vorstehende Arbeit selbständig und ohne fremde Hilfe angefertigt und alle Stellen, die ich wörtlich dem Sinne nach aus Veröffentlichungen entnommen habe, als solche kenntlich gemacht habe, mich auch keiner anderen als der angegebenen Literatur oder sonstiger Hilfsmittel bedient habe.

Ich versichere an Eides Statt, dass ich die vorgenannten Angaben nach bestem Wissen und Gewissen gemacht habe und dass die Angaben der Wahrheit entsprechen und ich nichts verschwiegen habe.

Die Strafbarkeit einer falschen eidesstattlichen Versicherung ist mir bekannt, namentlich die Strafandrohung gemäß § 156 StGB bis zu drei Jahren Freiheitsstrafe oder Geldstrafe bei vorsätzlicher Begehung der Tat bzw. gemäß § 161 Abs. 1 StGB bis zu einem Jahr Freiheitsstrafe oder Geldstrafe bei fahrlässiger Begehung.

_____

Ort, Datum Unterschrift

Acknowledgments

An erster Stelle möchte ich mich bei meiner Doktormutter Prof. Dr. Petra Swiderek für die Betreuung und Finanzierung meiner Arbeit bedanken, sowie für die zahlreichen konstruktiven Anmerkungen in meinen Publikationen.

Mein besonderer Dank gilt außerdem Dr. Jan Hendrik Bredehöft für die Betreuung meiner Arbeit und dass er mir stets viele Freiheiten in Bezug auf meine Experimente eingeräumt hat.

Ich danke Prof. Dr. Christopher Arumainayagam und Prof. Dr. Anne Lafosse dafür, dass sie sich bereit erklärt haben, meine Dissertation zu begutachten.

Außerdem danke ich Prof. Dr. Peter Spiteller für die Übernahme des Kommissionsvorsitzes.

Ich danke allen aktuellen und ehemaligen Mitgliedern der Arbeitsgruppe Swiderek für die gute Arbeitsatmosphäre und die vielen interessanten Diskussion. Hierfür möchte ich mich bei Dr. Tobias Borrmann, Vera Suling, Dr. Markus Rohdenburg, Petra Martinović, René Cartaya, Dr. Ralf Kather, Brigitte Neimeier, Fiona Rathe, Cornelia Rybarsch-Steinke, Fengmiao Zhang und Tina Zock bedanken. Insbesondere möchte ich die regelmäßig stattfindenden Café-Runden hervorheben, die wesentlich zu einem lockeren und angenehmen Arbeitsklima beigetragen haben.

Zu guter Letzt danke ich Svea Riek, meinen Freunden und meiner Familie für die moralische Unterstützung währendes meines Studiums und der Promotion.

Publications

This thesis is based on the following list of publications:

Publication I Schmidt, F.; Swiderek, P.; Bredehöft, J. H. Formation of Formic Acid, Formaldehyde, and Carbon Dioxide by Electron-Induced Chemistry in Ices of Water and Carbon Monoxide. *ACS Earth Space Chem.* **2019**, 3, 1974–1986.

https://pubs.acs.org/doi/10.1021/acsearthspacechem.9b00168

Publication II Schmidt, F.; Swiderek, P.; Bredehöft, J. H. Energetic Processing of Methanol Ice. *ACS Earth Space Chem.* **2021**, 5, 391–408.

https://pubs.acs.org/doi/10.1021/acsearthspacechem.0c00250

Publication III Schmidt, F.; Swiderek, P.; Bredehöft, J. H. Electron-Induced Formation of Ethyl Methyl Ether in Condensed Mixtures of Methanol and Ethylene. *J. Phys. Chem. A* **2019**, 123, 37–47.

https://pubs.acs.org/doi/10.1021/acs.jpca.8b10209

Publication IV Schmidt, F.; Swiderek, P.; Scheele, T.; Bredehöft, J. H. Mechanism of Methyl Formate Production During Electron-Induced Processing of Methanol–Carbon Monoxide Ices. *Phys. Chem. Chem. Phys.* **2021**, 23, 11649–11662.

https://dx.doi.org/10.1039/d1cp01255j

Additional publications that are not part of the present work:

Publication V Bredehöft, J. H.; Böhler, E.; Schmidt, F.; Borrmann, T.; Swiderek, P. Electron-Induced Synthesis of Formamide in Condensed Mixtures of Carbon Monoxide and Ammonia, *ACS Earth Space Chem.* **2017**, *1*, 50–59.

https://doi.org/10.1021/acsearthspacechem.6b00011

Publication VI Schrader, I.; Neumann, S.; Šulce, A.; Schmidt, F.; Azov, V.; Kunz, S. Asymmetric Heterogeneous Catalysis: Transfer of Molecular Principles to Nanoparticles by Ligand Functionalization, *ACS Catal.*, **2017**, *7*, 3979–3987.

https://doi.org/10.1021/acscatal.7b00422

Declaration on the contribution of the candidate to a multi-author article/manuscript which is included as a chapter in the submitted doctoral thesis

Publication I: "Formation of Formic Acid, Formaldehyde, and Carbon Dioxide by Electron-Induced Chemistry in Ices of Water and Carbon Monoxide"

Contributions of the candidate in % of the total workload (up to 100% for each of the following categories)

Experimental concept and design: 90%
Experimental work and/or acquisition of (experimental) data: 100%
Data analysis and interpretation: 90%
Preparation of Figures and Tables: 100%
Drafting of the manuscript: 70%

Publication II: "Electron-Induced Processing of Methanol Ice"

Contributions of the candidate in % of the total workload (up to 100% for each of the following categories)

Experimental concept and design: 90%
Experimental work and/or acquisition of (experimental) data: 100%
Data analysis and interpretation: 90%
Preparation of Figures and Tables: 100%
Drafting of the manuscript: 70%

Publication III: "Electron-Induced Formation of Ethyl Methyl Ether in Condensed Mixtures of Methanol and Ethylene"

Contributions of the candidate in % of the total workload (up to 100% for each of the following categories)

Experimental concept and design: 90%
Experimental work and/or acquisition of (experimental) data: 100%
Data analysis and interpretation: 90%
Preparation of Figures and Tables: 100%
Drafting of the manuscript: 70%

Publication IV: "Mechanism of Methyl Formate Production During Electron-Induced Processing of Methanol–Carbon Monoxide Ices"

Contributions of the candidate in % of the total workload (up to 100% for each of the following categories)

Experimental concept and design: 90%
Experimental work and/or acquisition of (experimental) data: 80%
Data analysis and interpretation: 90%
Preparation of Figures and Tables: 100%
Drafting of the manuscript: 70%

Date:

Signature:

Abbreviations

BEB	Binary-encounter-Bethe
DEA	Dissociative electron attachment
DI	Dissociative ionization
EE	Electronic excitation
EI	Electron impact ionization
ESD	Electron-stimulated desorption
HREELS	High-resolution electron energy loss spectroscopy
IR	Infrared
MGR	Menzel-Gomer-Redhead
ND	Neutral dissociation
PAH	Polycyclic aromatic hydrocarbon
PID	Proportional-Integral-Derivative
RGA	Residual gas analyzer
TDS	Thermal desorption spectrometry
TNI	Transient negative ion
UHV	Ultrahigh vacuum
UV	Ultraviolet
XPS	X-ray photoelectron spectroscopy

Abstract

Electron-induced reactions play a key-role in astrochemical processes as vast numbers of secondary electrons are released when any ionizing radiation such as UV photons, X-rays, or cosmic rays penetrate the icy mantle around interstellar dust particles. Subsequently, these secondary electrons can interact with molecules in their environment producing reactive fragments which, in turn, may trigger a reaction sequence. Eventually, new organic molecules are formed some of which might be important for the emergence of life on earth. However, while there are many data on the identification of irradiation products under various conditions, the mechanisms that drive their formation just start to emerge. In particular, there is a lack of knowledge on the electron-molecule interactions that underlie product formation.

In this thesis, electron-induced reactions have been investigated in pure CH_3OH, and in binary ices, namely CO/H_2O, C_2H_4/CH_3OH, and CO/CH_3OH. The results of these studies provide important insights into electron-induced reactions in interstellar ices as H_2O, CO, and CH_3OH are all major constituents of these ices. Detailed knowledge on the reaction mechanisms has been inferred from the dependences of product yields on electron energy which reveals the underlying electron-molecule interactions. Additional information on a mechanism were obtained by comparing the energy dependence of a particular product with those of its side products. This enables one to identify the relevant intermediates and to discriminate among several possible reaction scenarios. On the basis of this approach, several reaction classes were identified to play a role under electron-irradiation of the investigated mixtures. Namely, these are radical recombination, hydrogenation of CO and C_2H_4, oxidation of CO to CO_2, and addition reactions between a radical and CO or C_2H_4.

Kurzzusammenfassung

Elektronen-induzierte Reaktionen spielen eine Schlüsselrolle in astrochemischen Prozessen, da eine große Anzahl an Sekundärelektronen erzeugt wird, wenn ionisierende Strahlung wie beispielsweise UV-Strahlung, Röntgenstrahlung oder kosmische Strahlung in den Eismantel eines interstellaren Staubpartikels eindringt. Im Anschluss können diese Sekundärelektronen mit benachbarten Molekülen interagieren, wobei reaktive Fragmente entstehen, die weitere Reaktionen auslösen können. Auf diesem Wege bilden sich organische Moleküle, von denen einige für die Entstehung des Lebens auf der Erde von Bedeutung sein könnten. Obwohl bereits eine große Anzahl an Produkten bei solchen Experimenten nachgewiesen werden konnten, wird erst langsam ersichtlich, welche Mechanismen bei der Produktbildung eine Rolle spielen. Insbesondere existieren noch große Wissenslücken bezüglich der zugrunde liegenden Elektronen-Molekül-Wechselwirkungen.

In dieser Dissertation wurden Elektronen-induzierte Reaktionen in reinem CH_3OH, sowie in binären Mischungen aus CO/H_2O, C_2H_4/CH_3OH und CO/CH_3OH untersucht. Die Ergebnisse dieser Arbeiten liefern wichtige Einblicke in elektronen-induzierte Reaktionen in interstellarem Eis, da H_2O, CO und CH_3OH Hauptbestandteile von interstellarem Eis sind. Detailliertes Wissen über die Reaktionsmechanismen konnte aus der Abhängigkeit der Produktausbeute von der Elektronenenergie abgeleitet werden, was die Bestimmung der zugrunde liegenden Elektronen-Molekül-Wechselwirkungen ermöglichte. Weitere Informationen über die Mechanismen wurden durch den Vergleich der Energieabhängigkeiten verschiedener Produkte erhalten. Dies ermöglichte es, die relevanten Intermediate zu identifizieren und zwischen mehreren möglichen Reaktionsszenarien zu unterscheiden. Auf Grundlage dieses Ansatzes konnten mehrere Reaktionstypen identifiziert werden, die bei der Bestrahlung der untersuchten Mischungen eine Rolle spielen. Bei diesen handelt es sich um die Radikalrekombination, die Hydrierung von CO und C_2H_4, die Oxidation von CO zu CO_2, und die Additionsreaktionen zwischen einem Radikal und CO oder C_2H_4.

Table of Contents

1 Introduction

1.1 Chemical Transformations in the Interstellar Medium

The space between stars is not empty but is filled with gas and dust which are formed at the end of a star's life cycle by stellar winds or supernova events.[1–3] This space is referred to as the interstellar medium and is characterized by a wide range of particle densities (10^{-4}–10^{8} particles/cm^3), temperatures (10–10^6 K), and the presence of high energy radiation fields.[1–3] Up to the late 1960's, these conditions were considered to be too harsh to enable the formation and survival of polyatomic molecules. It was not before 1968 that Cheung and co-workers[4] discovered NH_3 in the interstellar medium.[5] Since then, more than 220 molecules have been observed in the interstellar medium and circumstellar shell[6–8] which has changed conceptions of astrochemistry dramatically.

A more comprehensive understanding of chemical processes in the interstellar and circumstellar medium is not only desirable to understand the formation of molecules but also to probe physical conditions, such as the density, temperature, velocity, and age of interstellar objects.[9] Furthermore, it has been recognized that the large inventory of organics in molecular clouds might have served as a feedstock for the building blocks of life[2] and thus may link astrochemical processes with the emergence of life on earth.

The interstellar medium is a rather inhomogeneous environment which contains regions of lower and higher densities reflective of the evolution from the diffuse interstellar medium to the formation of protostars. The regions with the lowest densities are called the diffuse interstellar medium (typical particle densities of 10^2–10^3 particles/cm^3)[1] where harsh UV radiation (typical fluxes of 10^8 UV photons/cm^2/s)[1,3] from nearby stars prevents the formation and survival of most molecules. Thus, the diffuse interstellar medium is mostly comprised of neutral atomic hydrogen, and ionized atoms (particularly carbon).[10] One of the rare molecular species are polycyclic aromatic hydrocarbons (PAHs) which are sufficiently robust to withstand UV photolysis.[2] Under the force of gravity, the diffuse interstellar medium collapses to form dense molecular clouds whose interior is effectively shielded from external UV radiation by dust particles which allows more complex molecules to survive.[2,11] Despite the absence of external UV radiation, molecular clouds are not devoid of ionizing radiation. This is because cosmic ray particles, i.e., highly energetic atomic nuclei most of which are protons with energies of >1 MeV, can penetrate much deeper into the interior of the molecular cloud.[3] On their track through the molecular cloud, these cosmic rays successively lose parts of their

kinetic energy by ionizing atoms and molecules. This leads to the formation of a high number of secondary electrons of which a small fraction is thought to lead to electronic excitation of H_2 and subsequent emission of UV photons in the Lyman and Werner bands.[1–3,12] By this mechanism, a flux of about 10^3–10^4 UV photons/cm^2/s is maintained in the interior of the molecular clouds which is several orders of magnitude lower than that in the diffuse interstellar medium.[1,3]

Due to the lower radiation flux, radiative heating is less effective than in the diffuse interstellar medium or in the vicinity of a star. The temperature in molecular clouds can thus drop to values as low as 10–15 K.[2,3] At these low temperatures, even highly volatile compounds are physisorbed when they strike the surface of a dust particle.[2] When the molecular cloud starts to form out of the diffuse medium, atoms dominate the gas phase.[11] Thus, H, O, C, and N atoms accrete onto the dust grains where they are thought to react by a Langmuir-Hinshelwood mechanism, i.e., the atoms are sufficiently mobile to diffuse over the grain surface until they encounter a partner to react with.[3,11,13–17] Other scenarios based on the Eley-Rideal or the hot atom mechanism, however, are also discussed to contribute to the formation of reaction products.[17] Due to the high mobility and abundance of hydrogen atoms, hydrogenation reactions are thought to prevail leading to the formation of H_2, H_2O, CH_4, and NH_3.[2,3,13–17] In the gas phase, CO is efficiently formed which accretes onto the dust grains where it can also be hydrogenated yielding H_2CO and CH_3OH.[11] Note that He atoms, which are also abundant in the gas phase, do not participate in chemical reactions due to their inert character. With ongoing accretion of atoms and molecules from the gas phase and subsequent surface reactions, an icy mantle is formed which is subject to further processing by UV photons and cosmic ray particles leading to the formation of more complex molecules (Figure 1).[1–3] Chemical reactions on the surface of dust grains provide two key advantages over gas phase reactions: First, they accommodate a large number of molecules in close proximity which increases the probability of two molecules to meet and, secondly, they also act as a third body that can dissipate excess energy released during chemical reactions.[1,2]

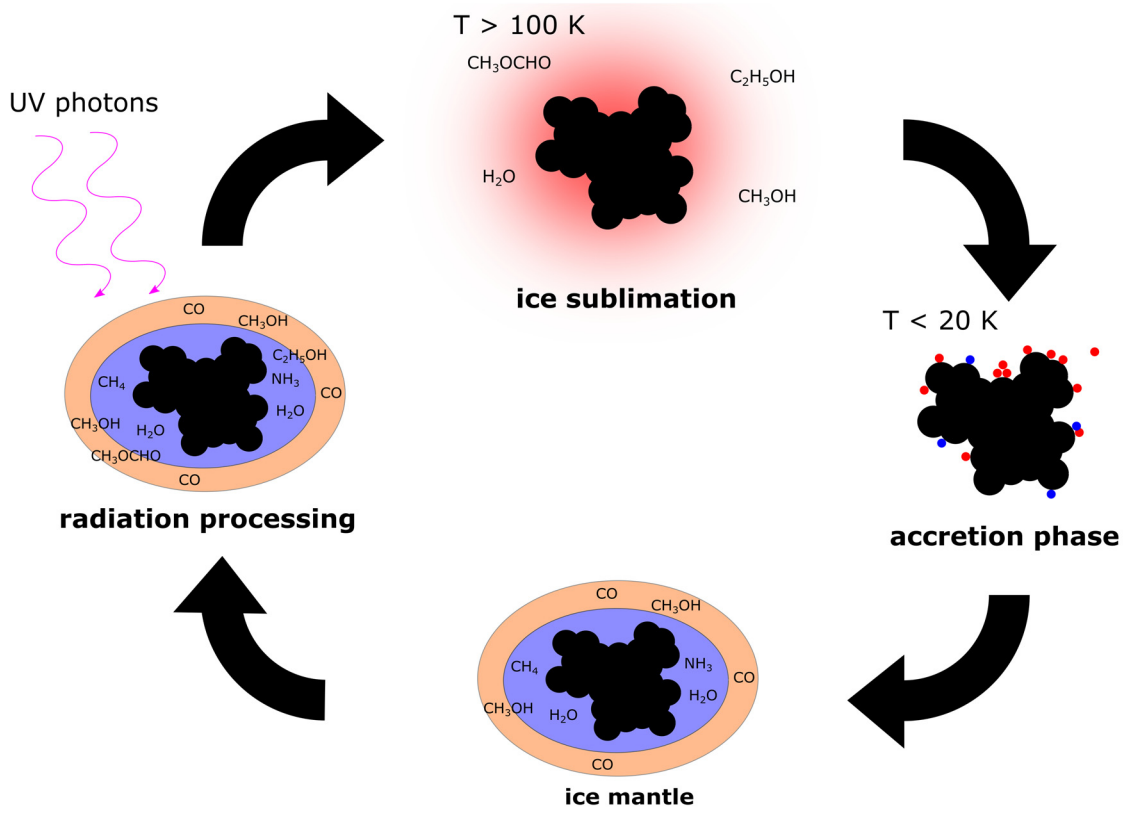

Figure 1. Life cycle of an interstellar dust grain. In the accretion phase, atoms are physisorbed on the surface of the bare grain where they can undergo surface reactions forming simple molecules like H_2O, NH_3, and CH_4. During later stages, CO from the gas phase is also accreted and can be hydrogenated yielding H_2CO and CH_3OH. With ongoing accretion, a thick ice mantle is formed around the dust grain. This ice mantle is subject to photolysis and radiolysis which leads to the formation of more complex molecules. Finally, the ice mantle sublimes into the gas phase once the grain is in an environment of sufficiently high temperature.[3]

Although the importance of dust grain chemistry is generally accepted nowadays, detailed knowledge about the reaction mechanisms just starts to emerge. This is because molecular clouds are separated from earth by large distances restricting any studies to remote observations using telescopes.[2] Furthermore, chemical transformations occur on a timescale of thousands of years which only allows one to understand chemical processes by analyzing the commonalities and differences in chemical composition over a wide range of different environments.[18] Finally, analysis of ice composition is restricted to infrared (IR) spectroscopy which, however, suffers from overlapping absorption bands and insufficient sensitivity for minor ice constituents.[17,18] Thus, the formation of many products has only been indirectly inferred from their detection in the gas phase by rotational spectroscopy, that is, after these molecules have sublimed in warmer environments.[17] Consequently, much of today's knowledge on the chemical processes in interstellar ices are based on laboratory experiments

as these enable the study of chemical reactions under well-defined conditions and with a variety of analytical techniques.

1.2 Laboratory Experiments

Experiments performed in the laboratory provide spectroscopic data which can be used to identify absorption bands observed by telescopes and to constrain molecular abundances.[3] On the other hand, laboratory experiments also serve to determine rate constants for gas phase reactions[19] and to study chemical reactions that occur when interstellar ices are exposed to various radiation sources.[20–23] With regard to the studies presented in this thesis, the following discussion is confined to those laboratory experiments that study radiation-induced chemistry in ices.

Typically, these experiments are performed in Ultrahigh vacuum (UHV) with base pressures of ~10^{-10} mbar in order to avoid contaminations of the samples. Ices are typically prepared by condensing gases or vapors on a substrate which is cooled down to temperatures as low as 5–35 K by He cryostats.[20,23,24] Subsequently, the ice is exposed to a radiation source which can deliver UV radiation,[11,21,25] X-rays,[26] keV electrons,[20,27–29] low-energy electrons,[23,30,31] or ions.[32] UV lamps typically operate with photon fluxes of about 10^{13}–10^{15} photons/cm^2/s[21,25,33] in order to keep irradiation times reasonable short. Electron sources typically operate at fluxes of 10^{11}–10^{15} electrons/cm^2/s and may thus be comparable to UV lamps.[20,23,29,30,34] Notable, radiation fluxes, vacuum quality, and ice composition can deviate significantly from those in the interstellar medium. Still, the data provide valuable information as chemical reactions can be studied under well-defined conditions. Laboratory experiments are thus essential for a comprehensive understanding of astrochemical processes.

During irradiation and/or after a defined radiation dose, the composition of the ice is analyzed by IR spectroscopy, mass spectrometry, or chromatography. Often, ice composition is chosen to match that of a "realistic" ice mixture consisting of three or more constituents which results in a very rich chemistry. For example, Caro et al.[35] investigated product formation in UV irradiated mixtures of $H_2O/CH_3OH/NH_3/CO/CO_2$, and Meinert et al.[36] investigated product formation in UV irradiated mixtures of $H_2O/CH_3OH/NH_3$. Analysis of the processed ices with gas chromatography in combination with mass spectrometry (GC-MS) revealed the formation of amino acids[35] and sugars[36], which are import building blocks in biochemistry. In those experiments, however, it is difficult to deduce specific reaction mechanisms as the reaction networks are already too complex to be unraveled. In order to facilitate the interpretation, mechanistic studies are thus typically performed in pure ices[21,23,25,28,30,31] or in binary

mixtures[20,21,29,34,37] which still provides very useful information. Typical questions that are of interest for the astrochemical community is how chemical reactions are affected by the ice temperature, morphology, thickness, and composition. Furthermore, there is an ongoing debate about the contributions of different types of radiation to the overall yields[1] as well as the emergence of homochirality, e.g., by circularly-polarized UV photons[11,38,39] and low-energy spin-polarized secondary electrons.[40–42]

A comprehensive understanding of a reaction mechanism often requires a number of studies that each shed light on different aspects of a reaction. These different aspects can be inferred from reaction kinetics, isotopic labeling of reactants, identification of intermediates and side products,[11,20] matrix isolation experiments,[43] computational modelling,[44] or by performing irradiations with different radiation sources.[45] Regarding the last aspect, it is worth noting that different kinds of ionizing radiation have in common that they produce huge numbers of low-energy secondary electrons when they interact with ices.[11,46–48] In fact, secondary electrons are thought to be the actual driving force behind a wide variety of radiation-induced chemical reactions.[1,46–48] These secondary electrons have kinetic energies which are typically below 20 eV. In this energy regime, different electron-molecule interactions are accessible which are electron impact ionization (EI), electronic excitation (EE) and electron attachment (EA) (see Section 2.1 for a more detailed description).[46,49] These electron–molecule interactions are often followed by dissociation of the molecule into radicals and/or ions in which case these processes are referred to as dissociative ionization (DI), neutral dissociation (ND), and dissociative electron attachment (DEA), respectively.[46,49] In interstellar ices as well as in many laboratory experiments that rely on high energy radiation, these events occur at the same time which makes it very difficult to identify the relevant electron-molecule interactions as well as to evaluate their individual contribution to the overall product yields.

In order to address this problem, it is important to consider that EI, EE, and EA show characteristic dependences on electron energy. The basic idea of the work summarized in this thesis is that this energy dependence is reflected in the product yields of an electron-induced reaction. Therefore, the underlying electron-molecule interactions can be identified by performing irradiation experiments with a range of different electron energies.

1.3 Electron-Induced Synthesis

Typically, electron irradiation is associated with its destructive nature which is widely utilized in mass spectrometry to identify molecules by their characteristic fragmentation pattern. Electron irradiation, however, can also lead to molecular synthesis, i.e., the formation of more

complex molecules from smaller entities.[49] In many cases, the underlying mechanisms are remarkably similar to those known from organic chemistry including nucleophilic displacement reactions,[50] acid-base reactions,[51] addition reactions,[51–53] and oligomerization.[54,55] This suggests that electron-induced synthesis is in fact not only a random re-assembly of atomic and molecular fragments but that it follows certain reaction principles.

Several examples of electron-induced syntheses in molecular ices were studied previously using the same approach as also applied in the present thesis. In particular, the electron-induced reactions between C_2H_4 and NH_3 yielding ethylamine ($CH_3CH_2NH_2$),[52,53] C_2H_4 and H_2O yielding ethanol (C_2H_5OH),[51] and CO and NH_3 yielding formamide (NH_2CHO)[37] were investigated and reaction mechanisms were proposed.

In the case of C_2H_4/NH_3 mixtures, formation of ethylamine, i.e., an electron-induced hydroamination, was observed for electron energies above the ionization thresholds of C_2H_4 and NH_3.[52] As the electron energies used in that study are still below the onset of DI at least for NH_3 and not much above the threshold for C_2H_4,[56] a mechanism on the basis of intact radical cations was proposed (Scheme 1). In this reaction model, ionization of either C_2H_4 or NH_3 leads to an attractive Coulomb force between the reactants which allows them to circumvent the reaction barrier that prevents a spontaneous reaction between the neutral molecules.[52] Reaction between C_2H_4 and NH_3 after EI yields a cationic adduct (structure **I** in Scheme 1) as an intermediate. Intramolecular rearrangement of **I** into the ethylamine cation (structure **II** in Scheme 1**)** and subsequent neutralization by a thermalized electron eventually yields ethylamine.

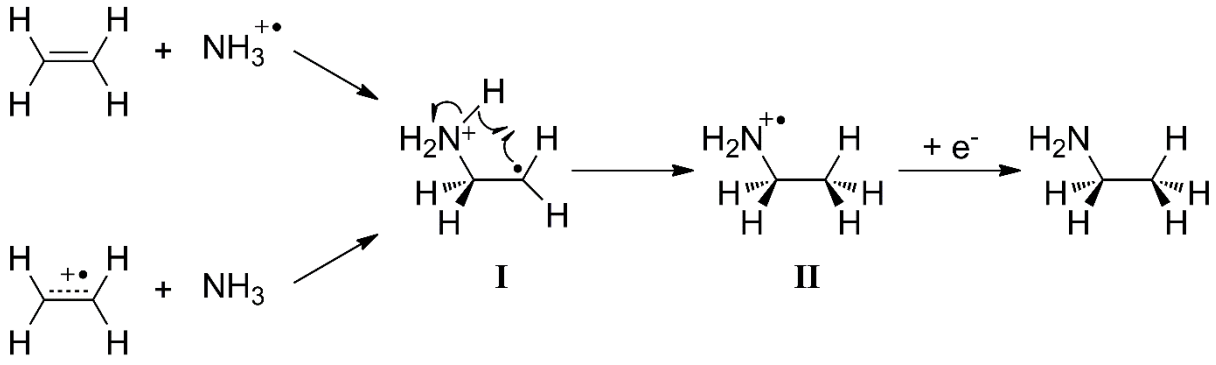

Scheme 1. Proposed mechanism for the ionization-driven formation of ethylamine in mixtures of C_2H_4 and NH_3 upon electron irradiation.[52,53]

The proposed mechanism has been examined more comprehensively in a subsequent study[53] by investigating the dependence of product yield on electron energy and sample composition, as well as the formation of side products. Furthermore, experiments were also performed

using NH_3 and propene (CH_2=$CHCH_3$), ethylamine and C_2H_4, and diethylamine ($(CH_3CH_2)_2NH$) and C_2H_4 in order to probe possible steric effects. While the mechanism in Scheme 1 is in accord with the observed energy dependences and successfully predicts the formation of the respective hydroamination products, it fails to predict some of the observed side products. For example, ethane (C_2H_6) and butane (C_4H_{10}) were formed as major side products in the C_2H_4/NH_3 mixture. Although these products were also formed upon electron irradiation of pure C_2H_4, the product yields were considerably enhanced in the presence of NH_3 suggesting that NH_3 acts as a reducing agent. This is supported by the observation that N_2 was a side product which signifies successive loss of hydrogen atoms from NH_3. With regard to gas phase studies, it has been suggested that DEA to NH_3 which yields NH_2^- and $H^{\bullet}$[57] might cause reduction of C_2H_4.[53] However, this hypothesis remained speculative as no obvious resonances have been observed in the energy dependent yields of ethylamine, C_2H_6, and N_2.

The results discussed so far signify that the mechanism in Scheme 1 does not represent a complete picture as dissociative channels are not included. This conclusion in general calls for a critical evaluation if a reaction mechanism that explains the formation of a specific product is in accord with the formation of all side products. For instance, the mechanism proposed in Scheme 1 does not include the reduction of C_2H_4 by NH_3, as well as the oxidation of NH_3 to N_2. Experimental and theoretical studies on ionized NH_3 clusters suggest that $NH_3^{\bullet+}$ can transfer a proton to a nearby NH_3 molecule yielding NH_4^+ and $NH_2^{\bullet}$.[58] Previous experiments on electron-irradiation of a bilayer of NH_3 at E_0 = 50 eV provided further evidence for the formation of chemisorbed $NH_2^{\bullet}$ radicals by high-resolution electron energy loss spectroscopy (HREELS) and X-ray photoelectron spectroscopy (XPS).[59] In addition, more recent experiments on thin[31,53] and thick[60] multilayer films revealed the formation of N_2H_4 by TDS,[31,53,60] which is thought to result from recombination of two $NH_2^{\bullet}$ moieties. Thus, a more favorable route to ethylamine might be initiated by ionization of NH_3 and subsequent proton transfer to a nearby NH_3 molecule yielding $NH_2^{\bullet}$ and NH_4^+.[61] The $NH_2^{\bullet}$ radical could then add to C_2H_4 yielding an intermediate $H_2N–C_2H_4^{\bullet}$ radical which may then abstract a hydrogen atom from a nearby NH_3 to yield ethylamine. In a competitive reaction, the intermediate radical might also capture a thermalized electron and then undergo proton transfer with the NH_4^+ cation yielding ethylamine and NH_3.

The mechanism in Scheme 1 has also been adopted to explain the formation of ethanol from C_2H_4/H_2O mixture[51] and the formation of formamide from CO/NH_3.[37] In addition to the ionization driven mechanism, however, further mechanisms on the basis of EA and DEA have

been proposed to explain resonant structures in the energy dependences of ethanol and formamide production. Considering first the case of C_2H_4/H_2O,[51] resonant formation of ethanol, C_2H_6, and butane was observed for E_0 < 6 eV which has been assigned to EA to C_2H_4 yielding a $C_2H_4^{\bullet -}$ radical anion which undergoes an acid-base reaction with H_2O yielding $C_2H_5^{\bullet}$ (Scheme 2). Subsequently, the $C_2H_5^{\bullet}$ radical can attack the double bond of another C_2H_4 moiety which initiates dimerization of C_2H_4 yielding $C_4H_9^{\bullet}$ which can react further in a chain reaction. If either of the radical alkyl intermediates reacts with H_2O, however, the chain propagation is terminated yielding, for instance, C_4H_{10} and a $HO^{\bullet}$ radical. The $HO^{\bullet}$ radical, in turn, can attack a nearby C_2H_4 moiety forming $HOC_2H_4^{\bullet}$. Finally, reaction with a nearby H_2O molecule again yields ethanol and $HO^{\bullet}$ (Scheme 2) potentially resulting in another chain reaction. It is also obvious here how consideration of side products leads to a more comprehensive view of the reaction.

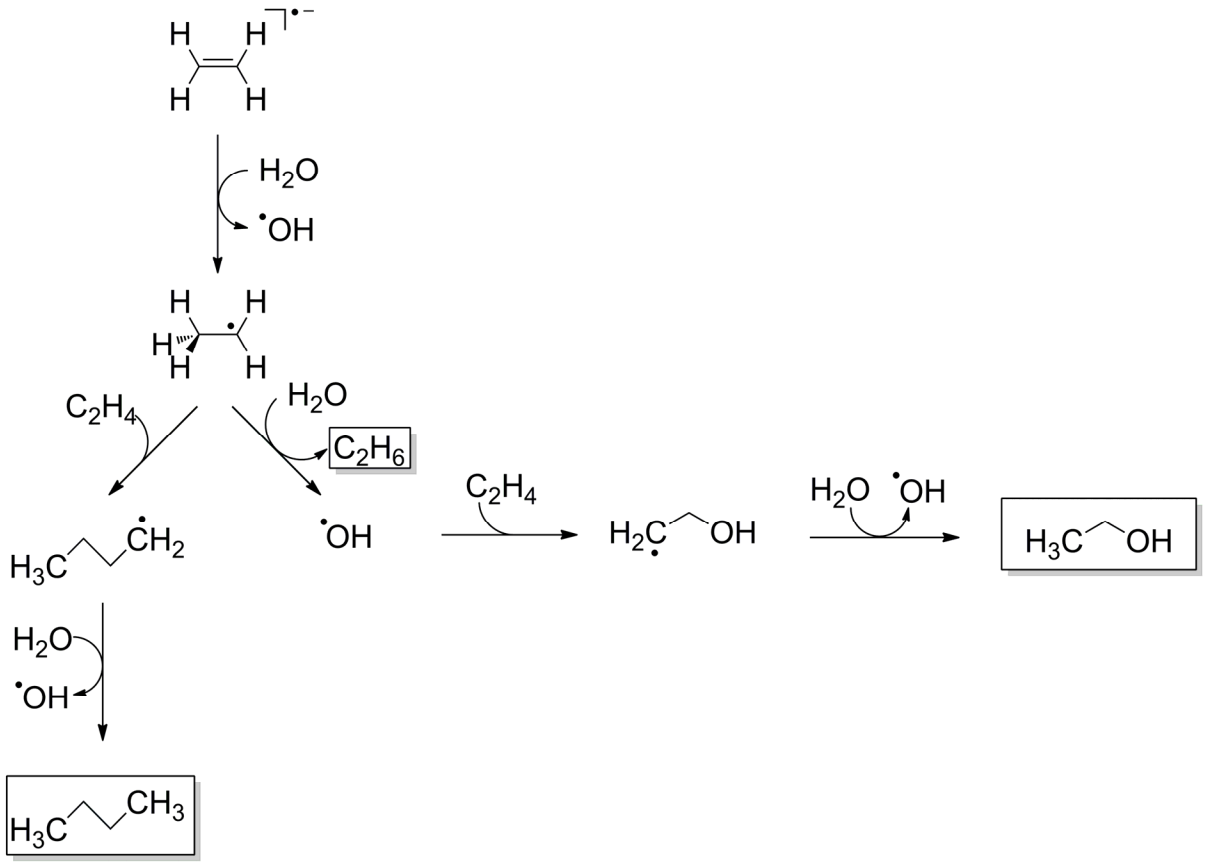

Scheme 2. Proposed mechanism for the electron-induced formation of ethanol in mixtures of C_2H_4 and H_2O by EA to C_2H_4 at E_0 < 6 eV. Side products of the reaction are C_2H_6 and butane.[51]

Considering next the case of CO/NH_3,[37] resonant formation of formamide was observed at 9 eV which has been assigned to DEA to NH_3 yielding H^- and $NH_2^{\bullet}$, or NH_2^- and $H^{\bullet}$.[57] Following DEA, either $NH_2^{\bullet}$ or $H^{\bullet}$ can attack a nearby CO molecule to yield $H_2NCO^{\bullet}$ or $HCO^{\bullet}$.

Finally, reaction with NH_3 yields formamide and either a $NH_2^{\bullet}$ or $H^{\bullet}$ radical (Scheme 3) potentially resulting in a chain reaction.

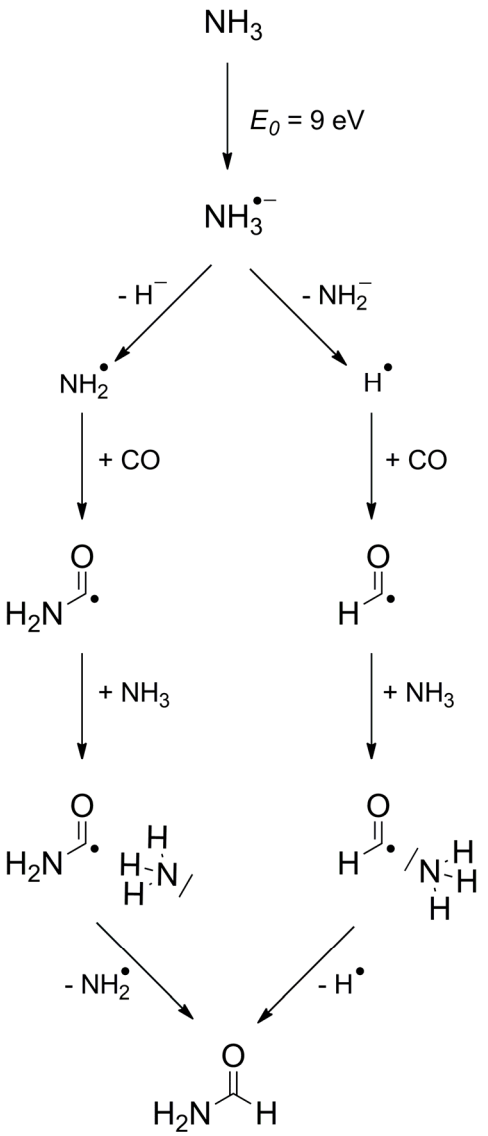

Scheme 3. Proposed mechanism for the formation of formamide in mixtures of CO and NH_3 by DEA to NH_3 at E_0 = 9 eV.[37]

A closer comparison of the formation of ethylamine in C_2H_4/NH_3 ices[53] and of formamide in CO/NH_3[37] reveals that the proposed mechanisms may not be fully consistent calling again for a more comprehensive reevaluation. In fact, it could be expected that DEA to NH_3 at 9 eV yielding either H^- and $^{\bullet}NH_2$, or NH_2^- and $H^{\bullet}$[57] which explains the resonant formation of formamide[37] should also contribute to the formation of ethylamine and/or C_2H_6. However, while the energy dependence of formamide evinces a resonance at 9 eV,[37] the energy dependences of ethylamine and C_2H_6 do not.[53] There might be several reasons for this discrepancy. Firstly, the resonance may have been overseen in the data for ethylamine and C_2H_6 production as their formation was not strictly studied in the regime where product

formation depends linearly on the electron dose. This hypothesis is, in fact, supported by the energy dependence of product yields which show saturation for E_0 > 10 eV.[53] Secondly, ionization of C_2H_4 may already start to contribute to the formation of ethylamine at 10 eV if it is considered that the ionization energy of C_2H_4, which is about 10.5 eV in the gas phase,[56] might be shifted to lower values in the condensed phase.[62,63] In contrast, the ionization energy of CO is 14.0 eV in the gas phase[56] and thus at considerably higher energies. Thus, resonant contributions to the overall product yields in the C_2H_4/NH_3 ice might be masked by higher contributions of the EI-driven mechanism. Finally, the resonance observed in the CO/NH_3 ice may also stem from DEA to CO rather than NH_3.[64–66] These arguments demonstrate that interpretation of the experimental data is still ambiguous and that more comprehensive studies are required to obtain a conclusive picture of the reaction mechanisms that underlie the product formation under electron irradiation in molecular ices.

This review of the previous work makes clear that it is essential to consider if any proposed reaction mechanism is also able to predict the reaction outcome in similar reaction systems. To this end, the present thesis is concerned with the question how a reaction mechanism is changed when an individual reactant is replaced by another. In particular, this question has been addressed by studying electron-induced reactions in C_2H_4/CH_3OH, CO/H_2O, and CO/CH_3OH mixed ices as summarized briefly in Sections 1.3.1 to 1.3.4. This work complements the results obtained from studying electron-induced reactions in C_2H_4/H_2O,[51] C_2H_4/NH_3,[53] and CO/NH_3 mixtures.[37] For example, the results allow us to directly compare the formation of formamide, formic acid, and methyl formate which are anticipated as products in the reaction of CO with NH_3, H_2O, and CH_3OH based on the mechanism depicted in Scheme 1, respectively (Table 1). This systematic approach leads to more general conclusions on the reaction mechanisms and thus contributes to a comprehensive picture of astrochemical processes.

Table 1. Addition products expected for the reaction of C_2H_4 and CO with NH_3, H_2O, and CH_3OH via the ionization-driven mechanism depicted in Scheme 1. Formation of ethylamine, ethanol, and formamide (black) has been investigated in previously studies.[37,51–53] In the present thesis, formation of ethyl methyl ether, formic acid, and methyl formate (red) have been studied.

	NH_3	H_2O	CH_3OH
C_2H_4	 Ethylamine	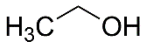 Ethanol	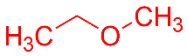 Ethyl methyl ether
CO	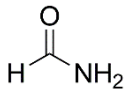 Formamide	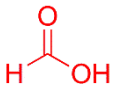 Formic acid	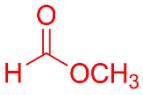 Methyl formate

1.3.1 Reactions in CO/H_2O Mixtures (Publication I)

Electron-induced reactions in mixed ices of CO and H_2O yield not only formic acid (HCOOH) anticipated according to Scheme 1 and Table 1 but also H_2CO and CO_2 (Figure 2). A detailed study on the energy dependent formation of HCOOH, H_2CO, and CO_2 revealed that product formation is mainly triggered by ND of H_2O yielding $HO^{\bullet}$ and $H^{\bullet}$, as well as H_2 and $O(^3P/^1D)$. In addition, formation of HCOOH also proceeds by DEA to CO or H_2O at 10 eV yielding a reactive $O^{\bullet-}$ radical anion. Finally, formation of H_2CO is also initiated by EA to CO at around 4 eV yielding an intermediate $CO^{\bullet-}$ radical anion.

The results have important implications for the formation of CO_2 under astronomical conditions as this is the first experimental study showing that CO_2 is mainly formed by the reaction of atomic oxygen with CO which is in contrast to most previous studies which proposed a formation route via an intermediate $HOCO^{\bullet}$ radical that decays into CO_2 and $H^{\bullet}$.

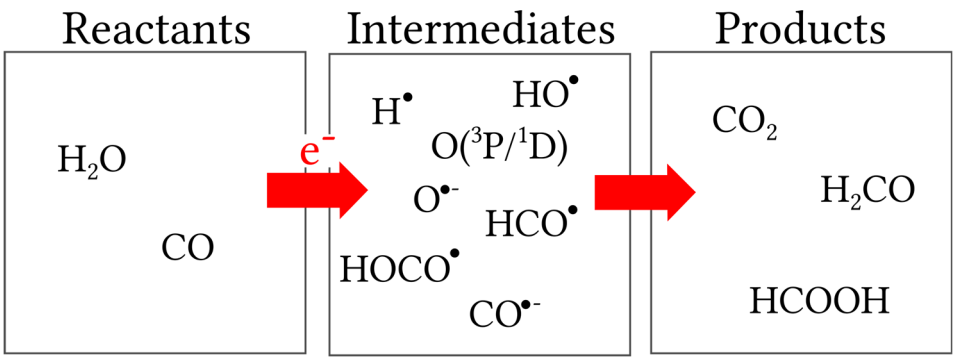

Figure 2. Products and relevant intermediates produced during electron irradiation of CO/H_2O ice.

1.3.2 Reactions in Pure CH_3OH (Publication II)

Upon electron irradiation of CH_3OH, cleavage of the different bonds leads to numerous products via a complex reaction network. In order to understand chemical reactions in mixed ices containing CH_3OH, it is thus essential to have a comprehensive knowledge of chemical processes in pure CH_3OH ice. Therefore, the formation of H_2CO, CH_4, ethylene glycol ($HOCH_2CH_2OH$), methoxymethanol (CH_3OCH_2OH), dimethyl ether (CH_3OCH_3), and ethanol (C_2H_5OH) (Figure 3) has been studied with respect to the dependence of product yields on electron energy.

The results revealed that electron-induced synthesis, i.e., the formation of larger molecules from smaller building blocks, mainly proceeds by radical recombination of CH_3OH fragments whereas H_2CO and CH_4 are also formed by unimolecular decay of CH_3OH following electron interaction. Below the ionization threshold, ND is the main driving force for the formation of products but DEA to CH_3OH also contributes to the yields of H_2CO and CH_4. Above the ionization threshold, EI of CH_3OH is the dominant electron–molecule interaction responsible for product formation. In addition, H_2CO is formed by EA to CH_3OH at E_0 = 13 eV followed by autodetachment and subsequent dissociation of the excited neutral into H_2CO and H_2. To a lower extent, this resonance may also yield radical species and thus contribute to the formation of ethylene glycol, methoxymethanol, dimethyl ether, and ethanol. This publication constitutes the most complete dataset on the energy dependence of product formation during irradiation with low-energy electrons of CH_3OH ice so far and thus serves as reference for studies on electron-induced processes in CH_3OH containing mixed ices.

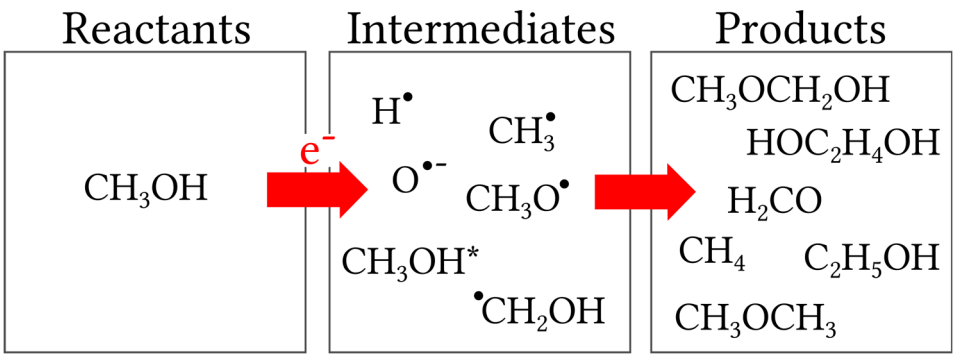

Figure 3. Products and relevant intermediates produced during electron irradiation of CH_3OH ice.

1.3.3 Reactions in C_2H_4/CH_3OH Mixtures (Publication III)

Electron-induced reactions in mixed ices of C_2H_4 and CH_3OH yield not only ethyl methyl ether ($CH_3OC_2H_5$) anticipated according to Scheme 1 and Table 1 but also hydrocarbons like ethane (C_2H_6) and butane (C_4H_{10}) (Figure 4). A detailed study on the energy dependence of ethyl methyl ether revealed that product formation is mainly triggered by EI. However, there is a minor reaction channel at lower electron energies which triggers product formation by DEA to CH_3OH.

The proposed reactions do probably not occur under conditions relevant for astrochemistry as C_2H_4 is none of the major ice constituents. However, this is the first experimental study demonstrating the role of DEA for electron-induced synthesis in CH_3OH containing ices.

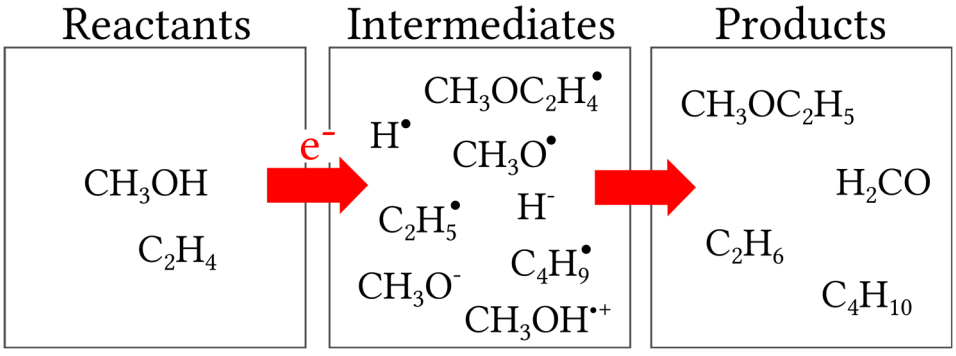

Figure 4. Products and relevant intermediates produced during electron irradiation of C_2H_4/CH_3OH ice.

1.3.4 Reactions in CO/CH_3OH Mixtures (Publication IV)

Electron-induced reactions between CO and CH_3OH yield not only methyl formate (CH_3OCHO) which was anticipated to form according to Scheme 1 and Table 1, but also H_2CO and CO_2. Based on the dependence of product yields on electron energy and supported by the

formation of specific side products, it could be inferred that methyl formate is mainly formed by an intermediate $CH_3OCO^{\bullet}$ radical and not by addition of the intact $CH_3OH^{\bullet+}$ radical cation to CO. The dominant reaction pathway leading to methyl formate is initiated by DEA to CO at 10 eV although ND and EI of CH_3OH contribute to its formation to some extent. At lower electron energies, methyl formate is also formed by DEA to CH_3OH at E_0 = 5.5 eV. This is the first study which provides evidence that methyl formate can be formed by an intermediate $CH_3OCO^{\bullet}$ radical. Furthermore, this study corroborates the importance of DEA for electron-induced synthesis in CH_3OH containing ices.

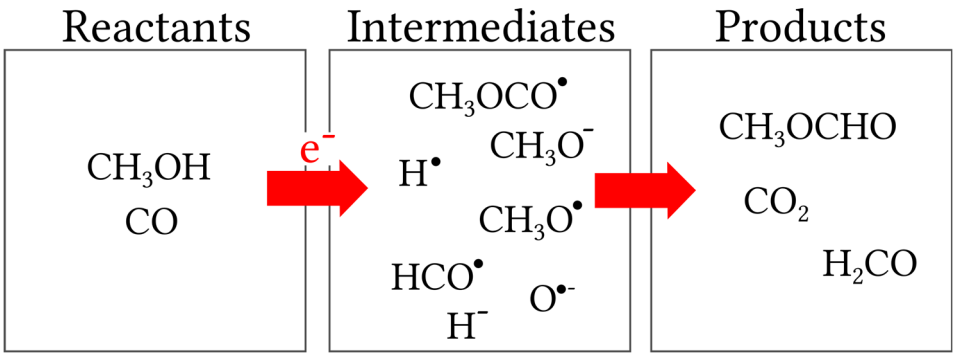

Figure 5. Products and relevant intermediates produced during electron irradiation of CO/CH_3OH ice.

2 Formation of Reactive Species by Electron–Molecule Interactions

Chemical reactions can be initiated when electrons interact with a molecule by electron impact ionization (EI), electronic excitation (EE), or electron attachment (EA).[46,49] The primary intermediates are typically unstable and decay by dissociation into one or more fragments. In the quasi-diatomic model, EI produces radical cations which can further dissociate into a radical and a cation. This process is referred to as dissociative ionization (DI):

$$AB + e^- \longrightarrow AB^{\bullet+} + 2e^-$$
$$AB^{\bullet+} \longrightarrow A^\bullet + B^+$$

EE produces an electronically excited molecule which can subsequently decay by neutral dissociation (ND) into two neutral fragments which are typically radicals:

$$AB + e^- \longrightarrow AB^* + e^-$$
$$AB^* \longrightarrow A^\bullet + B^\bullet$$

EA produces a transient negative ion (TNI) which can either be stabilized (not shown), reemit the excess electron by autodetachment (not shown) or decay by dissociative electron attachment (DEA) into an anion and a radical.

$$AB + e^- \longrightarrow AB^{\bullet-}$$
$$AB^{\bullet-} \longrightarrow A^\bullet + B^-$$

2.1 Non-Resonant Electron-Molecule Interactions

EI and EE are non-resonant processes which only occur when the kinetic energy of the electron exceeds the ionization energy or electronic excitation energy of the target molecule, respectively. DI requires sufficient excess energy to overcome the binding energy. In the case of a quasi-diatomic model, this excess energy equals the bond dissociation energy of the radical cation. For polyatomic molecules, however, this excess energy can be partially or fully compensated when molecular rearrangement leads to the formation of new chemical bonds. The cross section of EI and EE increases steadily with increasing electron energy once the thresholds for ionization or electronic excitation have been overcome. In the range from 50–100 eV, the cross section reaches a maximum and decreases again for higher electron energies (Figure 6). This is because the interaction time between an electron and a molecule decreases with the velocity of the electron and eventually becomes smaller than the time required for EE or EI.

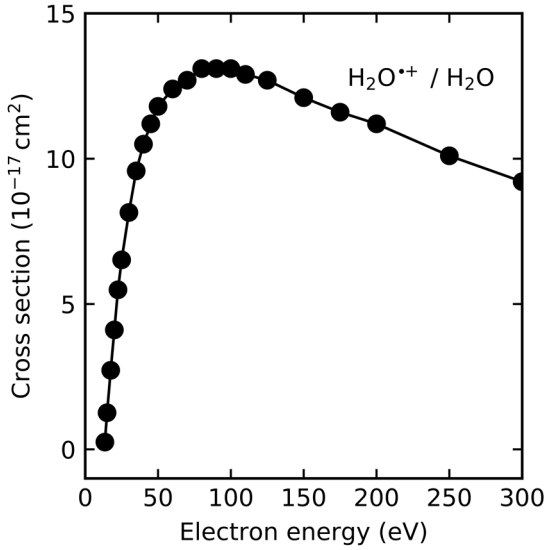

Figure 6. Energy dependence of the cross section for the formation of $H_2O^{\bullet+}$ from EI to H_2O as an example of the typical behavior of ionization cross sections. Data were taken from Itikawa and Mason.[67]

2.2 Resonant Electron-Molecule Interactions

In contrast to EI and EE, EA and DEA are resonant processes which only occur in narrow energy ranges (Figure 7). Intact radical anions $M^{\bullet-}$ formed by EA to a molecule M are usually only observed at near-zero electron energies where fragmentation is energetically not feasible.[49] The thermodynamic threshold for DEA, however, is often lower than those for ND and DI as the energy required to overcome the binding energy can be partially or fully compensated by the electron affinity of either of the fragments.[49]

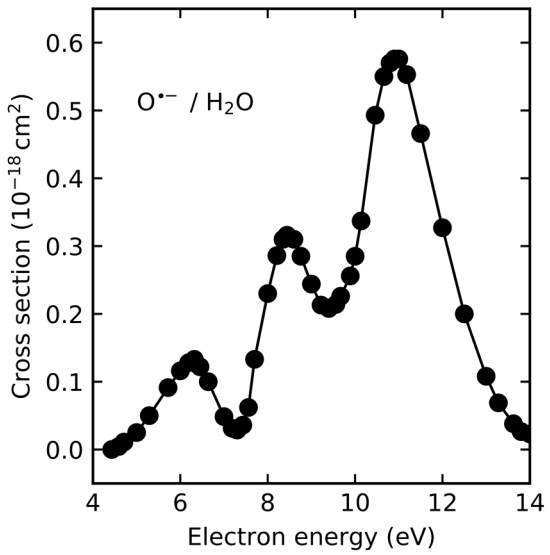

Figure 7. Energy dependence of the cross section for the formation of $O^{\bullet-}$ by DEA to H_2O as an example of the typical behavior of cross sections for DEA. Data were taken from Itikawa and Mason.[67]

EA and DEA can be categorized into either single-particle resonances or core-excited resonances which can be further divided into shape resonances and Feshbach resonances (Figure 8).[62,68] In a single-particle resonance, the incident electron occupies a previously unoccupied or half-occupied orbital. In a core-excited resonance, this electron capture goes along with an excitation of the neutral parent molecule into a higher electronic state. In a shape resonance, the TNI is metastable with respect to the neutral parent state and immediate autodetachment is only hindered by the centrifugal barrier. Shape resonances are typically short-lived states with lifetimes from femtoseconds to a few hundreds of picoseconds because the excess electron can tunnel through the centrifugal barrier.[62] In a Feshbach resonance, the TNI is lower in energy than the corresponding neutral parent state. The lifetimes of Feshbach resonances are thus considerably higher than those of shape resonances.

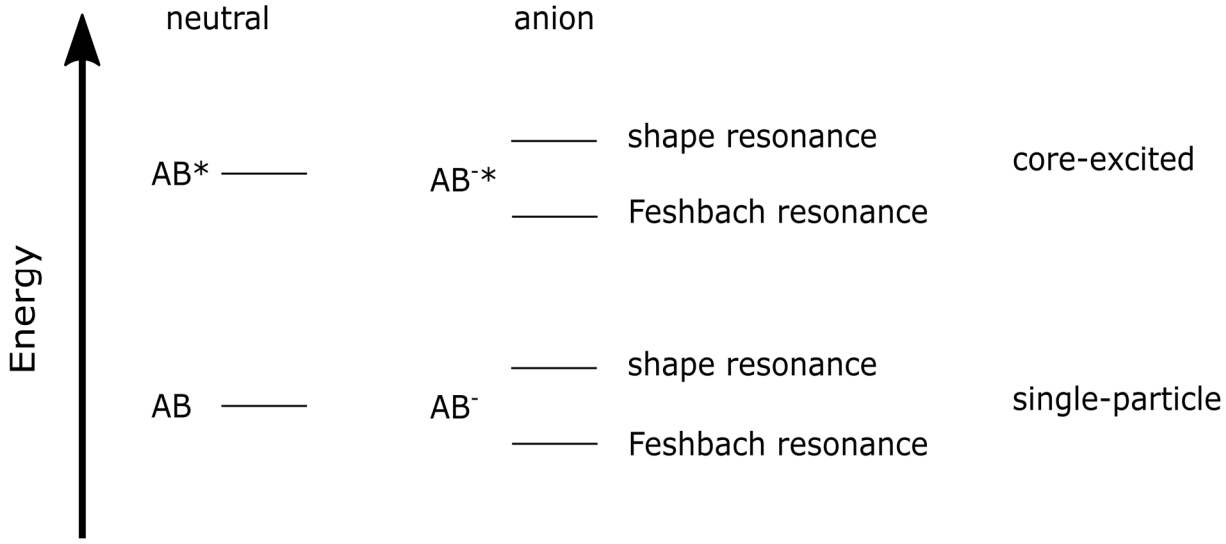

Figure 8. Types of resonances in electron attachment (EA) to a molecule AB. In a single-particle resonance, the electron occupies a previously unoccupied orbital. In a core-excited resonance, EA is accompanied by electronic excitation of the molecule. Core-excited and single-particle resonances can be further categorized into shape and Feshbach resonances. For shape resonances, the TNI has a higher energy than its neutral parent state whereas the TNI is lower in energy in case of a Feshbach resonance.

Typically, the kinetic energy of the electron where resonant DEA occurs is slightly higher than the thermodynamic threshold for the reaction. This is because DEA proceeds by a vertical transition to the anionic potential energy surface (Figure 9). The kinetic energy of the electron must thus match the energy difference between the ground state and electronically excited state. Subsequently, the TNI decays by increasing the internuclear distance which eventually leads to dissociation into a radical and an anion. During this progression, the TNI can return to the parent electronic state by autodetachment of the excess electron. Beyond the critical point where both potential energy surfaces crosses (R_c in Figure 9), however, it is energetically not feasible for the molecule to return to its parent state which leads to irreversible dissociation of the TNI unless the parent anion is sufficiently stabilized.

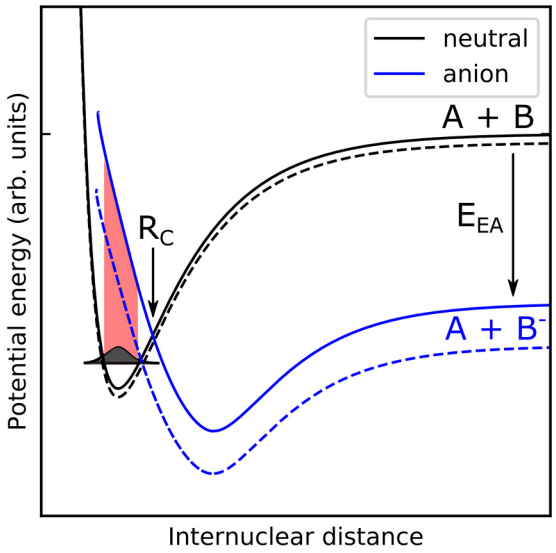

Figure 9. Potential energy curves of the electronic ground state of a diatomic molecule AB and that of the $AB^{\bullet-}$ radical anion. Potential energy curves are shifted to lower energies when going from the gas phase (solid lines) to the condensed phase (dotted lines) due to polarization of the surrounding medium. Compared to dissociation in the neutral state, the dissociation limit of the molecule AB in DEA is lowered by the electron affinity of B (E_{EA}) which can enable dissociation of the molecule at near-zero electron energies.

2.3 Effects in the Condensed Phase

In the condensed phase, molecules and in particular ions are stabilized by polarization of the surrounding medium which can modify electron-molecule interactions regarding their energetic thresholds, cross sections, and fragmentation behaviour.[46,50,62,69]

Considering first the resonant electron-molecule interactions, the potential energy surface of the TNI is shifted to lower energies, typically by about 1 eV, which may also be reflected in the position of the resonance depending on the experimental method that is used.[46] In addition, stabilization of the TNI in the condensed phase leads to a shift of R_c to a smaller distance between the two nuclei (Figure 9) which decreases the chance of autodetachment and, consequently, enhances the DEA cross section.[49,62,63] In the extreme case, shape resonances can become Feshbach resonances in the condensed phase because the anion is stabilized by the surrounding matrix making it more stable than the corresponding neutral state.[62] DEA is thus considered to be particularly important in the condensed phase. These promoting factors, on the other hand, might be counteracted by different quenching processes which affect the lifetime and stability of the TNI. In the gas phase, associative attachment yielding an intact radical anion rarely ever occurs because the TNI can only get rid of the excess energy by radiative cooling which is much less efficient than autodetachment.[46] In the

condensed phase, however, associative attachment might become feasible as the excess energy of the TNI can be accommodated by the surrounding medium.[46,63] In close proximity to metal surfaces, electron-transfer from the TNI to the metal surface can also decrease the cross section for DEA.[63] In order to minimize this effect, experiments are typically performed with sufficiently high film thicknesses, or by using a noble gas spacer.[46]

In contrast, the effect of condensation on non-resonant electron-molecule interactions is less well studied than for DEA. It is generally assumed, however, that ionization thresholds shift to lower energies upon condensation.[25,31,51,70] This assumption is, in fact, backed up by the ultraviolet photoelectron spectra of a number of molecules which suggest a shift of the ionization threshold of about 1–2 eV to lower energies.[71] The threshold for ND may also be shifted to lower energies although to a lower amount compared to EI as neutrals are typically less stabilized in the condensed phase compared to ions.

In the gas phase, EI of a molecule at sufficiently high electron energies is typically followed by various bond ruptures as is reflected in the mass spectra of most molecucles.[72] In the condensed phase, however, the excess energy can be accommodated by the surrounding medium which might lower the degree of fragmentation or, in the extreme case, even suppress bond dissociation. Such a quenching process, for example, has been observed in cluster experiments with CH_3OH. Under single collision conditions, isolated CH_3OH molecules show considerable fragmentation at $E_0 = 70$ eV[72] whereas in CH_3OH clusters, proton transfer from $CH_3OH^{\bullet+}$ to an adjacent CH_3OH molecule prevails over fragmentation.[73] Similarly, fragmentation of $Fe(CO)_5$ clusters by DI has been studied which revealed significantly reduced cross sections for the formation of fragments compared to those of isolated $Fe(CO)_5$ molecules.[74]

3 Experimental Setup

All experiments were carried out in an ultrahigh–vacuum (UHV) chamber (Figure 10) with a base pressure of ≤ 10^{-10} mbar which was maintained by turbomolecular pumps. The pressure inside the vacuum chamber was constantly monitored by a hot-cathode ionization gauge.

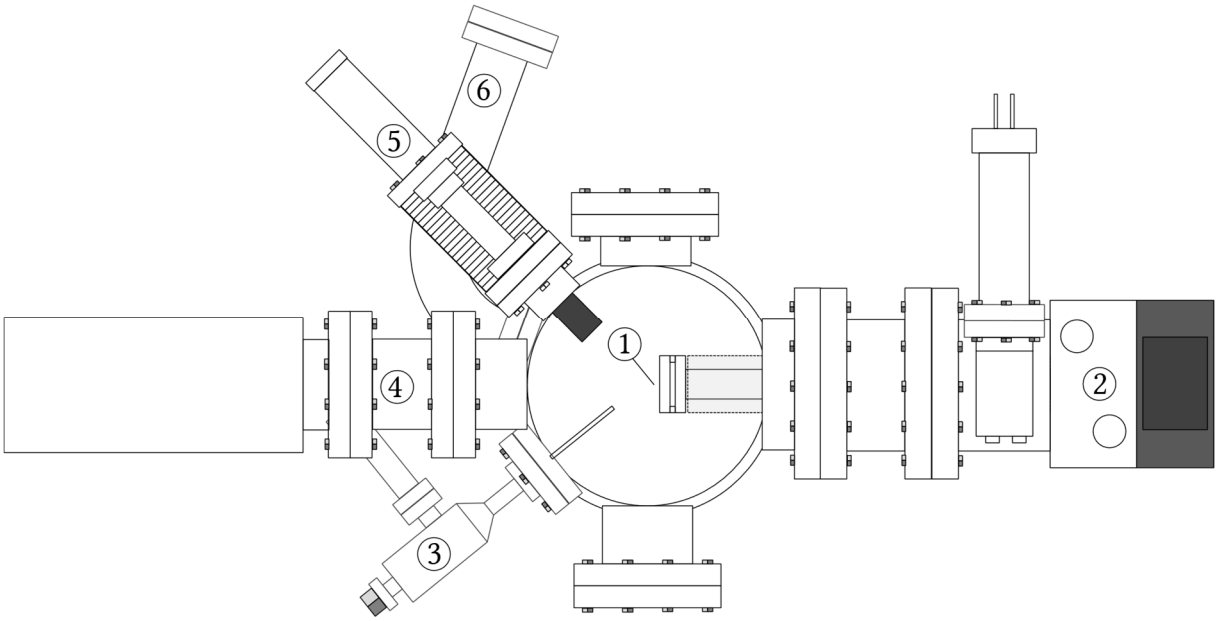

Figure 10. Schematic representation of the UHV chamber with (1) sample, (2) cryostat, (3) valve to the dosing line, (4) residual gas analyzer (RGA), (5) electron source, and (6) ion gauge.

The use of chemicals is limited to gases and to liquids or solids that have a sufficiently high vapor pressure. Gaseous compounds were typically purchased in a pressurized cylinder which could be mounted to the dosing line (Figure 11) via an adapter and an Ultra-Torr (Swagelok) vacuum fitting. In contrast, solid and liquid compounds were transferred into a round bottom flask which was then mounted to the vacuum fitting. In the case of liquid samples, several freeze-pump-thaw cycles with liquid N_2 were performed in order to remove any dissolved gases whereas solid samples were used without further purification. By opening the valve between the flask and the dosing line, the vapor of the head space was allowed to diffuse into the reservoir (blue part in Figure 11). From this reservoir, a small fraction of the gas or vapor was leaked into the upper part of the dosing line (red part in Figure 11) by use of a precision leak valve. There, it could be mixed with a second reactant. Mixing ratios of two reactants were controlled by a capacitance manometer (MKS Baratron) that monitored the change in absolute pressure inside this upper part of the dosing line after injection of the first and second reactant, respectively. Similarly, the amounts of gases or vapors leaked into the UHV chamber were controlled by monitoring the pressure drop inside the upper part of the dosing line with the capacitance manometer. Between two consecutive experiments, the upper part of the

dosing line was evacuated by a turbomolecular pump. The purities of the reactants stored in the reservoirs were frequently verified by mass spectrometry. Gases or vapors injected into the main vacuum chamber were allowed to condense on a polycrystalline Ta foil held at 30–35 K by a closed cycle helium cryostat.

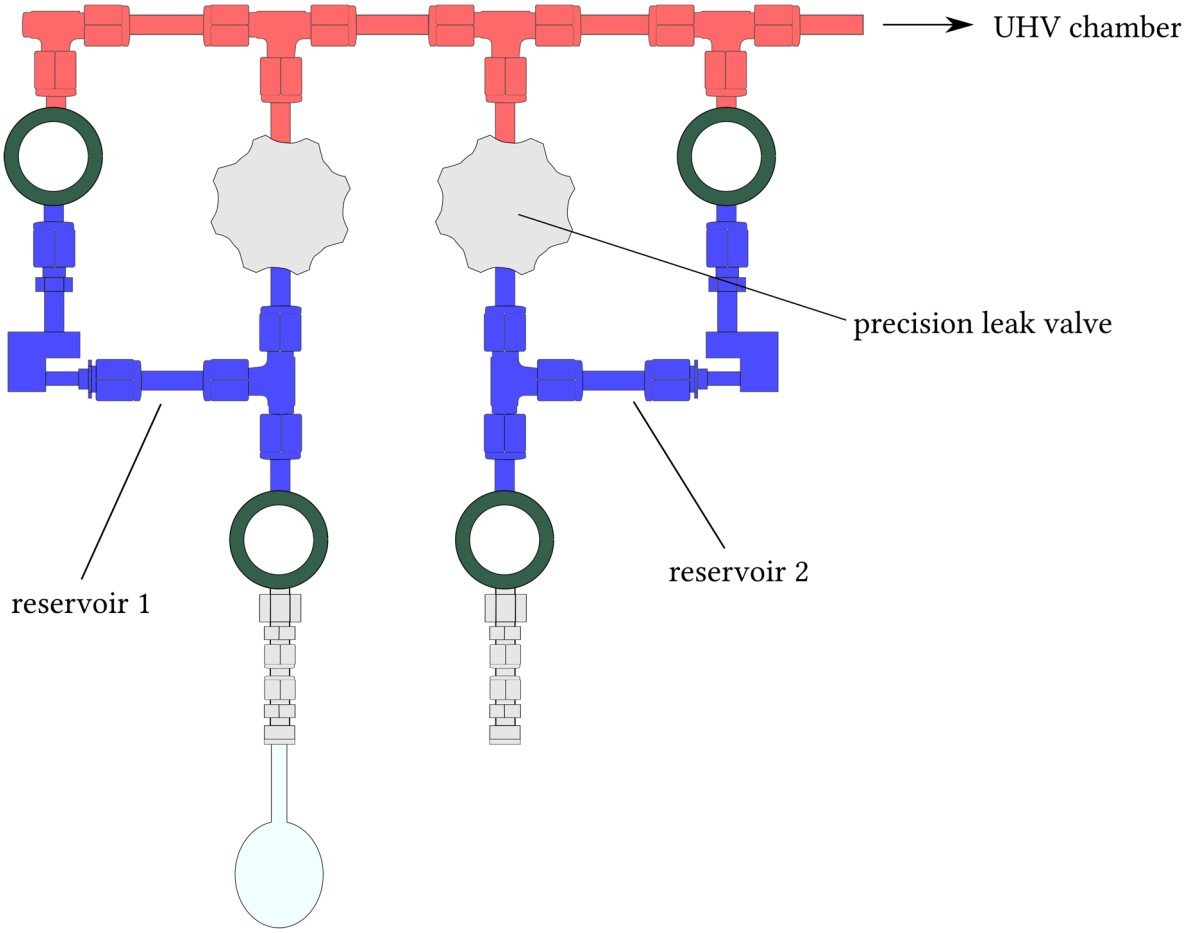

Figure 11. Schematic representation of the dosing line. Gases or vapors of the reactants are stored in either of the two reservoirs (depicted in blue). From either of the two reservoirs, defined amounts of a reactant can be dosed into the upper part of the dosing line (depicted in red) by a precision leak valve. The upper part of the dosing line (depicted in red) is used to mix the reactants before they are leaked into the UHV chamber.

The temperature of the Ta substrate can be monitored by a thermocouple type K which is spot-welded to the sample. Electron irradiation was performed with a commercial electron source (STAIB NEK-150-1) which is operated continuously to avoid contaminations. To suppress unintended irradiation during sample preparation and TDS, the electron beam was deflected by a negative sample bias of −25 V to prevent any electrons from reaching the sample. Upon electron irradiation, the electron beam was allowed to illuminate the entire sample evenly. The electron exposure was inferred by integrating the transmitted current as measured on the Ta foil by use of a picoamperemeter over time. After irradiation, samples

were annealed to 450 K by resistive heating with a rate of 1 K/s as was controlled by an Omega CN8200 controller using a Proportional-Integral-Derivative (PID) algorithm (Figure 12). Subsequently, the temperature was held at 450 K for 1–2 min in order to remove residual molecules from the surface. Cleanliness of the sample was frequently verified by performing TDS on the pure substrate. During electron irradiation and TDS, desorbing molecules were detected by a residual gas analyzer (RGA SRS 200). In a typical ESD or TDS experiment, not more than four mass-to-charge ratios were monitored simultaneously to maintain a good signal-to-noise ratio.

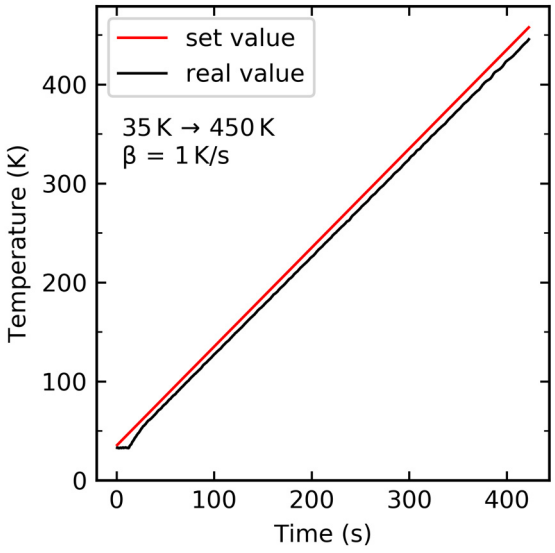

Figure 12. Temperature ramp (black curve) as was controlled by a PID-Controller and set temperature (red curve) during a typical TDS experiment from 35–450 K with a heating rate of 1 K/s.

4 Experimental Methods

4.1 Electron-Stimulated Desorption

ESD of adsorbate molecules or fragments thereof occurs when electrons of sufficiently high kinetic energy hit a sample surface. In principle, the impinging electron can transfer its energy to the adsorbate by elastic or inelastic scattering, the latter leading to excitation, ionization, or electron attachment. Considering the electron-adsorbate interaction as a central elastic collision, the maximum energy transfer ΔE is given by[75*]

$$\Delta E = \frac{4m_e m_A E_0}{(m_e + m_A)^2} \approx \frac{4m_e}{m_A} E_0 \quad (1)$$

where E_0 is the kinetic energy of the impinging electron, m_e is the electron mass, and m_A is the mass of the adsorbate. For E_0 = 20 eV, and H_2 as the adsorbed molecule, the kinetic energy transfer is about 0.018 eV which is still lower than typical adsorption energies of physisorbed species (0.07 eV for N_2 on Au; 0.5 eV for H_2O on Au).[76] Thus, for low-energy electrons, only conversion of the electron kinetic energy into internal energy of the substrate-adsorbate complex can account for ESD.[75]

A conceptual framework for ESD is provided by the Menzel-Gomer-Redhead (MGR) model.[77–81] Briefly, the MGR model states that upon electron irradiation, the adsorbate undergoes a Franck-Condon transition to a repulsive state. During the subsequent relaxation process which forces the adsorbate to move away from the sample surface, desorption competes with recapture. Note that the description of the MGR model is kept very general, i.e., the specific nature of the repulsive state and the relevant quenching mechanisms are not specified. It has thus been modified several times to describe more specific situations.[80,82,83]

In a very simple scenario, a molecule adsorbed onto a surface undergoes electronic excitation into a repulsive state with respect to the molecule-surface bond (Figure 13). In order to desorb, the molecule must reach a critical distance from the surface (R_c in Figure 13) beyond which the kinetic energy of the molecule is sufficiently high to overcome the recapture barrier (E_{rec}) even if the excited state is quenched.[80,81] If the excited state is quenched before the molecule has reached the critical distance, on the other hand, it gets recaptured by the surface, that is, it stays adsorbed.[80,81] Consequently, the desorption rate depends critically on quenching of the excited state by energy transfer, or, in the case of desorbing ions, charge transfer with the

[*] In Ref. 75, eq 1 states that $\Delta E/E_0 = (2m_e m_A)(1-\cos\theta)/(m_e+m_A)^2$ where θ is the scattering angle. For $\theta = 180°$, the term on the right-hand side of the equation becomes maximum yielding $\Delta E/E_0 = 4m_e m_A/(m_e+m_A)^2$.

substrate.[79] Typically, the desorption rates of neutrals are higher than those of ions by several orders of magnitudes[84] which is mainly due to the following reasons: First, ions are stabilized by a higher amount of energy than neutrals due to polarization of the surrounding medium and by interaction of the ion with its image charge induced in metallic substrates. Secondly, ions are prone to neutralization as electrons can tunnel between the metal surface and the ion and vice versa.[85]

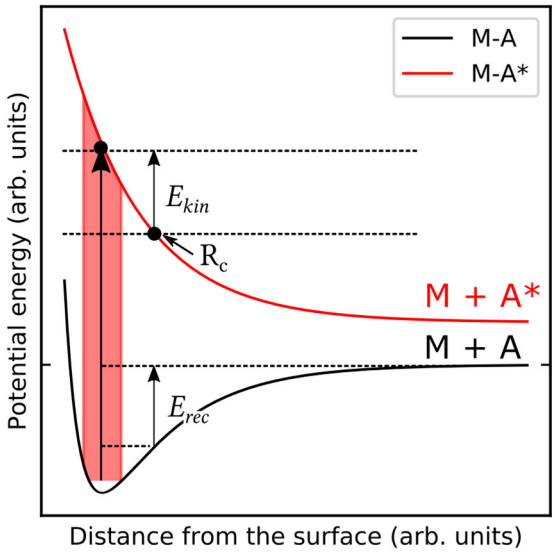

Figure 13. Potential energy curve of a substrate-adsorbate complex. Upon ESD, the complex undergoes electronic transition into an antibonding state which decays by moving away from the surface. Beyond the critical distance R_c, desorption proceeds irreversibly as the kinetic energy (E_{kin}) of the desorbing particle is higher than the barrier (E_{rec}) required to overcome the adsorption potential.

Electron irradiation, however, does not only lead to desorption of intact molecules but also to desorption of neutral and ionic fragments produced by ND, DI, or DEA.[23,86–88] In contrast to the example above, relaxation of the excited adsorbate progresses by increasing the internuclear distance within a molecule. Similar to the MGR model, the molecule can undergo quenching throughout this progression which may prevent dissociation of the molecule or desorption of fragments.[85] If a fragment has acquired enough kinetic energy during dissociation, however, it may overcome the desorption barrier and escape into vacuum.

Desorption of neutral and, in particular, ionic fragments is frequently studied to unravel the primary electron-molecule interactions that occur upon electron irradiation.[23,86,89,90] In such ESD experiments, the energy of the impinging electrons is increased within a defined range while desorbing cations, anions, or neutrals are monitored by a mass spectrometer. The signal as a function of electron energy then reflects the cross section of the respective electron-

molecule interaction. Experiments with isotopically labeled reactants further allow to study site selective bond cleavages.[91] However, ESD experiments can also be used to obtain information on chemical kinetics if the temporal evolution of a mass spectrometric signal is studied.[92] For example, when CO is used as a reactant, its signal intensity in the ESD shows a sharp onset once the sample is irradiated followed by an exponential decay of the ESD signal which is characteristic of a first order reaction kinetic (Figure 14, left panel). When CO is produced during irradiation of CH_3OH, however, desorption is limited by its formation rate and thus shows a delayed increase which, in this case, follows a (pseudo) first order kinetic (Figure 14, right panel).

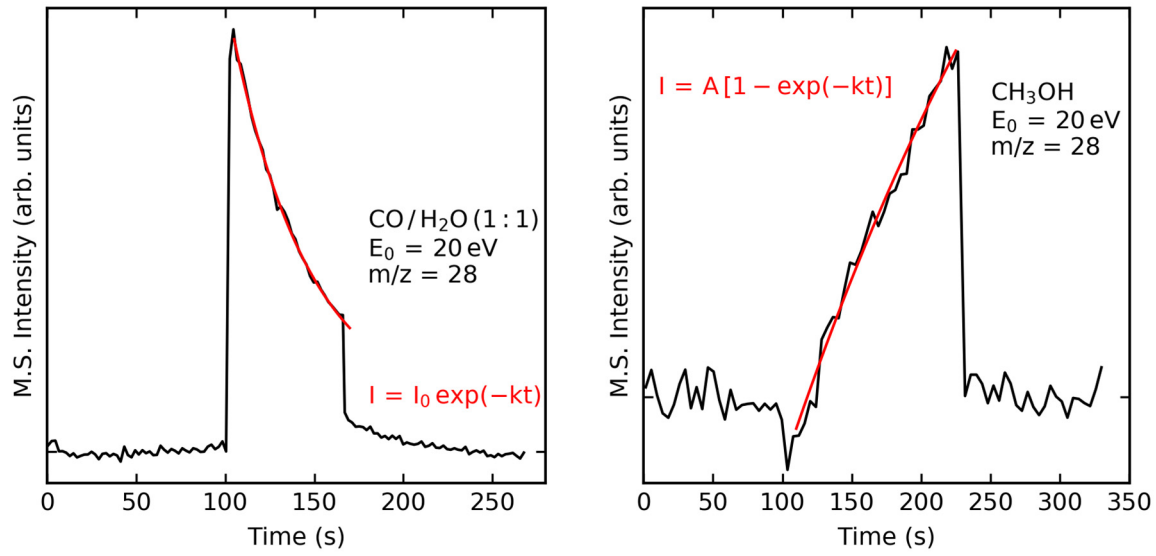

Figure 14. Temporal evolution of the ESD signal of CO upon irradiation of CO/H_2O (1:1) mixtures (left panel) and CH_3OH (right panel) at E_0 = 20 eV. In the left panel, CO is a reactant; its ESD intensity thus follows an exponential decay. In the right panel, desorption of CO during electron irradiation of CH_3OH is limited by its formation as indicated by the delayed increase of intensity; The temporal evolution can be described by the denoted function which corresponds to a first-order reaction kinetic.

4.2 Thermal Desorption Spectrometry

Thermal desorption spectrometry (TDS) is a surface science technique that is typically used to determine surface coverages of adsorbates, and their adsorption enthalpies.[93] It can also be used to probe chemical changes that occur on the substrate surface which makes this technique suitable for studying electron-induced reactions.[46,49,94,95] Typically, TDS is used in combination with mass spectrometry as this can detect molecules even at very low partial pressures, and because molecules can be identified by their characteristic fragmentation pattern.

Mathematically, thermal desorption is described by the Polanyi Wigner equation[93,96] which can be derived by combination of eq 2 which is the chemical rate equation for desorption and the Arrhenius equation which yields eq 3

$$-\frac{\mathrm{d}\theta}{\mathrm{d}t} = \theta^n k \tag{2}$$

$$-\frac{\mathrm{d}\theta}{\mathrm{d}t} = \theta^n \nu \exp\left(-\frac{E_{\mathrm{des}}}{RT}\right) \tag{3}$$

where k is the rate constant, θ is the surface coverage, n is the desorption order, ν is the frequency factor, and E_{des} is the desorption energy. During TDS, the temperature of the substrate is typically increased linearly which leads to the following form of the Polanyi Wigner equation

$$-\frac{\mathrm{d}\theta}{\mathrm{d}T} = \frac{\theta^n}{\beta} \nu \exp\left(-\frac{E_{\mathrm{des}}}{RT}\right) \tag{4}$$

where β is the heating rate. In the simplest scenario, the desorption energy, frequency factor, and desorption order are fixed parameters, i.e., they are independent of coverage. Kinetic parameters can be then be obtained from experimental data by a number of methods like Redhead analysis and Leading edge analysis.[97,98]

In general, however, desorption energy and the frequency factor are functions of the surface coverage which requires a more sophisticated approach. For coverages in the monolayer regime, it is often observed that the maximum of the desorption signal shifts to lower temperatures with increasing coverage.[24,99–103] In Figure 15, this is illustrated for the case of C_2H_4 where the monolayer desorption peak shifts from 90 K at low coverage to 70 K at saturation. Traditionally, this coverage dependence of the desorption temperature can be explained by the multistate model which assumes a set of different binding sites.[93,96] When the adsorbed molecules are sufficiently mobile, the different binding sites are sequentially occupied from higher to lower adsorption energy. The overall signal can then be regarded as a convolution of individual desorption signals, each representative of desorption from a specific binding site.[100–102] As molecules adsorbed on less favorable binding sites desorb first upon heating, the maximum of the overall desorption signal shifts to lower temperatures with increasing coverage while the trailing edges of the different desorption signals overlap. However, it is now widely accepted that lateral interactions among adsorbed molecules also affect the adsorption energy.[93,96,97,103] Consequently, the shift of the desorption maximum to lower temperatures can also be interpreted as repulsive forces among the adsorbed molecules leading to lowering of the desorption energy with increasing coverage.

For multilayer coverages, desorption rates become independent of coverage because desorption occurs only from the topmost layer of the sample. In the TDS, this is reflected by a shared leading edge corresponding to a desorption order of zero (see multilayer peak of C_2H_4 in Figure 15).[96,99,101]

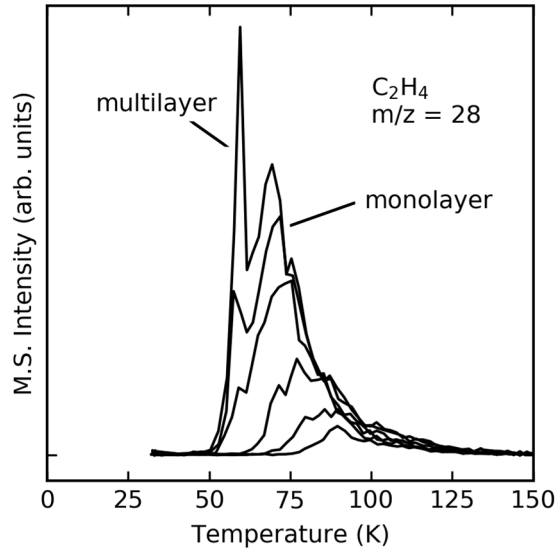

Figure 15. Thermal desorption spectra for increasing amounts of C_2H_4. The monolayer desorption peak shifts from 90 K at low coverages to 70 K at higher coverages. When the monolayer approaches saturation, a second peak emerges at 59 K which is assigned to multilayer desorption. Note that the leading edges of the multilayer peaks coincide.

TDS of volatile compounds which are embedded in a less volatile matrix (Figure 16, panel A) are often much more complex than TDS of the pure ices as additional signals can occur due to volcano- and co-desorption. Volcano desorption occurs when volatile compounds, typical small gas molecules like CO, N_2, or CH_4, are trapped in the pores of an amorphous deposit (Figure 16, panel B). Upon heating the film, the amorphous deposit tends to crystallize which produces small cracks (Figure 16, panel C). These cracks, in turn, enable the trapped volatiles to diffuse to the surface and escape into vacuum. Finally, residues of the volatiles that have not desorbed by the molecular volcano process co-desorb along with the surrounding matrix (Figure 16, panel D).[104–106] These mixing effects have been extensively studied in H_2O ices due

to its high abundances in icy mantles. However, there are also a few studies that revealed analogous effects in CH_3OH,[107] ethanol,[108] and CO_2[109] matrices.

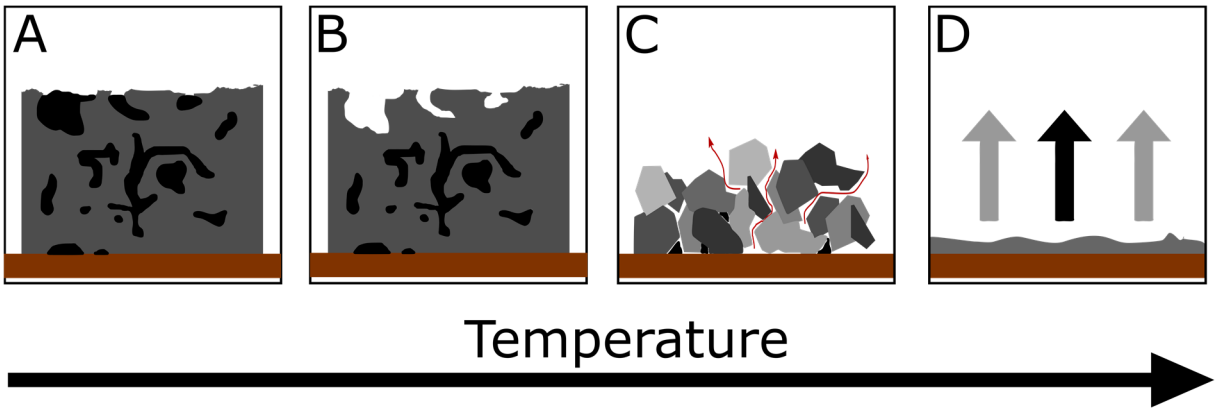

Figure 16. (A) Co-adsorption of two adsorbates. (B) Desorption of the more volatile compound. Molecules that are trapped in the porous network, stay embedded in the adsorbate. (C) Volcano-desorption: Crystallization of the matrix leads to the formation of cracks which form pathways from the pores to the surface of the sample. (D) Desorption of the matrix leads to co-desorption of last residues of the more volatile compounds.

Thermal desorption of more massive molecules in mixed ices is less well studied compared to that of volatile molecules. For a number of organic molecules co-adsorbed with H_2O, the desorption spectra also exhibit signals corresponding to volcano- and co-desorption.[110] However, if the guest molecule is much less volatile than the matrix, desorption of the guest molecule might be completely independent from desorption of the matrix as has been demonstrated for desorption of glycine[111] and formamide[112] from amorphous H_2O ice.

4.3 Quantification of Products

The mass spectrometric signal monitored during ESD and TDS is proportional to the desorption rate if the pumping speed is sufficiently high.[93] However, the individual compounds typically have different ionization efficiencies and fragmentation properties. Thus, mass spectrometric signals of two different compounds cannot be compared directly in a quantitative sense.

In principle, this problem can be addressed by either of two strategies: The first strategy is to prepare a number of reference mixtures containing increasing amounts of the anticipated product in the reactant matrix (Figure 17, left panel).[95] The data set constitutes a calibration curve (Figure 17, right panel) which allows to quantify the amount in the irradiated mixture by comparing the peak area in the irradiated sample with those of the reference mixtures. This approach, however, requires that the sticking coefficients of all components of the reference mixtures are known. In a similar approach, defined amounts of the anticipated

product are added to the irradiated samples. The amount that is initially present after irradiation can then be calculated by extrapolation (see Publication II). This approach is similar to the method of standard addition and has the advantage that matrix effects are already incorporated.

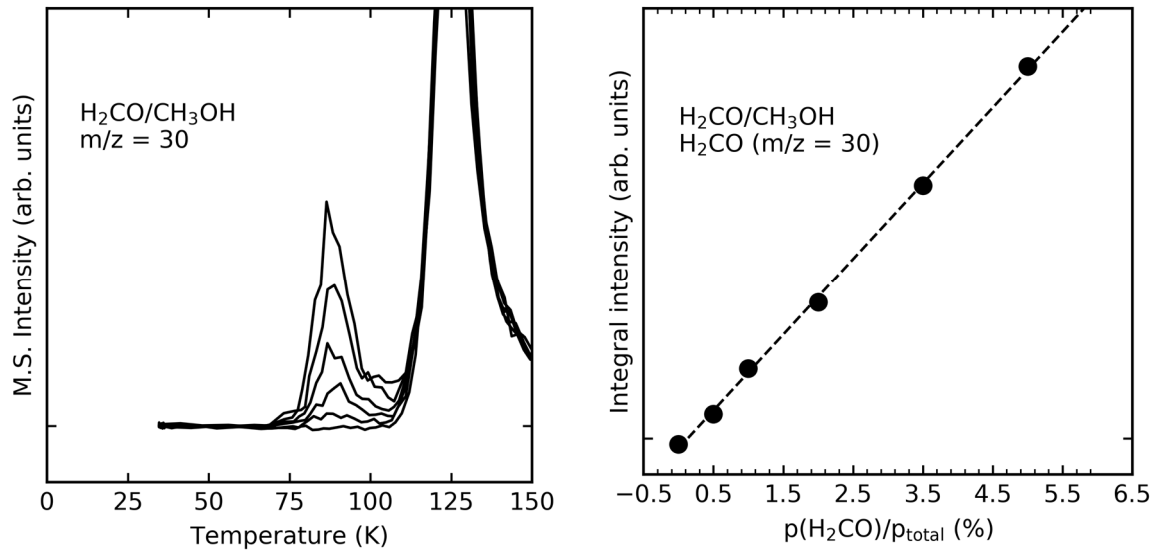

Figure 17. (Left panel) Thermal desorption spectra for increasing amounts of H_2CO in CH_3OH. H_2CO shows a desorption feature at 88 K. The desorption feature at 130 K is due to the m/z = 30 fragment of CH_3OH. (Right panel) Integral intensities of the H_2CO desorption signals with increasing amount of H_2CO in a H_2CO/CH_3OH mixture. The fraction of H_2CO was deduced from the pressure drops of H_2CO and CH_3OH in the dosing line.

The second strategy is to deduce the amounts by correcting the mass spectrometric signals for different ionization efficiencies and ion intensities. Although fragmentation patterns are accessible for a wide range of molecules in reference databases like NIST,[72] it is more accurate to deduce ion intensities with the same setup used throughout the ESD and TDS experiments. This is because the intensity pattern of the mass spectrum can differ from those in reference data due to different transmission and detection efficiencies of the mass spectrometer and due to a different geometry of the vacuum chamber. In contrast, it is much more difficult to obtain the ionization cross section for a particular molecule by experiment. For some selected molecules, experimental ionization cross sections have been published in reference databases.[113] For most molecules, however, ionization cross sections have not been reported and need to be calculated which is typically performed on the basis of the Binary-Encounter-Bethe (BEB) model.[114,115] The formation cross section of a specific ion following EI is usually termed as the partial ionization cross section. In contrast to the total ionization cross section, the partial ionization cross section describes the probability to end up with a particular ion.

Its value can be obtained by correcting the total ionization cross section for the fractional intensity of a specific ion which can be deduced from the respective mass spectrum by eq 5

$$\sigma_{\mathrm{p},i} = \frac{I_{\mathrm{rel},i}\sigma_{\mathrm{total}}}{\sum_{i=1}^{N} I_{\mathrm{rel},i}} \tag{5}$$

where $I_{\mathrm{rel},i}$ is the relative intensity of the ith fragment, N is the number of fragments, $\sigma_{\mathrm{p},i}$ is the partial ionization cross section for the ith fragment, and σ_{total} is the total ionization cross section. The yield a particular product P with respect to the initial abundance of the reactant R can then be calculated by scaling the integrated desorption signals ($\mathrm{area_P}$ and $\mathrm{area_R}$) with the respective cross sections according to eq 6:

$$yield = \frac{area_P}{area_R} \cdot \frac{\sigma_{p,R}}{\sigma_{p,P}} \tag{6}$$

Note that eq 6 can equally be applied to calculate relative yields between two arbitrary molecules or the mixing ratio of two reactants. The advantage of this strategy is that it does not require additional experiments. Furthermore, this strategy might be the only one that is feasible for compounds that are difficult to handle or commercially not available.

5 Classification of Electron-Induced Reactions

Electron-irradiation can trigger a number of different reactions depending on the electron energy. In a first step, electron irradiation typically leads to depletion of the reactants which is accompanied by the formation of reactive species, i.e., radicals and ions. EE and EI processes can be identified based on their characteristic threshold behavior. In contrast, DEA resonances show a more complex dependence on energy which is different for each individual compound. Thus, Figure 18 provides an overview over the known gas phase resonances of CH_3OH, H_2O, CO, and C_2H_4 which serves as reference for the discussion throughout the following sections.

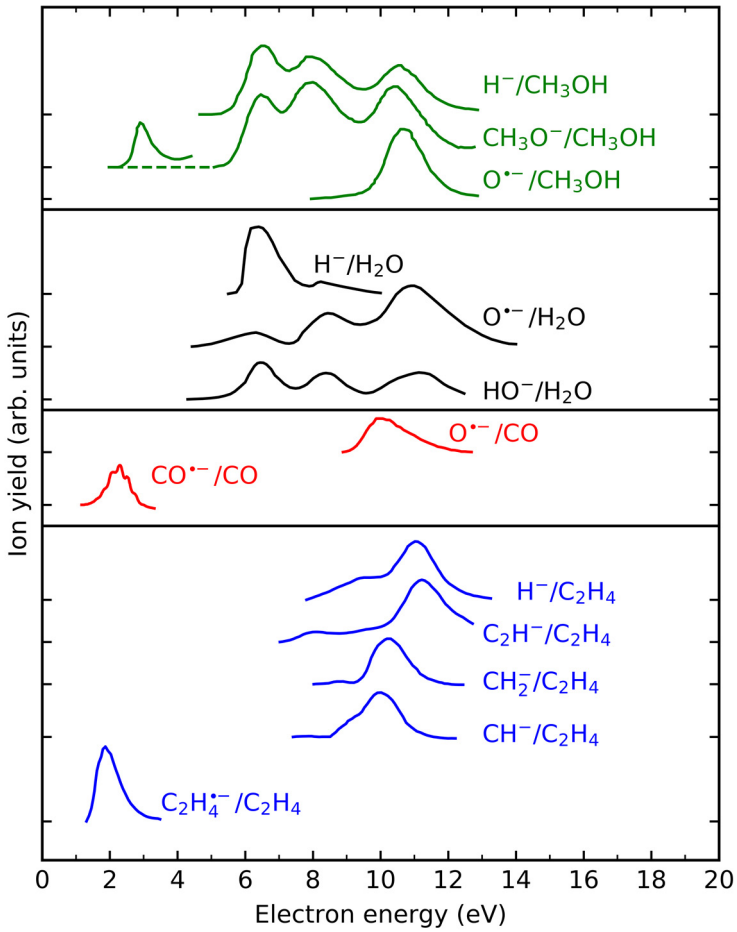

Figure 18. Overview over the known gas phase resonances of CH_3OH (green), H_2O (black), CO (red), and C_2H_4 (blue). Data are taken from Ibănescu et al.,[116] Itikawa and Mason,[67] Gope et al.,[65] Rempt (obtained from charge trapping experiments),[117] Thynne and MacNeil,[118] Trepka and Neuert,[119] and Walker (obtained by HREELS).[120] In the case of C_2H_4, only the most intense signals are displayed. See Ref. [121] for data on minor fragments. Note that the individual curves are scaled by an arbitrary factor in order to facilitate comparison. Tick marks on the y-axis indicate the vertical offset.

Following their formation, reactive species can undergo reactions with molecules in their environment eventually leading to electron-induced synthesis, i.e., the formation of larger

molecules from smaller building blocks. The mechanisms by which chemical transformation occur is not a random re-assembly of atomic and molecular fragments but often follows certain reaction principles. This allows one to classify chemical reactions according to their underlying mechanisms. However, differences among analogous reactions of the same reaction type can arise from thermodynamic or kinetic restrictions. The following sections aim to reconcile the results of the individual publications by discussing the fundamental reaction types underlying the specific reaction mechanisms triggered by formation of reactive species in the initial electron-molecule interaction.

5.1 Radical Recombination

Current astrochemical models assume that radical recombination is the dominant mechanism by which molecular synthesis occurs in interstellar ices.[20,21,29,30] However, neutral radicals which are produced in ices by the interaction of molecules with electrons or UV photons are typically surrounded by reactant molecules only. Radical–molecule reactions thus require no diffusion through the ice but are limited by activation barriers which might not be accessible at cryogenic temperatures. Diffusion, on the other hand, requires less energy allowing the radicals to travel until they encounter a second radical where a typically barrierless recombination reaction can occur. As will be shown in the following sections, this paradigm does not necessarily hold true because radicals released during dissociation of the parent molecule might have considerable excess energy which can be sufficiently high to overcome the activation barriers of radical-molecule reactions even at low electron energies. Furthermore, several theorical studies suggest that disproportionation of two radicals, that is, the transfer of a hydrogen atom from one radical to another, might dominate over recombination.[122–125] An example of such a disproportionation reaction would be the reaction between two $CH_3O^{\bullet}$ radicals yielding H_2CO and CH_3OH (Publication II). A similar case has been observed in matrix isolation experiments for the reaction between two $HCO^{\bullet}$ radicals which disproportionate to H_2CO and CO rather than recombine to glyoxal (HC(O)CH(O)).[122] Without doubt, however, radical recombination is an important reaction type in the processing of ices.

Among the ices studied in this thesis, radical recombination is particularly important in the case of CH_3OH containing ices. In CH_3OH, three different bonds can be cleaved yielding $CH_3O^{\bullet}$, $^{\bullet}CH_2OH$, $CH_3^{\bullet}$, $HO^{\bullet}$, and $H^{\bullet}$ radicals. The experiments of Publication II have identified the expected recombination products methoxymethanol (CH_3OCH_2OH), ethanol (C_2H_5OH), ethylene glycol (HOC_2H_4OH), and dimethyl ether (CH_3OCH_3). The very similar energy

dependences for these products (Figure 19) indicate that the different radicals are all produced by the same electron-molecule interactions. Assuming that radical recombination is in fact the dominant reaction, the relative yields would reflect branching ratios with which the different radicals recombine. Branching ratios for photodissociation of CH_3OH into $CH_3O^{\bullet}$, $^{\bullet}CH_2OH$, and $CH_3^{\bullet}$ radicals were previously deduced from the relative yields of ethanol, dimethyl ether, and ethylene glycol.[21] However, considering the recent theoretical predictions that disproportionation dominates over radical recombination,[122–125] it becomes impossible to deduce the branching ratios by which $CH_3O^{\bullet}$, $^{\bullet}CH_2OH$, and $CH_3^{\bullet}$ radicals are formed because, unlike for recombination products, the products of disproportionation are not linked to specific primary radicals. For example, it is not possible to distinguish between H_2CO that is formed by disproportionation between two $CH_3O^{\bullet}$ radicals, two $^{\bullet}CH_2OH$ radicals, or between a $CH_3O^{\bullet}$ and a $^{\bullet}CH_2OH$ radical.

Considering the identified recombination products as listed above, it is obvious that more compounds could be formed, such as dimethylperoxide (CH_3OOCH_3) and C_2H_6. These, however, were not detected (see Publication II). Dimethyl peroxide, which would result from recombination of two $CH_3O^{\bullet}$ radicals, could only be detected by the Kaiser group using a very sensitive photoionization reflectron time-of-flight mass spectrometer.[126] This suggests that dimethyl peroxide is produced in much smaller yields than other recombination products which prevents its detection in the present work. In fact, the competition of radical recombination with disproportionation could provide a reasonable explanation why certain recombination products are observed in high yields while others are not. The competitive disproportionation reaction between two $CH_3O^{\bullet}$ radicals yielding CH_3OH and H_2CO could thus be more efficient than recombination to yield dimethyl peroxide.

Similarly, there are no reports on the formation of C_2H_6 under irradiation of CH_3OH ice which is expected to form by coupling of two $CH_3^{\bullet}$ moieties. Öberg proposed that this is because of the higher abundances of $CH_3O^{\bullet}$ and $^{\bullet}CH_2OH$ radicals which favors reactions of $CH_3^{\bullet}$ with either $CH_3O^{\bullet}$ or $^{\bullet}CH_2OH$ over recombination of two $CH_3^{\bullet}$ radicals.[21] In addition, $CH_3^{\bullet}$ radicals have a higher mobility at 35 K than $CH_3O^{\bullet}$ and $^{\bullet}CH_2OH$[21,127] which might enable quick trapping of $CH_3^{\bullet}$ radicals before the majority of $CH_3O^{\bullet}$ and $^{\bullet}CH_2OH$ radicals are consumed by other reactions. Disproportionation between two $CH_3^{\bullet}$ radicals would yield methylene (CH_2) and CH_4 which, however, is an endothermic reaction[†] and should thus not be very

[†] Standard enthalpies of formation are 145.69 kJ/mol for $CH_3^{\bullet}$, 386.39 kJ/mol for CH_2, and −74.6 kJ/mol for CH_4.[181] This yields a reaction enthalpy of 20.41 kJ/mol (0.21 eV) for the disproportionation of two $CH_3^{\bullet}$ radicals yielding CH_2 and CH_4.

efficient. However, $CH_3^{\bullet}$ radicals could react with CH_3OH by hydrogen atom abstraction, which yields CH_4 as also observed in Publication II and either $CH_3O^{\bullet}$ or $^{\bullet}CH_2OH$. Thus, hydrogen atom abstraction which competes with radical recombination might be a crucial factor that prevents formation of C_2H_6.

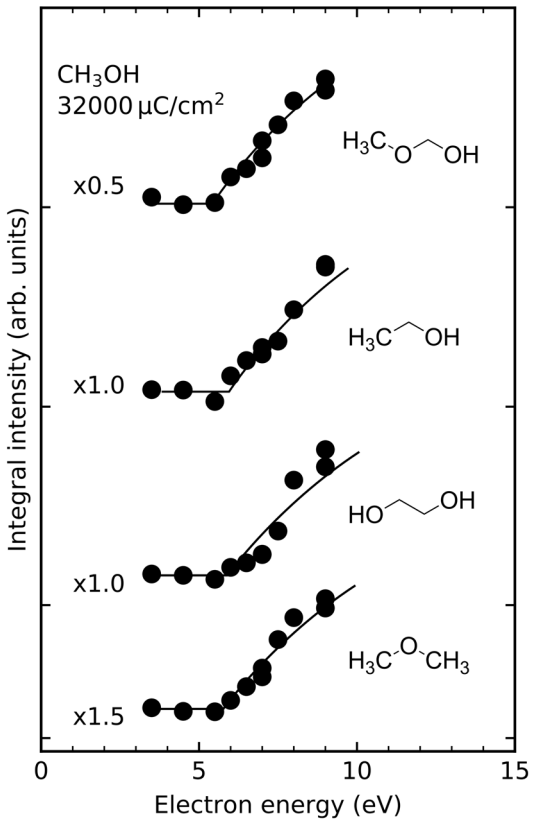

Figure 19. Dependence of integral intensities of methoxymethanol, ethanol, ethylene glycol, and dimethyl ether on electron energy obtained by TDS after irradiating pure CH_3OH with 32 000 µC/cm^2 in the range from 3.5–9 eV. Adapted with permission from Publication II. Copyright 2021 American Chemical Society.

Recombination of radicals is also observed in the mixed CO/CH_3OH (Publication IV) and C_2H_4/CH_3OH ices (Publication III) although the yields are typically lower compared to pure CH_3OH ice samples with the same film thickness as obvious from the examples of methoxymethanol and ethylene glycol (Figure 20). On one hand, this is because of the dilution of CH_3OH with a second reactant which lowers the overall amount of CH_3OH. On the other hand, radical recombination competes with concurrent reactions such as hydrogenation of CO and C_2H_4 (Sections 5.2–5.4), oxidation of CO (Section 5.5), and addition of a radical to CO or C_2H_4 (Section 5.6). Notably, hydrogenation of CO and C_2H_4 can progress via different mechanisms which are based on the transfer of a proton to a radical anion (Section 5.2),

addition of free hydrogen radicals (Section 5.3), or the transfer of a hydrogen atom from $CH_3O^{\bullet}$ to another molecule (Section 5.4).

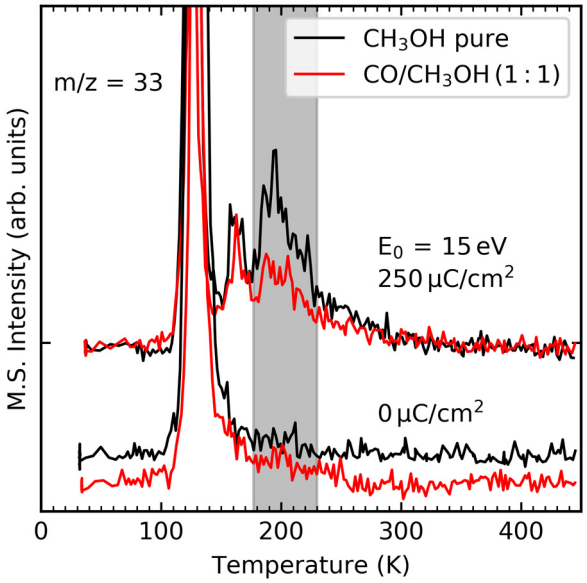

Figure 20. Thermal desorption spectra of pure CH_3OH (black lines) and a CO/CH_3OH (1:1) mixtures (red lines) after irradiation with 250 µC/cm^2 and without electron exposure (denoted as 0 µC/cm^2). The signals at 160 K and 195 K in the $m/z = 33$ curves are assigned to methoxymethanol and ethylene glycol (shaded in grey), respectively. The desorption signal at ~130 K is due to the $^{13}CH_3OH$ isotopologue. The TDS data show that signal intensities of the products decrease upon mixing CH_3OH with CO. Reproduced from Publication IV with permission from the PCCP Owner Societies.

5.2 Transfer-Hydrogenation of CO and C_2H_4 After Electron Attachment

Transfer hydrogenation is an important reaction class in organic chemistry which subsumes all hydrogenation reactions where the reducing agent is not gaseous H_2.[128] Many of those reactions rely on the proton transfer between a radical anion and a proton donor, often an alcohol. A prominent example of such reactions is the Birch reduction[129,130] which can be used to reduce aromatic compounds. The classical reaction employs solvated electrons as reducing agents which are provided by dissolving either Na or Li in liquid NH_3. Subsequently, these electrons add to an arene yielding a radical anion. In a final reaction step, the radical anion is protonated by an alcohol, leading to hydrogenation. Depending on the reaction conditions, the molecule can undergo this reaction sequence multiple times leading to further hydrogenation. Several variations of Birch reduction have been developed including electrochemical[131] and photochemical[132] all of which, however, rely on the initial formation of a radical anion.

Similar to the mechanism of Birch reduction, EA to CO at E_0 = 4 eV (Figure 21) yields an intact $CO^{\bullet-}$ radical anion which can undergo proton transfer with H_2O yielding $HCO^{\bullet}$ and HO^-. Subsequently, $HCO^{\bullet}$ can react with a nearby H_2O molecule yielding H_2CO and $HO^{\bullet}$ (Publication I). Recall that the resonance at 4 eV can only be due to EA to CO as DEA to H_2O occurs at considerably higher energies (Figure 18). Notably, an analogous reaction was also observed after EA to C_2H_4 yielding $C_2H_4^{\bullet-}$ which undergoes proton transfer with H_2O to yield $C_2H_5^{\bullet}$ and HO^- (see Scheme 2).[51] Such a reaction, however, was not observed in C_2H_4/NH_3 mixtures[53] suggesting that a sufficiently high acidity of the proton donor is essential for the reaction to occur.

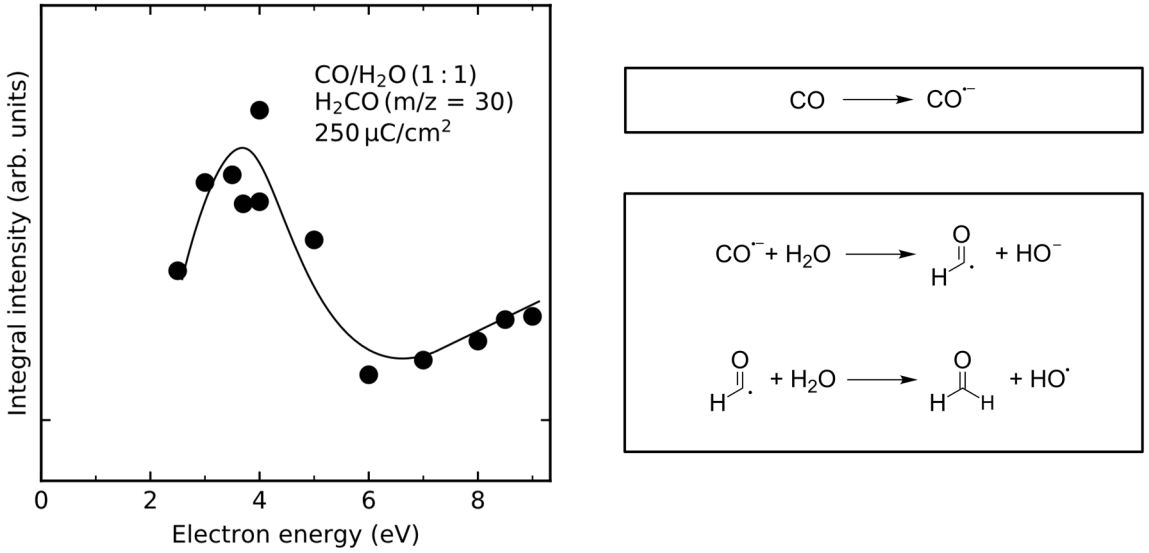

Figure 21. Energy dependence for the formation of H_2CO obtained by TDS after electron irradiation of CO/H_2O (1:1) mixtures with 250 µC/cm^2. The resonance at 4 eV was assigned to EA to CO yielding $CO^{\bullet-}$. Data were taken from Publication I.

This type of reaction has also neither been observed in C_2H_4/CH_3OH nor CO/CH_3OH mixtures. It is not immediately obvious why this protonation step does not occur in the presence of CH_3OH as the gas phase acidity of CH_3OH is in fact higher than that of H_2O.[133] One reason for this could be the effect of the molecular environment which, for example, leads to a reversed order of acidities of H_2O and CH_3OH in aqueous solution as HO^- is better stabilized than CH_3O^-.[134,135†] Thus, depending on the stability of the CH_3O^- anion in a CH_3OH matrix, the acidity of CH_3OH might be too low to enable proton transfer. Another key factor might be the effect of different molecular environments on the stability of the radical anion

† In an aqueous environment, the pK_a value of H_2O is 14.0 and that of CH_3OH is 15.6. Note that in many chemistry textbooks, a wrong value of 15.7 is given for pK_a of H_2O. For a comprehensive discussion on this issue see for example Ref. 182.

as has been reported for acetonylacetone.[136] Thus, H_2O might be able to sufficiently stabilize the $CO^{\bullet-}$ and $C_2H_4^{\bullet-}$ radical anions so that they have a sufficient lifetime to undergo subsequent chemistry whereas CH_3OH is not. Of course, these hypotheses need to be studied more closely before a definite explanation can be provided. However, the finding that H_2CO is formed via EA to CO in mixed CO/H_2O ice clearly demonstrates the relevance of transfer hydrogenation reactions for electron-induced chemistry of molecular ices.

5.3 Reduction of CO and C_2H_4 by Atomic Hydrogen

ESD and crossed beam experiments on DEA to H_2O and CH_3OH revealed the production of HO^-[137] and CH_3O^- (see Figure 18),[23,116,138] respectively, which must be accompanied by the release of hydrogen atoms. In addition, there is clear evidence that hydrogen atoms are produced by ND of H_2O.[88] Following these initial electron-molecule interactions, the released hydrogen atoms can react with unsaturated compounds such as CO or C_2H_4 enabling reaction pathways that are neither accessible in pure H_2O nor in CH_3OH. Hydrogenation of CO has been previously reported to occur during electron irradiation of CO/H_2O and CO/CH_3OH ices yielding H_2CO, CH_3OH, and intermediate radicals (reaction 1).[20,29,34,139,140]

$$CO \xrightarrow{H} HCO^{\bullet} \xrightarrow{H} H_2CO \xrightarrow{H} {}^{\bullet}CH_2OH/CH_3O^{\bullet} \xrightarrow{H} CH_3OH \qquad (1)$$

The hydrogenation of CO by H_2O and CH_3OH was investigated in this work by studying the energy dependent formation of H_2CO (Publications I and IV). In the case of CO/H_2O ice mixtures (Publication I), reaction 1 is mainly triggered by ND of H_2O into $H^{\bullet}$ and $HO^{\bullet}$. This is obvious from the onset of H_2O production which coincides with the electronic excitation threshold of H_2O which is about 7 eV in the gas phase.[67,141] Also, the lack of obvious resonances in the energy range from 6–13 eV (Figure 22) suggests that DEA of H_2O into HO^- and $H^{\bullet}$ (Figure 18) does not significantly contribute to the hydrogenation of CO. Note that the resonant formation of H_2CO at 4 eV is due to EA to CO and subsequent protonation of the intermediate $CO^{\bullet-}$ radical anion by H_2O (Section 5.2).

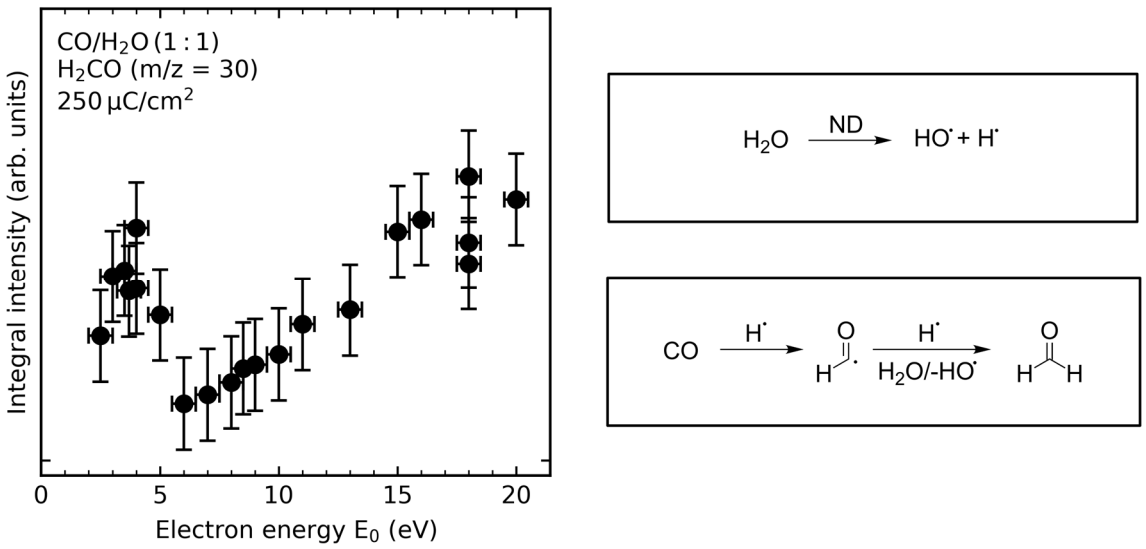

Figure 22. (Left panel) Dependence of H_2CO yield on electron energy after irradiation of a CO/H_2O (1:1) mixture with 250 µC/cm^2. Note that the data points below 10 eV are identical to those in Figure 21. (Right panel) Reactions leading to the formation of H_2CO by ND of H_2O. Adapted with permission from Publication I. Copyright 2019 American Chemical Society.

In CO/CH_3OH ice mixtures (Publication IV), it is more challenging to study reaction 1 as H_2CO is not only formed by hydrogenation of CO but also by fragmentation of CH_3OH (see also Publications II and IV). Previous studies differentiated between these two possibilities by using ^{13}C and ^{18}O labelled CH_3OH and CO.[20,29] However, isotopic labeling is not required in the present work. This is because the energy dependence of H_2CO formation in CO/CH_3OH mixtures differs from that in pure CH_3OH due to contributions of reaction 1 to the overall yield (Figure 23). The energy dependence of this additional formation channel shows an onset at ~7 eV, in good agreement with the electronic excitation energy of CH_3OH which is about 6.4 eV in the gas phase[142] and 6.7 eV in the condensed phase.[143] Furthermore, contribution of this channel to the overall H_2CO yield increases steadily with electron energy (red markers in Figure 23, left panel) indicative of a non-resonant process. This agrees well with the hypothesis that ND of CH_3OH yields hydrogen atoms which then reduce CO according to reaction 1. Notably, there is no further threshold at higher electron energies suggesting that EI does not contribute to hydrogenation of CO. This implies that EI of CH_3OH does not produce significant amounts of free hydrogen atoms.

A similar result was observed at lower electron energies. Here, the two DEA channels of CH_3OH at 5–6 eV yielding CH_3O^- and $H^\bullet$, and $CH_3O^\bullet$ and H^- (Figure 18) are responsible for product formation. In pure CH_3OH ice, a linear increase of the H_2CO yield is observed with electron energy (Figure 23, right panel). This linear increase is ascribed to an overlap of the

DEA channel yielding $CH_3O^{\bullet}$ and H^- (Figure 18)[23,144] with the onset of ND.[142,143] Subsequently, two $CH_3O^{\bullet}$ radicals can undergo disproportionation to yield H_2CO and CH_3OH. The DEA channel yielding CH_3O^- and $H^{\bullet}$ (Figure 18), on the other hand, does not contribute to H_2CO formation in pure CH_3OH. However, in the presence of CO, the released H atoms can react with CO (reaction 1) enabling formation of additional H_2CO. This additional reaction channel is reflected in the energy dependence of H_2CO where the linear increase of product yield is overlaid with the DEA resonance at ~6 eV (Figure 23, right panel).

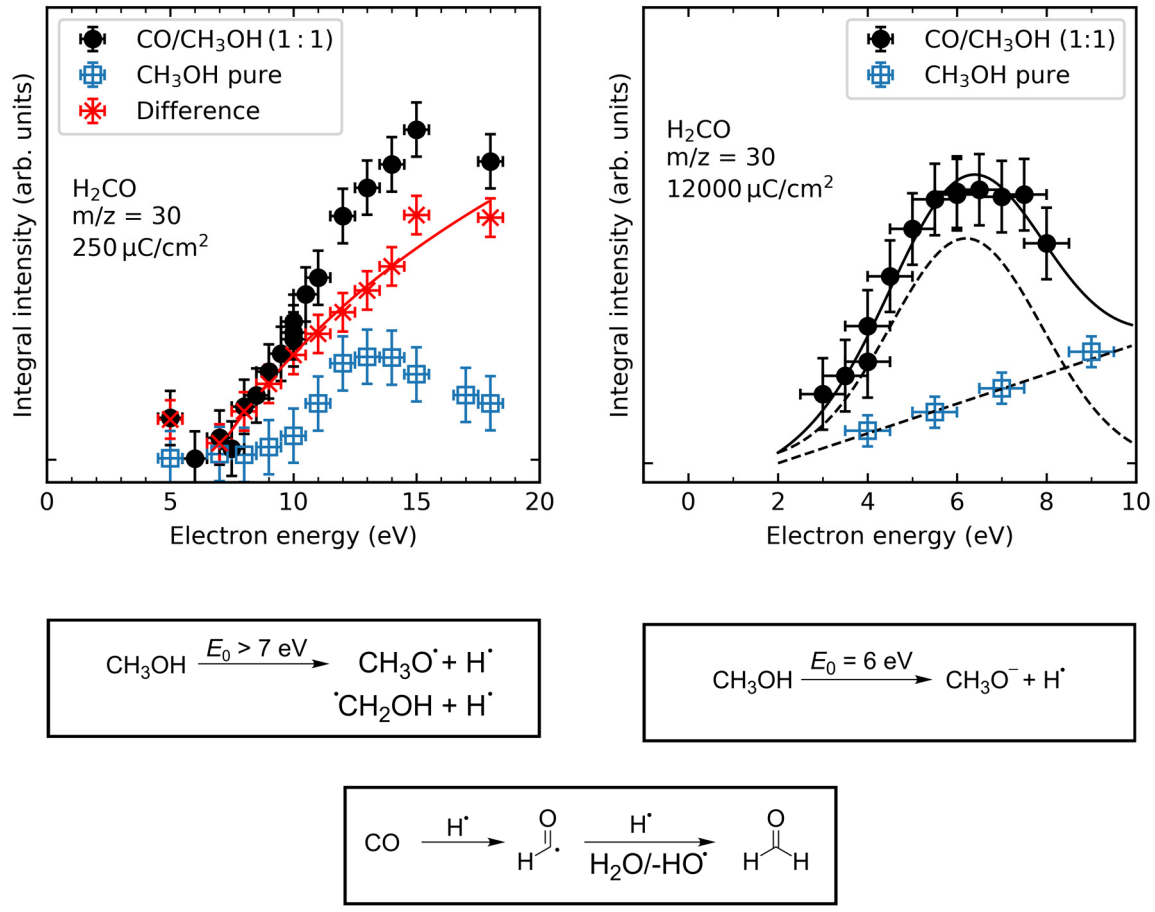

Figure 23. Dependence of H_2CO yield on electron energy after irradiation of pure CH_3OH (blue □), and CO/CH_3OH (1:1) (black ●) with 250 µC/cm² (left panel) and 12000 µC/cm² (right panel). The difference curve (red ×) in the left panel is reflective of an additional reaction channel that is not accessible in pure CH_3OH. The reaction schemes (bottom) denote the processes that lead to the enhanced production rate of H_2CO in the CO/CH_3OH mixture. Reproduced from Publication IV with permission from the PCCP Owner Societies.

In the CO/CH_3OH mixed ice, the DEA channel yielding CH_3O^- and $H^{\bullet}$ (Figure 18) does not only lead to the formation of H_2CO but also produces methoxymethanol (CH_3OCH_2OH) which is not observed after electron irradiation of pure CH_3OH at E_0 = 5.5 eV (Figure 24). This is because the DEA channel at 5.5 eV only yields $CH_3O^{\bullet}$ and H^- but no $^{\bullet}CH_2OH$ radicals[144] which prevents the recombination reaction needed for formation of methoxymethanol in pure

CH_3OH at this low electron energy. In CO/CH_3OH mixtures, however, $^{\bullet}CH_2OH$ radicals are formed by successive hydrogenation of CO (reaction 1) which enables the formation of methoxymethanol by recombination of $CH_3O^{\bullet}$ and $^{\bullet}CH_2OH$ radicals.

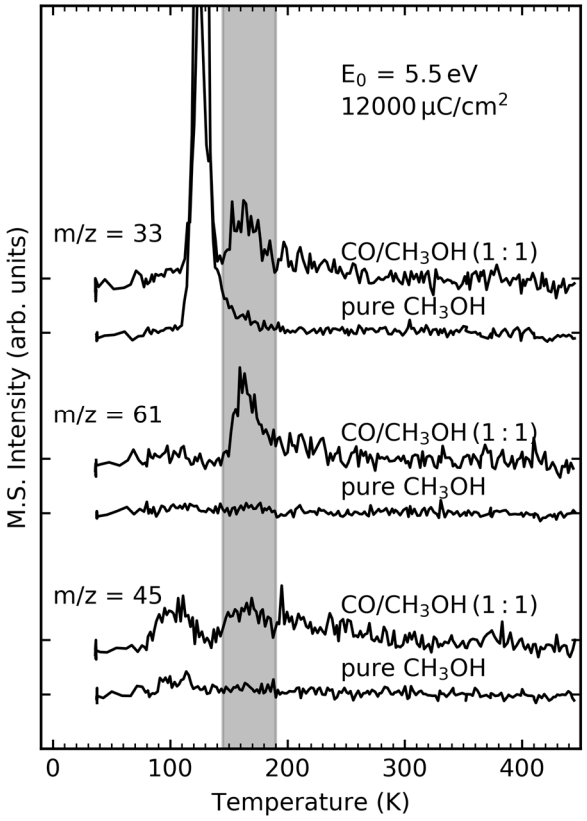

Figure 24. Identification of methoxymethanol by its desorption signal at 161 K (shaded in grey) in the *m/z* = 33, 45, and 61 curves of the TDS after irradiation of CO/CH_3OH (1:1) with 12000 µC/cm^2 at 5.5 eV. Notably, methoxymethanol is not observed in pure CH_3OH. Reproduced from Publication IV with permission from the PCCP Owner Societies.

The DEA resonance of CH_3OH at E_0 = 5.5 eV is also observed in the C_2H_4/CH_3OH ice mixtures where it causes hydrogenation of C_2H_4 yielding ethane (C_2H_6). (Figure 25, left panel, shaded in grey) (Publication III). Note that no significant amounts of C_2H_6 are formed after irradiation of pure CH_3OH (Section 5.1) or C_2H_4 at E_0 = 5.5 eV (Figure 25, left panel) suggesting that formation of C_2H_6 mainly occurs by a reaction between CH_3OH and C_2H_4. Two reaction mechanisms contribute to the formation of C_2H_6 which are based on the two competitive DEA channels of CH_3OH yielding CH_3O^- and $H^{\bullet}$, and $CH_3O^{\bullet}$ and H^- (Figure 18).[138,144] Following the first of these two DEA channels, the released hydrogen radicals can add to C_2H_4 producing an intermediate $C_2H_5^{\bullet}$ radical. Subsequently, the $C_2H_5^{\bullet}$ radical can abstract a hydrogen atom from a nearby CH_3OH molecule to yield C_2H_6 and $CH_3O^{\bullet}$. The proposed mechanism is supported by the concomitant appearance of butane (C_4H_{10}) (Figure 25, right panel) which is

formed when the intermediate $C_2H_5^{\bullet}$ radical reacts with a second C_2H_4 molecule to yield $C_4H_9^{\bullet}$ before it abstracts a hydrogen atom from a nearby CH_3OH molecule. The reactions of the $CH_3O^{\bullet}$ radical and the outcome of the second DEA channel are discussed in more detail in Section 5.4. Note that the relevance of reduction by atomic hydrogen has also been noted in the case of the electron-induced reactions of C_2H_4 with NH_3,[53] of cisplatin which is a complex carrying a NH_3 ligand,[145] and of η^3-allyl ruthenium tricarbonyl chloride in the presence of NH_3.[146]

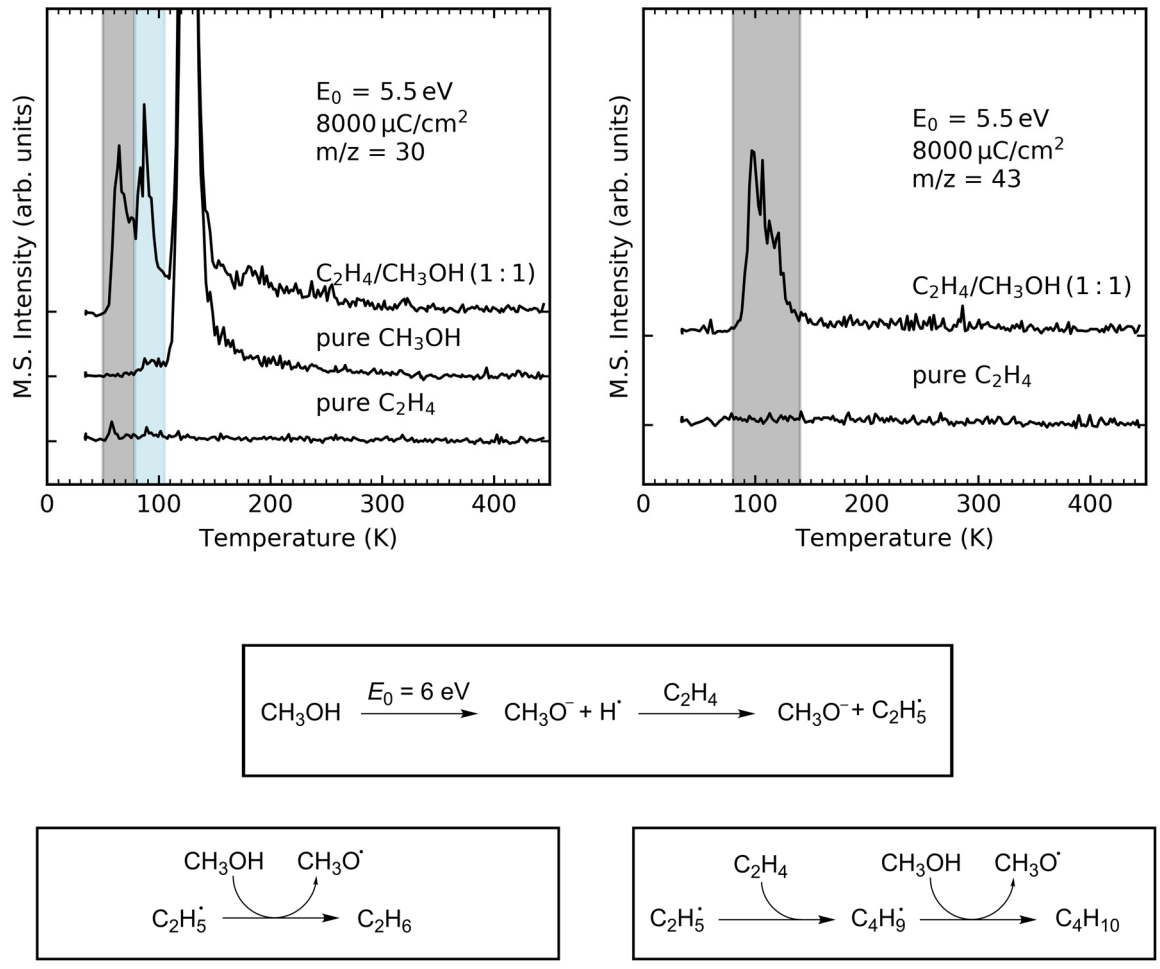

Figure 25. Thermal desorption spectra obtained after irradiation of a C_2H_4/CH_3OH (1:1) mixture and of pure C_2H_4 and pure CH_3OH at 5.5 eV with 8000 µC/cm^2. The desorption signal at 60 K in the m/z = 30 curve (grey, left panel) was assigned to ethane (C_2H_6) whereas the signal at 100 K in the m/z = 43 curve (right panel) was assigned to butane (C_4H_{10}). Notably, no significant amounts of ethane and butane are formed in pure C_2H_4 and CH_3OH. Furthermore, the intensity of the desorption signal of H_2CO (shaded in blue, left panel) in the irradiated C_2H_4/CH_3OH mixture is significantly higher than in pure CH_3OH. The reaction scheme (bottom) denotes the formation of ethane and butane following DEA to CH_3OH yielding CH_3O^- and $H^{\bullet}$. Data were taken from Publication III.

5.4 Hydrogenation of Unsaturated Compounds by Methoxy Radicals

Unsaturated compounds cannot only be reduced by free hydrogen radicals as discussed in Section 5.3, but also by $CH_3O^\bullet$ radicals which are produced by DEA to CH_3OH at E_0 = 5.5 eV along with H^- (Figure 18), ND yielding $CH_3O^\bullet$ and $H^\bullet$, and EI yielding a $CH_3OH^{\bullet+}$ radical cation which can then protonate a nearby CH_3OH molecule to yield $CH_3OH_2^+$ and $CH_3O^\bullet$. The $CH_3O^\bullet$ radical can transfer a hydrogen atom to C_2H_4 yielding H_2CO and $C_2H_5^\bullet$ (reaction 2). This is supported by the increase of the H_2CO yield by a factor of about 9 when CH_3OH is mixed with C_2H_4 (see blue shaded signal in left panel of Figure 25). Analogous to the reactions following addition of free hydrogen radicals to C_2H_4 (Section 5.3), the so formed $C_2H_5^\bullet$ radical can react with a CH_3OH molecule to yield C_2H_6 and $CH_3O^\bullet$ (reaction 3). In a concurrent process, the intermediate $C_2H_5^\bullet$ radical can add to a second C_2H_4 molecule before it reacts with CH_3OH to finally yield butane (reaction 4).

$$CH_3O^\bullet + C_2H_4 \rightarrow H_2CO + C_2H_5^\bullet \quad (2)$$

$$C_2H_5^\bullet + CH_3OH \rightarrow C_2H_6 + CH_3O^\bullet \quad (3)$$

$$C_2H_5^\bullet + C_2H_4 + CH_3OH \rightarrow C_4H_9^\bullet + CH_3OH \rightarrow C_4H_{10} + CH_3O^\bullet \quad (4)$$

Note that the $CH_3O^\bullet$ radical is recovered at the end of reactions 3 and 4 so that the net chemical equations simplify to:

$$CH_3OH + C_2H_4 \rightarrow H_2CO + C_2H_6 \quad (5)$$

$$CH_3OH + 2C_2H_4 \rightarrow H_2CO + C_4H_{10} \quad (6)$$

The overall contribution of hydrogen transfer from $CH_3O^\bullet$ radicals to the hydrogenation of C_2H_4 can be estimated by comparing the relative yields of H_2CO, C_2H_6, and C_4H_{10}. Considering the stoichiometry of reactions 5 and 6, the amount of H_2CO should be equal to the total amount of C_2H_6 and butane. Analysis of the molecular abundances reveals, that after irradiation at 5.5 eV with 8000 μC/cm^2 (Publication III), the yields of H_2CO, C_2H_6, and C_4H_{10} are 1.5%, 2.6%, and 1.3% with respect to the amount of CH_3OH in a nonirradiated sample. Consequently, the total amount of C_2H_6 and butane is 2.6 times higher than the amount of H_2CO. Thus, hydrogen transfer from $CH_3O^\bullet$ to C_2H_4 accounts for about 40% of the formed C_2H_6 and C_4H_{10}, whereas the addition of free $H^\bullet$ radicals to C_2H_4 (see Section 5.3) accounts for about 60% of these products. Reaction 2 has been studied in particular after DEA to CH_3OH at 5.5 eV (Publication III) but may also play a significant role for the reduction of C_2H_4 following $CH_3O^\bullet$ formation after ND or EI of CH_3OH. Recall that the amount of H_2CO after

irradiation of pure CH_3OH at E_0 = 5.5 eV is significantly lower than in the C_2H_4/CH_3OH mixture (Figure 25) suggesting that unimolecular dissociation of $CH_3O^\bullet$ into H_2CO and $H^\bullet$ (reaction 7) is not efficient at this low electron energy.

$$CH_3O^\bullet \nrightarrow H_2CO + H^\bullet \tag{7}$$

Notably, CO is not reduced by $CH_3O^\bullet$ radicals (reaction 8) (Publication IV).

$$CH_3O^\bullet + CO \nrightarrow H_2CO + HCO^\bullet \tag{8}$$

This has been inferred by comparing the energy dependence of H_2CO with that of methyl formate (CH_3OCHO). As the production of methyl formate relies on $CH_3O^\bullet$ radicals (see Section 5.6), it can be used as a proxy for $CH_3O^\bullet$ formation. Notably, the energy dependence of methyl formate shows a resonance at 10 eV (Figure 26). As discussed in Section 5.6, this resonance can be assigned to DEA to CO yielding C and $O^{\bullet-}$ (Figure 18). The latter of which undergoes an ion-molecule reaction with a nearby CH_3OH molecule yielding HO^- and $CH_3O^\bullet$.[147] In contrast to methyl formate, the energy dependence of H_2CO does not show a resonance at 10 eV (Figure 26) suggesting that hydrogen transfer from $CH_3O^\bullet$ to CO is not efficient.

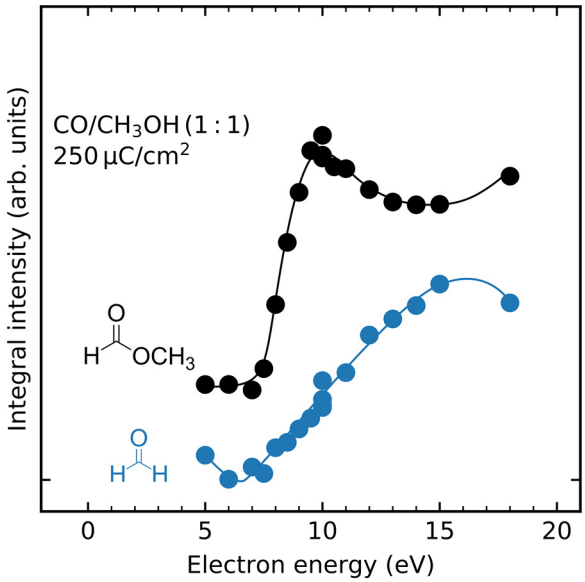

Figure 26. Comparison of the energy dependences of methyl formate (black ●) and H_2CO (blue ●) after irradiation of a CO/CH_3OH (1:1) mixture with 250 µC/cm^2. Data were taken from Publication IV.

The different reactivity of $CH_3O^\bullet$ with regard to hydrogen transfer to CO and C_2H_4 might be rationalized by considering the energy profiles of these reactions. To this end, quantum

chemical calculations were performed with the ORCA 4.0.1.2 software package.[148,149] All geometries were optimized at the DFT UB3LYP/aug-cc-pVTZ level of theory. The optimized geometries were characterized by their harmonic frequencies as minima (reactants or products) and saddle points (transition states). Improved single point energies were calculated for all minima and saddle points at the CCSD(T)/aug-cc-pVTZ level of theory. These were corrected by the zero-point vibrational energies (ZPEs) which were obtained during the DFT calculation. The calculated reaction energies and barriers for the decomposition of $CH_3O^\bullet$ into H_2CO and $H^\bullet$, and the hydrogen transfer from $CH_3O^\bullet$ to CO to yield H_2CO and $HCO^\bullet$ agree well with published data (Figure 27, panels A and B).[150,151] The values for the hydrogen transfer from $CH_3O^\bullet$ to C_2H_4, which have not been reported so far, should thus be reasonably accurate (Figure 27, panel C).

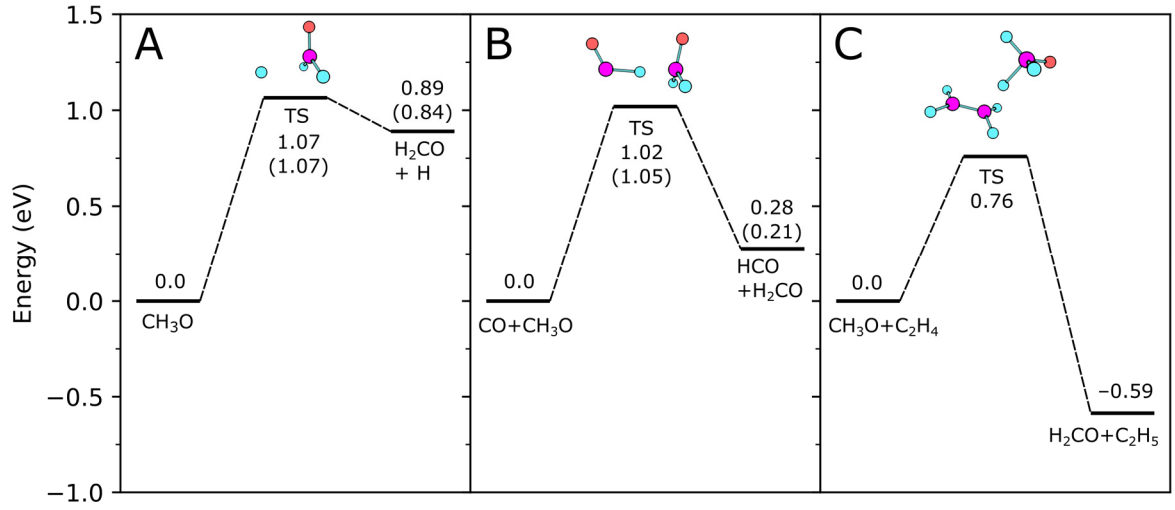

Figure 27. Zero-point energy corrected energy profiles for the (A) hydrogen loss from $CH_3O^\bullet$ yielding H_2CO and $H^\bullet$, (B) hydrogen transfer reaction from $CH_3O^\bullet$ to CO yielding H_2CO and $HCO^\bullet$, and (C) hydrogen transfer reaction from $CH_3O^\bullet$ to C_2H_4 yielding H_2CO and $C_2H_5^\bullet$. The calculations were performed on the CCSD(T)/aug-cc-pVTZ level of theory with ZPEs obtained at the B3LYP/aug-cc-pVTZ level of theory. Previous values are given in parentheses and were reported for (A) by Kamarchik et al.,[150] and (B) by Wang et al.[151]

The computations reveal that the unimolecular decomposition of $CH_3O^\bullet$ into H_2CO and $H^\bullet$ is endothermic by 0.89 eV and has a reaction barrier of 1.07 eV (Figure 27, panel A). The presence of CO, which acts as a hydrogen acceptor, significantly lowers the reaction energy although the reaction is still endothermic by 0.28 eV. The reaction barrier, however, is not significantly lowered compared to dissociation of $CH_3O^\bullet$ into H_2CO and $H^\bullet$ (Figure 27, panel B). In the case of $CH_3O^\bullet$ and C_2H_4, the reaction is exothermic by −0.59 eV, and the reaction barrier is lowered to a value of 0.76 eV (Figure 27, panel C). Thus, the trend seen in the

calculated reaction barriers agrees with the observation that only hydrogen transfer from $CH_3O^\bullet$ to C_2H_4 is experimentally observed. Note, however, that even in the case of reaction with C_2H_4 the $CH_3O^\bullet$ radical must have a sufficiently high excess energy to overcome the reaction barrier of 0.76 eV. A simple estimate based on the conservation of momentum and energy[144] reveals that the kinetic energy of the $CH_3O^\bullet$ radical would only be about 0.055 eV at E_0 = 5.5 eV if vibrational excitation is neglected.‡ Obviously, the kinetic energy of $CH_3O^\bullet$ is not sufficient to overcome the reaction barrier suggesting that a considerable amount of the released excess energy must be stored in the rovibrational modes of $CH_3O^\bullet$.

In addition to the classical over-the-barrier mechanism, tunneling might also play a role for hydrogen transfer. In fact, it is known that tunneling is the dominant mechanism by which hydrogen transfer reactions occur over a wide range of temperatures[152–159] as is indicated by exceptionally large kinetic isotope effects and non-linear Arrhenius plots. In contrast to the over-the-barrier mechanism, the barrier width is more important for tunneling than its height. Thus, detailed knowledge on the individual barrier width would be required for a theoretical understanding. However, as the barrier effectively narrows when one moves upwards from the bottom of the energy profile to the top of the barrier,[152,159] tunneling is particularly efficient when the reactants have energies below but close to the top of the reaction barrier. Thus, a tunneling mechanism would probably lead to the same trend in reactivity as the over-the-barrier mechanism. In order to verify the role of tunneling for the hydrogen transfer from $CH_3O^\bullet$ to C_2H_4 experimentally, one could repeat the same reaction with CD_3OH or CD_3OD. As tunneling reactions show unusually large kinetic isotope effects,[152,155,157,158] the efficiency of hydrogen transfer from $CD_3O^\bullet$ to C_2H_4 should be considerably lower than in the case of $CH_3O^\bullet$.

The study on the hydrogen transfer from $CH_3O^\bullet$ to C_2H_4 clearly demonstrates the relevance of this mechanism in molecular ices. However, as could be shown for the CO/CH_3OH mixture, this mechanism only operates if the reaction barrier for hydrogen transfer is sufficiently low and/or $CH_3O^\bullet$ has sufficient excess energy.

5.5 Oxidation of CO to CO_2

Upon electron irradiation of CO/H_2O and CO/CH_3OH ices, CO is readily oxidized to CO_2 (Publications I and IV). In previous studies, CO_2 formation has typically been attributed to

‡ The thermodynamic threshold for the formation of $CH_3O^\bullet$ and H^- is 3.75 eV.[144] Under the assumption that the excess energy is only released as kinetic energy of the fragments, the kinetic energy of the $CH_3O^\bullet$ fragment can be calculated by[137] $(1-31/32)\times(E_0-3.75\text{ eV})$ which yields 0.055 eV at E_0 = 5.5 eV.

either of two mechanisms: Formation and decay of an intermediate ROCO• radical (R = H, CH_3), or reaction of atomic O with CO.[28,34,139,160,161] Considering the first mechanism, reaction of HO• or CH_3O• with CO yields the intermediate HOCO• or CH_3OCO• radicals, respectively. These intermediates can either be stabilized which favors their subsequent conversion to formic acid (HCOOH) or methyl formate (CH_3OCHO), respectively, or they can decay into CO_2, and H• or CH_3•.

In the case of mixed CO/H_2O ices (Publication I), the results of the present thesis suggest that HOCO• is sufficiently stabilized by the H_2O matrix to enable its further reaction to formic acid (see Section 5.6). In contrast, decay of HOCO• does not play a significant role for the formation of CO_2. This has been inferred by comparing the energy dependences of CO_2 with those of H_2CO and formic acid (Figure 28). As H_2CO can only be formed via an intermediate HCO• radical, the resonant formation of formic acid at 10 eV must proceed by the HOCO• radical. Conversely, it can be excluded that a significant amount of CO_2 is formed by decay of HOCO• as the resonance at 10 eV is not reflected in the energy dependence of CO_2. It was thus proposed that CO_2 is mainly formed by the competitive ND channel of H_2O into H_2 and O(^{3}P/^{1}D) and subsequent reaction of the latter with CO.

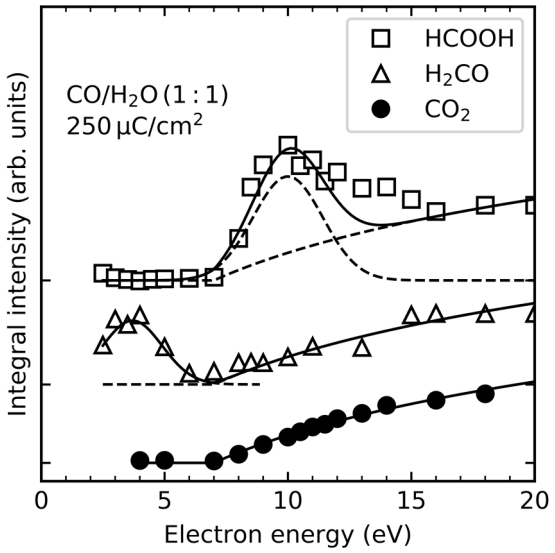

Figure 28. Integral intensities of the *m/z* = 45 signal of formic acid (HCOOH, □), the *m/z* = 30 signal of H_2CO (△), and of the *m/z* = 44 signal of CO_2 (●) after irradiation of a CO/H_2O (1:1) mixture with 250 µC/cm^2. Individual curves are scaled by an arbitrary factor to facilitate comparison. The solid and broken lines serve as a guide to the eye. Adapted with permission from Publication I. Copyright 2019 American Chemical Society.

In contrast, the CH_3OCO• radical which is formed upon irradiation of CO/CH_3OH (Publication IV) readily dissociates into CO_2 and CH_3• which has been inferred from the formation of

dimethyl ether (CH_3OCH_3) and methyl acetate ($CH_3C(O)OCH_3$) which are specific side products at E_0 = 5.5 eV formed by recombination of the $CH_3^\bullet$ radical with $CH_3O^\bullet$ and $CH_3OCO^\bullet$, respectively. Notably, dimethyl ether and methyl acetate are not formed upon irradiation of pure CH_3OH at E_0 = 5.5 eV so that direct production of $CH_3^\bullet$ radicals by dissociation of CH_3OH can be ruled out at this low energy (Publication II and IV). ND of CH_3OH into CH_4 and $O(^3P/^1D)$ may also contribute to CO_2 formation to some extent as has been suggested previously.[27,28] However, fundamental data on this decay channel have not been reported yet. This question needs to be addressed in future studies by measuring the dependence on electron energy for the formation of CO_2 in the CO/CH_3OH ice.

The different reactivities of $HOCO^\bullet$ and $CH_3OCO^\bullet$ with respect to dissociation might be explained by their electronic structures and the molecular environment in which these radicals are formed. $HOCO^\bullet$ exists in *cis*- and *trans*-conformations which can be interconverted by rotation around the C–O bond. Elongation of the O–H bond in the *cis*-isomer directly leads to the formation of CO_2 and $H^\bullet$. In contrast, formation of CO_2 from *trans*-$HOCO^\bullet$ progresses via an intermediate $HCOO^\bullet$ radical which, however, is rather unstable and quickly reacts further to CO_2 and $H^\bullet$ (Figure 29, top panel).[162–164] Theoretical studies suggest that decay of the $HOCO^\bullet$ radical is hindered by a reaction barrier which is about 1.47 eV for the *trans*-isomer and 1.07 eV for the *cis*-isomer (Figure 29, top panel).[164] However, the transition states are energetically only 0.37 and 0.04 eV above the asymptote of the reactants CO and $HO^\bullet$.

Similar to $HOCO^\bullet$, $CH_3OCO^\bullet$ has a *cis*- and *trans*-conformer. Decay of $CH_3OCO^\bullet$ into CO_2 and $CH_3^\bullet$ has a reaction barrier of 1.49 eV for the *trans*-isomer and only 0.63 eV for the *cis*-isomer (see Figure 29, lower panel).[161] For the *cis*-isomer, the exit barrier is below the asymptotic level of the reactants $CH_3O^\bullet$ and CO by −0.04 eV. Thus, the rate determining step is the entrance barrier which is about 0.25 eV in the gas phase (Figure 29, lower panel).

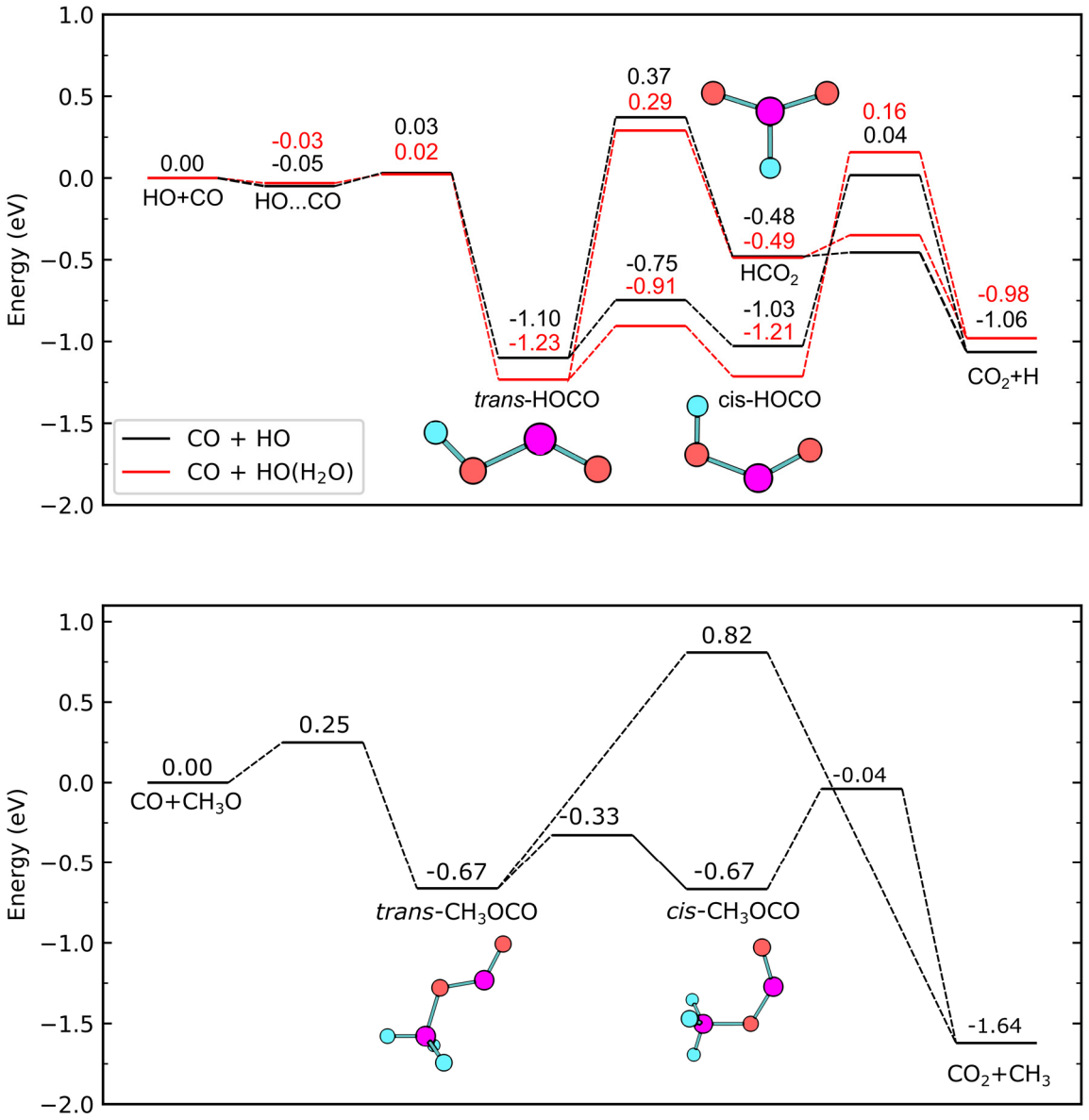

Figure 29. (Top panel) Energetic profile of the reaction of HO• with CO yielding an intermediate HOCO• radical which can further react to CO_2 and H•. Data are given for the hydrated (red) and non-hydrated (black) complex. Note that the hydrated complex is an aggregate of HOCO• and H_2O. Energetic data are taken from Zhang et al.[164] and have been calculated at the FCC/CBS level of theory with ZPE calculated on the M06-2X/ADVZ level of theory. (Bottom panel) Energetic profile of the reaction of CH_3O• with CO yielding an intermediate CH_3OCO• radical which can further react to CO_2 and CH_3•. Energetic data are taken from McCunn et al.[161] and have been calculated on the CCSD(T)/aug-cc-pV/(Q+d)Z level of theory with ZPE calculated at the CCSD(T)/6-311G(2df,p) level of theory.

In order to unravel the factors that prevent the HOCO• radical from dissociation, a more detailed analysis of the radical energies is required as HO• is not formed in its energetic ground state but has a certain amount of excess energy. This amount can be estimated by the electron energy E_0, the bond dissociation energy D_0 of the O–H bond in H_2O which is 5.1 eV,

and the relative masses of HO• and H_2O.[67,165§] At the experimentally observed threshold of E_0 = 7 eV for the formation of CO_2 (Figure 28)(Publication I), the HO• radical already has a minimum excess energy of 0.1 eV which is already sufficient to overcome the entrance barrier of 0.03 eV (Figure 29, top panel). Note that this calculation assumes that the impinging electron loses all of its kinetic energy. Thus, the calculated values represent an upper limit of the excess energy. If the HO• radical is formed in a vibrationally excited state, the energy of the HO• radical is even higher. For the first fundamental, the excess energy of HO• would be about 0.50 eV based on the threshold for vibrational excitation of HO• which is 0.42 eV.[166] This energy is already sufficient to overcome the dissociation barriers of *cis*- and *trans*-HOCO• to form CO_2 and H• which are 0.04 and 0.37 eV above the asymptotic level of HO• and CO, respectively (Figure 29, top panel). However, even if the excess energy of HO• is not sufficient to overcome the dissociation barriers in a classical way, HOCO• should be formed in a highly excited vibrational state close to the dissociation barrier unless considerable amounts of energy are dissipated by a third body. From such a state, hydrogen tunneling plays a significant role for the decay of HOCO• as could be shown by Johnson and Continetti who produced vibrationally excited HOCO• by photodetachment of $HOCO^-$.[167]

The reaction barrier for addition of CH_3O• to CO is about 0.25 eV and thus considerably lower than for the observed hydrogen transfer from CH_3O• to C_2H_4 discussed in Section 5.4. The excess energy of CH_3O• should thus be sufficient to react with CO to yield CH_3OCO•. Once the *trans*-CH_3OCO• radical is formed, its excess energy is sufficient to undergo isomerization to *cis*-CH_3OCO• and subsequent dissociation of the O–CH_3 bond. Thus, the fragmentation dynamics of CH_3OH following DEA at E_0 = 5.5 eV are in agreement with the proposed formation mechanism of CO_2 via the CH_3OCO• radical. In particular, energy dissipation by the matrix does not significantly affect the decomposition of the CH_3OCO• radical into CO_2 and CH_3•. In contrast, the energetic estimates described above for the reaction of CO with fragments of H_2O resulting from ND cannot explain why CO_2 is not formed via the HOCO• pathway. This suggests that the molecular environment plays a crucial role for the reactivity of HOCO•. Studies applying molecular mechanics suggest that in water ice, HOCO• loses all of its excess energy within a few picoseconds[168] which makes it impossible for HOCO• to overcome the barriers toward CO_2 and H• in a classical sense. Thus, only tunneling could contribute to the formation of CO_2 and H•. In N_2 and Ar matrices, however, no production of

§ The kinetic energy of the HO• fragment can be calculated to be E_{kin} = (1-17/18)×(E_0−5.1 eV−E_{vib}) where E_0 is the energy of the incident electron, and E_{vib} is the vibrational energy of the HO• fragment which is 0.42 eV[166] for the fundamental mode. The total excess energy can then be calculated by $E_{tot} = E_{kin} + n \times E_{vib}$ where n is zero for the vibrational ground state and unity for the first fundamental.

CO_2 was observed after vibrational excitation of the O–H stretching fundamental of *cis*-HOCO• at 3400 cm^{-1} (0.42 eV), and of *trans*-HOCO• at 3600 cm^{-1} (0.45 eV).[169] This suggests that the tunneling probability from the first vibrationally excited state is not significant, in agreement with the energy of this state which is considerably below the dissociation barrier (Figure 29, top panel).

In a H_2O matrix, the probability for decay of HOCO• might be even lower than in N_2 and Ar matrices as HOCO• can form strong hydrogen bonds to adjacent H_2O molecules yielding cyclic or linear complexes (Figure 30).[163,164,170] In fact, when HOCO• forms a complex with a H_2O molecule, it is even more stable than the reaction products CO_2 and H• by about 0.23 eV (Figure 29, top panel).[164] Thus, tunneling cannot occur from the ground vibrational state of HOCO•. Note that suppression of quantum tunneling due to the formation of hydrogen bonds between an organic molecule and H_2O has been previously reported for the isomerization of formic acid between its *cis*- and *trans*-form.[171] Thus, such a scenario provides a reasonable explanation why CO_2 is not formed by dissociation of HOCO•. Instead, CO_2 formation progresses by ND of H_2O into H_2 and O(^{1}D/^{3}P) and subsequent addition of the latter to CO. No calculations have been reported on the stabilization of CH_3OCO• by other CH_3OH radicals. However, the stabilization should be much smaller than in the case of HOCO• as CH_3OCO• can only act as a hydrogen bond acceptor due to substitution of the –OH group by a $–OCH_3$ group. Furthermore, CH_3OH can only form a single hydrogen bond to CH_3OCO•. Thus, decay of CH_3OCO• into CO_2 and CH_3• should be less affected by its molecular environment than HOCO•.

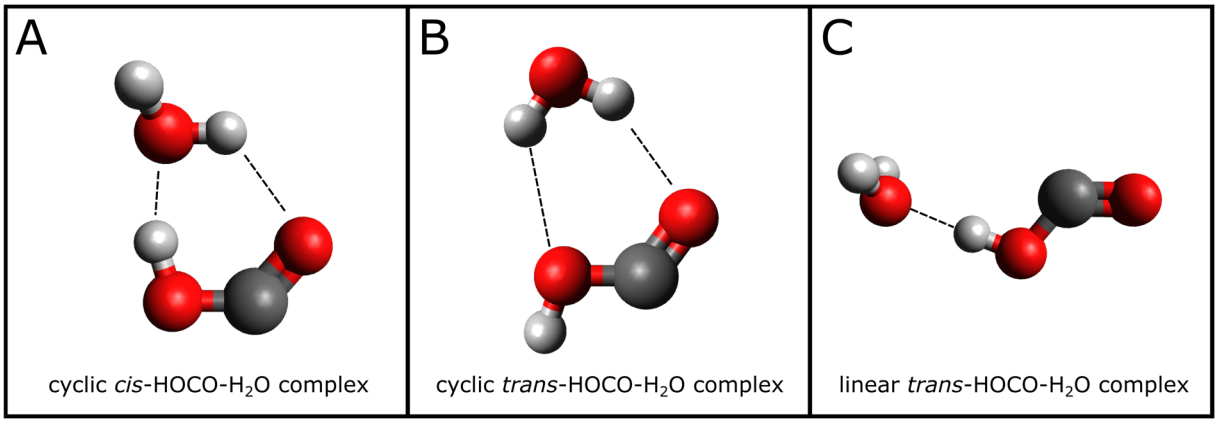

Figure 30. Molecular structures of the cyclic *cis*-HOCO•–H_2O complex (A), the cyclic *trans*-HOCO•–H_2O complex (B), and the linear *trans*-HOCO•–H_2O complex (C). Coordinates are taken from Oyama et al.[170] Dashed lines indicate hydrogen bonds.

5.6 Addition Reactions

In an addition reaction, two reactant molecules formally combine to form a larger adduct which contains all atoms of the reactant molecules. As such, the reaction is inherently atom-efficient. An example is the reaction between C_2H_4 and NH_3 which yields ethylamine ($C_2H_5NH_2$). In previous studies, the formation of ethylamine was only observed at electron energies where ionization of either C_2H_4 or NH_3 occurs.[53] Based on this observation, a mechanism was proposed which relies on the ionization of either C_2H_4 or NH_3 as the initial step which yields a radical cation (Scheme 1). Subsequently, this radical cation can react with the neutral second reactant yielding a cationic adduct. This adduct, in turn, undergoes hydrogen migration and finally yields ethylamine after neutralization by a thermalized electron. In fact, this mechanism describes well the energy dependent formation of ethyl methyl ether ($CH_3OC_2H_5$) after irradiation of C_2H_4/CH_3OH mixtures (Publication III). However, the formation of recombination products such as ethylene glycol (HOC_2H_4OH), methoxymethanol (CH_3OCH_2OH), and ethanol (C_2H_5OH) in CH_3OH containing ices (see Section 5.1) suggests that dissociation of CH_3OH into smaller fragments dominates over the production of an intact radical cation (Publication II–IV) which is not considered by the mechanism in Scheme 1. Notably, the formation of adduct molecules by the reaction of a radical with an unsaturated compound has already been proposed for the formation of ethanol after electron-irradiation of C_2H_4/H_2O mixtures at E_0 < 6 eV (Scheme 2), and for the formation of formamide (H_2NCHO) from CO/NH_3 mixtures after DEA to NH_3 at 9 eV (Scheme 3). Thus, an alternative mechanism is proposed for the formation of formic acid, methyl formate, and ethyl methyl ether which is based on addition of a $RO^{\bullet}$ radical (R = H, CH_3) to CO or C_2H_4, respectively. Any differences in the energy dependences of the adducts can then be reduced to the available reaction channels that yield a $RO^{\bullet}$ radical (R = H, CH_3).

The energy dependences of methyl formate in CO/CH_3OH mixtures (Publication IV) and formic acid in CO/H_2O mixtures (Publication I) revealed resonant product formation at E_0 = 10 eV (Figure 31). Assignment of this resonance to a specific DEA resonance is not immediately obvious because CO, H_2O, C_2H_4 and CH_3OH do all evince DEA resonances at around 10–11 eV in both gas phase (Figure 18)[65,144] and condensed phase[23,66,87,172–174] experiments. However, no resonances at E_0 = 10 eV are observed for the formation of ethyl methyl ether in C_2H_4/CH_3OH mixtures (Figure 31, left panel) and for the formation of ethanol in C_2H_4/H_2O mixtures (see Figure 2 in Ref. 51), suggesting that the 10 eV resonance is due to DEA to CO yielding C and $O^{\bullet-}$. Note that addition of $CH_3O^{\bullet}$ to CO and C_2H_4 have very similar barriers of 0.26 eV and 0.29 eV, respectively.[161,175] Therefore, a resonance should be visible in

both the formation of ethyl methyl ether in C_2H_4/CH_3OH mixtures and of methyl formate in CO/CH_3OH mixtures if $CH_3O^{\bullet}$ was formed by DEA to CH_3OH, either directly or via $O^{\bullet-}$ that then reacts with another CH_3OH to yield HO^- and $CH_3O^{\bullet}$. Furthermore, addition of $HO^{\bullet}$ to C_2H_4 and CO also have similar barriers of 0.037 eV[175] and 0.03 eV (Figure 29, top panel),[164] respectively. Therefore, a resonance should not only be visible for the formation of formic acid in CO/H_2O mixtures but also for the formation of ethanol in C_2H_4/H_2O mixtures if $HO^{\bullet}$ was formed by DEA to H_2O yielding $O^{\bullet-}$ (Figure 18) which then reacts with a second H_2O to yield HO^- and $HO^{\bullet}$. Thus, in contrast to the hydrogen transfer reaction between $CH_3O^{\bullet}$ and CO (Section 5.4), it is unlikely that the missing DEA resonance in the C_2H_4/CH_3OH (Publication III) and C_2H_4/H_2O mixtures[51] is due to kinetic discrimination.

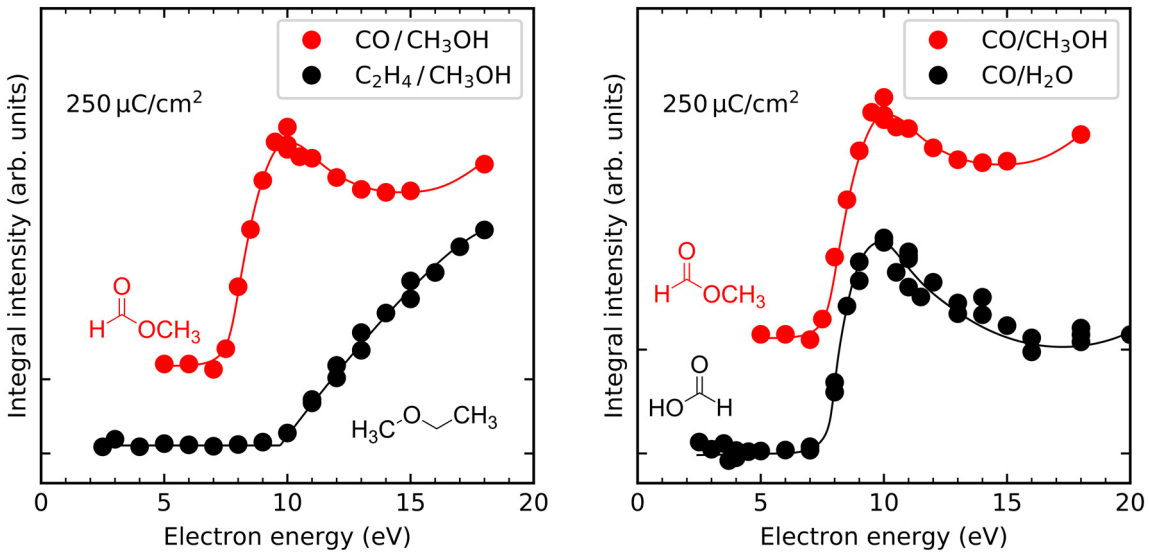

Figure 31. (Left panel) Energy dependences for the formation of methyl formate in CO/CH_3OH (1:1) mixtures and of ethyl methyl ether in C_2H_4/CH_3OH (1:1) mixtures. A resonance is only observed in the mixtures containing CO suggesting that the resonance is due to DEA to CO. (Right panel) Energy dependences for the formation of methyl formate in CO/CH_3OH (1:1) mixtures and of formic acid in CO/H_2O (1:1) mixtures. The resonance at 10 eV is observed in both mixtures, in agreement with the interpretation that the resonance is due to DEA to CO. Data are scaled to facilitate comparison. The solid lines serve as a guide to the eye. Data were taken from Publications I, III, and IV.

Thus, in the ice mixtures investigated in this work, DEA to CO clearly dominates over DEA to H_2O and CH_3OH at 10 eV. This is in contrast to the gas phase where the cross sections for the formation of $O^{\bullet-}$ by DEA at 10 eV are 2×10^{-19} cm^2 for CO[176] and 5.76×10^{-19} cm^2 for H_2O, respectively.[67] No absolute cross sections have been reported for the production of H^- and $O^{\bullet-}$ from DEA to CH_3OH at 10 eV. However, Kühn et al.[138] estimated the cross section for the production of $O^{\bullet-}$ to be in the order of 10^{-19} cm^2. This signifies that the relative cross sections

in the condensed phase can differ significantly from those in the gas phase, in agreement with previous reports on $Fe(CO)_5$ clusters[177] and methyl iodide (CH_3I).[178]

In addition to the 10 eV resonance, there are non-resonant contributions to the formation of formic acid, methyl formate, and ethyl methyl ether which are due to ND and/or EI of H_2O and CH_3OH. In the case of CH_3OH containing ices, EI clearly dominates over ND as can be seen by the onset for the formation of ethyl methyl ether at ~10 eV (Figure 31, left panel). This value agrees nicely with the ionization threshold of CH_3OH which is at 10.84 eV in the gas phase,[56] and at 9.8 eV in the condensed phase.[71] In the case of methyl formate and formic acid, the non-resonant contributions to product formation cannot be unambiguously identified to be dominated by ND or EI as the onset of this second formation channel is masked by the DEA resonance at 10 eV (Figure 31). However, both ND and EI of H_2O and CH_3OH can produce $RO^{\bullet}$ (R = H, CH_3) radicals and thus contribute to some extent to the formation of formic acid and methyl formate.

In the case of CO/CH_3OH and C_2H_4/CH_3OH, DEA to CH_3OH at E_0 = 5.5 eV produces $CH_3O^{\bullet}$ and H^- (Figure 18) which contributes to the production of methyl formate and ethyl methyl ether, respectively (Figure 32). Note that DEA to C_2H_4 cannot be responsible for the observed resonance as the known DEA resonances in the gas phase are at considerably higher energies (Figure 18).[118,119,121] Moreover, the competitive DEA channel yielding CH_3O^- and $H^{\bullet}$ (Figure 18) contributes to the production of methyl formate by hydrogenation of CO to $CH_3O^{\bullet}$ (reaction 1).

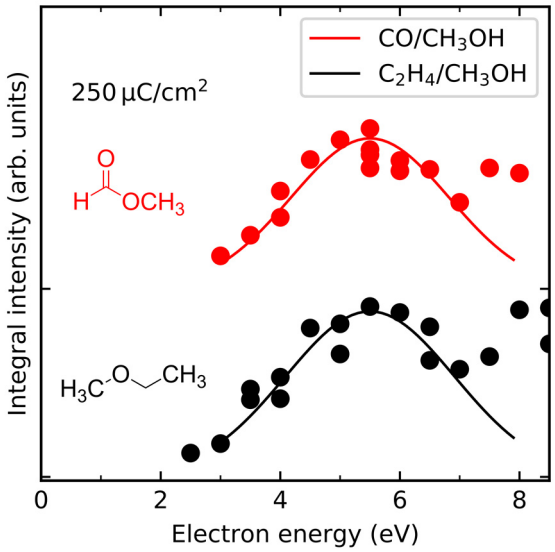

Figure 32. Energy dependences for the formation of methyl formate in CO/CH_3OH (1:1), and of ethyl methyl ether in C_2H_4/CH_3OH (1:1). The resonance at 5.5 eV is observed in both cases suggesting that the resonance is due to DEA to CH_3OH. Data were taken from Publications III and IV.

Based on the electron–molecule interactions described above, mechanisms have been proposed for the formation of formic acid, methyl formate and ethyl methyl ether. In each case, the key-step is the production of a $HO^\bullet$ or $CH_3O^\bullet$ radical. DEA to CO at 10 eV yields C and $O^{\bullet-}$ (Figure 18), the latter of which can react with a nearby H_2O or CH_3OH molecule to yield $HO^\bullet$ or $CH_3O^\bullet$, respectively (reactions 9 and 10).[147]

$$O^{\bullet-} + H_2O \rightarrow HO^- + HO^\bullet \quad (9)$$

$$O^{\bullet-} + CH_3OH \rightarrow HO^- + CH_3O^\bullet \quad (10)$$

After EI of H_2O or CH_3OH, the respective radical cation can transfer a proton to a nearby H_2O or CH_3OH molecule to yield a $HO^\bullet$ or a $CH_3O^\bullet$ radical, respectively, along with a protonated H_2O or CH_3OH molecule (reactions 11 and 12).

$$H_2O^{\bullet+} + H_2O \rightarrow HO^\bullet + H_3O^+ \quad (11)$$

$$CH_3OH^{\bullet+} + CH_3OH \rightarrow CH_3O^\bullet + CH_3OH_2^+ \quad (12)$$

Furthermore, ND of H_2O or CH_3OH yields $HO^\bullet$ or $CH_3O^\bullet$, and a $H^\bullet$ radical (reactions 13 and 14) once the electron energy is higher than the electronic excitation energy.

$$H_2O \rightarrow HO^\bullet + H^\bullet \quad (13)$$

$$CH_3OH \rightarrow CH_3O^\bullet + H^\bullet \quad (14)$$

Finally, DEA to CH_3OH yields $CH_3O^\bullet$ and H^- (Figure 18). Note that in the CO/CH_3OH mixture, additional $CH_3O^\bullet$ radicals are also produced by hydrogenation of CO (reaction 1) following DEA of CH_3OH into $CH_3O^-$and $H^\bullet$ (Figure 18) and by ND of CH_3OH.

Subsequently, the $HO^\bullet$ or $CH_3O^\bullet$ radical can attack CO to yield an intermediate $HOCO^\bullet$ or $CH_3OCO^\bullet$ radical which can subsequently abstract a H atom from a nearby H_2O or CH_3OH molecule to yield formic acid or methyl formate, respectively (Scheme 4). Similarly, $CH_3O^\bullet$ can attack C_2H_4 to yield an intermediate $CH_3OC_2H_4^\bullet$ radical which can abstract a H atom from a nearby CH_3OH molecule to yield ethyl methyl ether (Scheme 4). Note that at the end of the reaction, the $CH_3O^\bullet$ radical, or more generally $RO^\bullet$, is recovered, potentially inducing a chain reaction. Starting from the radicals, formation of the adducts can thus be described by the same elementary steps over the entire range of electron energies. Consequently, any differences in the energy dependences of the addition products can be reduced to the initial formation of radicals.

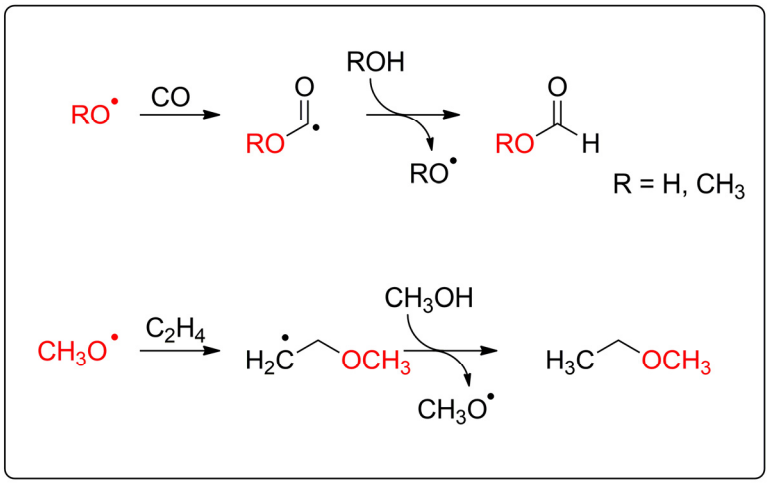

Scheme 4. Reaction of H_2O or CH_3OH with CO yielding formic acid and methyl formate, respectively, and reaction of CH_3OH with C_2H_4 yielding ethyl methyl ether. The reactions can be initiated by DEA to CO at E_0 = 10 eV yielding C and $O^{\bullet-}$, or by ND, EI, or DEA to CH_3OH. Note that DEA to CO is not accessible in the C_2H_4/CH_3OH mixture.

6 Summary and Outlook

Electron-induced reactions play an important role in astrochemistry as numerous secondary electrons are released when ionizing radiation such as cosmic rays penetrate the icy mantle around interstellar dust grains. A comprehensive understanding of the mechanisms that underlie electron-induced product formation is thus essential for a more complete picture of astrochemical processes. In the present thesis, electron-induced reaction in CO/H_2O, CO/CH_3OH, and C_2H_4/CH_3OH mixed simple ices have been studied to complement previous results on electron-induced reactions in CO/NH_3,[37] C_2H_4/H_2O,[51] and C_2H_4/NH_3 mixtures.[52,53] In particular, this work was concerned with the question how a mechanism is changed when one reactant is replaced by another. Important insights were obtained by studying the dependence of product formation on electron energy which enables one to identify the relevant electron–molecule interactions that underlie product formation. In particular, comparison of the energy dependences of different products enables one to distinguish among several possible mechanisms.

The results obtained in this thesis reveal that the observed products can be formed by recombination of radicals, hydrogenation of an unsaturated compound, oxidation of CO, and addition reactions. Recombination of two radicals is a reaction type that is particularly efficient in CH_3OH containing ices. Its efficiency, however, depends on the occurrence of competitive side reactions such as disproportionation of two radicals and radical-molecule reactions. In the extreme case, such side reactions may even prevent the detection of particular recombination products.

Hydrogenation occurs by either of three mechanisms: Transfer-hydrogenation after electron attachment, addition of free hydrogen atoms, and hydrogen transfer from $CH_3O^{\bullet}$ to an unsaturated compound. Transfer-hydrogenation after electron attachment was only observed in the CO/H_2O mixture and relies on a proton transfer from H_2O to the $CO^{\bullet-}$ radical anion. In previous experiments,[51] a similar reaction was observed after electron attachment to C_2H_4 in a C_2H_4/H_2O mixture. However, analogous reactions where not observed when H_2O was replaced by CH_3OH which can be explained by the lower ability of CH_3OH to stabilize the radical anion. In addition, the acidity of CH_3OH might be lower than that of H_2O. However, this needs to be further studied in the future due to a lack of reference data on the acidity of CH_3OH in a CH_3OH matrix which could be studied by theoretical calculations. Furthermore, it remains unclear how the lifetime of a $CO^{\bullet-}$ or $C_2H_4^{\bullet-}$ radical anion is affected by nearby

H_2O or CH_3OH molecules. In future studies, this question could be addressed by HREELS as the lifetime of a TNI affects the overtone intensities of a particular vibrational mode.[179,180]

Hydrogenation of CO and C_2H_4 by atomic hydrogen was observed in all three mixtures. It is likely that reduction of C_2H_4 by free hydrogen atoms also occurs upon irradiation of the C_2H_4/H_2O mixtures,[51] and possibly also upon irradiation of the C_2H_4/NH_3 and CO/NH_3 mixtures studied previously.[37,52,53] As this reaction could shed light on the role of ND of H_2O and NH_3, hydrogenation of CO and C_2H_4 in these mixtures should be studied in future experiments. From the experiments of the present thesis, it is expected that at least in the case of the C_2H_4/H_2O mixture, ND of H_2O should contribute significantly to the hydrogenation of C_2H_4 which would yield C_2H_6 and C_4H_{10}. In addition, studies on formation of H_2CO in the CO/NH_3 mixture could help to reveal whether the resonant formation of formamide at about 9 eV progresses via an $HCO^{\bullet}$ or $H_2NCO^{\bullet}$ intermediate.

Finally, reduction of C_2H_4 occurs also by hydrogen transfer from a $CH_3O^{\bullet}$ radical to C_2H_4. An analogous reaction, however, was not observed when C_2H_4 was replaced by CO which can be explained by the higher reaction barrier in the case of CO. In future experiments, the role of hydrogen tunneling for this reaction should be studied by using deuterated CH_3OH isotopologues.

Upon electron-irradiation of the CO/H_2O and CO/CH_3OH simple ices, CO is readily oxidized to CO_2. In the case of CO/CH_3OH, CO_2 is formed by reaction of $CH_3O^{\bullet}$ with CO to yield an intermediate $CH_3OCO^{\bullet}$ radical which can further decay to CO_2 and $CH_3^{\bullet}$. An analogous reaction is not observed in the case of CO/H_2O because the intermediate $HOCO^{\bullet}$ radical, which is formed by reaction of $HO^{\bullet}$ with CO, is considerably stabilized by the matrix. Instead, CO_2 formation in CO/H_2O progresses mainly by ND of H_2O into H_2 and $O(^1D/^3P)$ and subsequent addition of $O(^1D/^3P)$ to CO. In future experiments, it should be studied if the analogous ND channel of CH_3OH into CH_4 and $O(^1D/^3P)$ also contributes to the formation of CO_2 in CO/CH_3OH mixtures.

In each simple ice mixture, formation of the addition products was observed which are formic acid (HCOOH) in the case of CO/H_2O, methyl formate (CH_3OCHO) in the case of CO/CH_3OH, and ethyl methyl ether ($CH_3OC_2H_5$) in the case of C_2H_4/CH_3OH. In contrast to previous studies,[37,51–53] the results of the present thesis suggest that these addition reactions predominantly progress by radical-molecule reactions. By studying the formation of side products, it could also be shown that ND must contribute to product formation to some extent.

The different reaction classes identified in this work can serve as guideline to predict the formation of particular products in future studies. In addition, this work provides a reference for identifying the relevant electron–molecule interactions that underlie product formation in simple ice mixtures.

References

(1) Arumainayagam, C. R.; Garrod, R. T.; Boyer, M. C.; Hay, A. K.; Bao, S. T.; Campbell, J. S.; Wang, J.; Nowak, C. M.; Arumainayagam, M. R.; Hodge, P. J. Extraterrestrial Prebiotic Molecules: Photochemistry vs. Radiation Chemistry of Interstellar Ices. *Chem. Soc. Rev.* **2019**, *48*, 2293–2314.

(2) Sandford, S. A.; Nuevo, M.; Bera, P. P.; Lee, T. J. Prebiotic Astrochemistry and the Formation of Molecules of Astrobiological Interest in Interstellar Clouds and Protostellar Disks. *Chem. Rev.* **2020**, *120*, 4616–4659.

(3) van Dishoeck, E. F. Astrochemistry of Dust, Ice and Gas: Introduction and Overview. *Faraday Discuss.* **2014**, *168*, 9–47.

(4) Cheung, A. C.; Rank, D. M.; Townes, C. H.; Thornton, D. D.; Welch, W. J. Detection of NH_3 Molecules in the Interstellar Medium by Their Microwave Emission. *Phys. Rev. Lett.* **1968**, *21*, 1701–1705.

(5) Herzberg, G. Historical Remarks on the Discovery of Interstellar Molecules. *J. R. Astron. Soc. Can.* **1988**, *82*, 115–127.

(6) Müller, H. S. P.; Thorwirth, S.; Roth, D. A.; Winnewisser, G. The Cologne Database for Molecular Spectroscopy, CDMS. *Astron. Astrophys.* **2001**, *370*, L49–L52.

(7) Endres, C. P.; Schlemmer, S.; Schilke, P.; Stutzki, J.; Müller, H. S. P. The Cologne Database for Molecular Spectroscopy, CDMS, in the Virtual Atomic and Molecular Data Centre, VAMDC. *J. Mol. Spectrosc.* **2016**, *327*, 95–104.

(8) Müller, H. S. P.; Schlöder, F.; Stutzki, J.; Winnewisser, G. The Cologne Database for Molecular Spectroscopy, CDMS: A Useful Tool for Astronomers and Spectroscopists. *J. Mol. Struct.* **2005**, *742*, 215–227.

(9) Townes, C. H. Introduction: Radio and IR Studies of Molecular Clouds. In *The Structure and Content of Molecular Clouds 25 Years of Molecular Radioastronomy*; Wilson, T. L., Johnston, K. J., Eds.; Springer: New York City, NY, USA, 1993; pp 1–12.

(10) Snow, T. P.; McCall, B. J. Diffuse Atomic and Molecular Clouds. *Annu. Rev. Astron. Astrophys.* **2006**, *44*, 367–414.

(11) Öberg, K. I. Photochemistry and Astrochemistry: Photochemical Pathways to Interstellar Complex Organic Molecules. *Chem. Rev.* **2016**, *116*, 9631–9663.

(12) Prasad, S. S.; Tarafdar, S. P. UV Radiation Field Inside Dense Clouds: Its Possible Existence And Chemical Implications. *Astrophys. J.* **1983**, *267*, 603–609.

(13) Williams, D. A.; Herbst, E. It's a Dusty Universe: Surface Science in Space. *Surf. Sci.* **2002**, *500*, 823–837.

(14) d'Hendecourt, L. B.; Allamandola, L. J.; Greenberg, J. M. Time Dependent Chemistry in Dense Molecular Clouds. *Astron. Astrophys.* **1985**, *152*, 130–150.

(15) Winnewisser, G.; Herbst, E. Interstellar Molecules. *Rep. Prog. Phys.* **1993**, *56*, 1209–1273.

(16) Tielens, A. G. G. M.; Hagen, W. Model Calculations of the Molecular Composition of Interstellar Grain Mantles. *Astron. Astrophys.* **1982**, *114*, 245–260.

(17) Herbst, E.; van Dishoeck, E. F. Complex Organic Interstellar Molecules. *Annu. Rev. Astron. Astrophys.* **2009**, *47*, 427–480.

(18) Boogert, A. C. A.; Gerakines, P. A.; Whittet, D. C. B. Observations of the Icy Universe. *Annu. Rev. Astron. Astrophys.* **2015**, *53*, 541–581.

(19) Smith, I. W. M. Laboratory Astrochemistry: Gas-Phase Processes. *Annu. Rev. Astron. Astrophys.* **2011**, *49*, 29–66.

(20) Maity, S.; Kaiser, R. I.; Jones, B. M. Formation of Complex Organic Molecules in Methanol and Methanol–Carbon Monoxide Ices Exposed to Ionizing Radiation – A Combined FTIR and Reflectron Time-of-Flight Mass Spectrometry Study. *Phys. Chem. Chem. Phys.* **2015**, *17*, 3081–3114.

(21) Öberg, K. I.; Garrod, R. T.; van Dishoeck, E. F.; Linnartz, H. Formation Rates of Complex Organics in UV Irradiated CH_3OH-Rich Ices. *Astron. Astrophys.* **2009**, *504*, 891–913.

(22) Modica, P.; Palumbo, M. E. Formation of Methyl Formate After Cosmic Ion Irradiation of Icy Grain Mantles. *Astron. Astrophys.* **2010**, *519*, A22.

(23) Boyer, M. C.; Boamah, M. D.; Sullivan, K. K.; Arumainayagam, C. R.; Bazin, M.; Bass, A. D.; Sanche, L. Dynamics of Dissociative Electron-Molecule Interactions in Condensed Methanol. *J. Phys. Chem. C* **2014**, *118*, 22592–22600.

(24) Fayolle, E. C.; Balfe, J.; Loomis, R.; Bergner, J.; Graninger, D.; Rajappan, M.; Öberg, K. I. N_2 and CO Desorption Energies From Water Ice. *Astrophys. J., Lett.* **2016**, *816*, L28.

(25) Schneider, H.; Caldwell-Overdier, A.; Coppieters ʻt Wallant, S.; Dau, L.; Huang, J.; Nwolah, I.; Kasule, M.; Buffo, C.; Mullikin, E.; Widdup, L.; Hay, A.; Bao, S. T.; Perea, J.; Thompson, M.; Tano-Menka, R.; Van Tuyl, M.; Wang, A.; Bussey, S.; Sachdev, N.; Zhang, C.; Boyer, M. C.; Arumainayagam, C. R. Detection of Methoxymethanol as a Photochemistry Product of Condensed Methanol. *Mon. Not. R. Astron. Soc.: Lett.* **2019**, *485*, L19–L23.

(26) Chen, Y.-J.; Ciaravella, A.; Muñoz Caro, G. M.; Cecchi-Pestellini, C.; Jiménez-Escobar, A.; Juang, K.-J.; Yih, T.-S. Soft X-Ray Irradiation of Methanol Ice: Formation of Products as a Function of Photon Energy. *Astrophys. J.* **2013**, *778*, 1–11.

(27) Bennett, C. J.; Kaiser, R. I. On the Formation of Glycolaldehyde ($HCOCH_2OH$) and Methyl Formate ($HCOOCH_3$) in Interstellar Ice Analogs. *Astrophys. J.* **2007**, *661*, 899–909.

(28) Bennett, C. J.; Chen, S.; Sun, B.; Chang, A. H. H.; Kaiser, R. I. Mechanistical Studies on the Irradiation of Methanol in Extraterrestrial Ices. *Astrophys. J.* **2007**, *660*, 1588–1608.

(29) Maity, S.; Kaiser, R. I.; Jones, B. M. Infrared and Reflectron Time-of-Flight Mass Spectroscopic Study on the Synthesis of Glycolaldehyde in Methanol (CH_3OH) and Methanol-Carbon Monoxide (CH_3OH-CO) Ices Exposed to Ionization Radiation. *Faraday Discuss.* **2014**, *168*, 485–516.

(30) Boamah, M. D.; Sullivan, K. K.; Shulenberger, K. E.; Soe, C. M.; Jacob, L. M.; Yhee, F. C.; Atkinson, K. E.; Boyer, M. C.; Haines, D. R.; Arumainayagam, C. R. Low-Energy Electron-Induced Chemistry of Condensed Methanol: Implications for the Interstellar Synthesis of Prebiotic Molecules. *Faraday Discuss.* **2014**, *168*, 249–266.

(31) Shulenberger, K. E.; Zhu, J. L.; Tran, K.; Abdullahi, S.; Belvin, C.; Lukens, J.; Peeler, Z.; Mullikin, E.; Cumberbatch, H. M.; Huang, J.; Regovich, K.; Zhou, A.; Heller, L.; Markovic, M.; Gates, L.; Buffo, C.; Tano-Menka, R.; Arumainayagam, C. R.; Böhler, E.; Swiderek, P.; Esmaili, S.; Bass, A. D.; Huels, M.; Sanche, L. Electron-Induced Radiolysis of Astrochemically Relevant Ammonia Ices. *ACS Earth Space Chem.* **2019**, *3*, 800–810.

(32) Baratta, G. A.; Castorina, A. C.; Leto, G.; Palumbo, M. E.; Spinella, F.; Strazzulla, G. Ion Irradiation Experiments Relevant to the Physics of Comets. *Planet. Space Sci.* **1994**, *42*, 759–766.

(33) Allamandola, L. J.; Sandford, S. A.; Valero, G. J. Photochemical and Thermal Evolution of Interstellar/Precometary Ice Analogs. *Icarus* **1988**, *76*, 225–252.

(34) Petrik, N. G.; Monckton, R. J.; Koehler, S. P. K.; Kimmel, G. A. Distance-Dependent Radiation Chemistry: Oxidation versus Hydrogenation of CO in Electron-Irradiated H_2O/CO/H_2O Ices. *J. Phys. Chem. C* **2014**, *118*, 27483–27492.

(35) Munñoz Caro, G. M.; Meierhenrich, U. J.; Schutte, W. A.; Barbier, B.; Arcones Segovia, A.; Rosenbauer, H.; Thiemann, W. H.-P.; Brack, A.; Greenberg, J. M. Amino Acids from Ultraviolet Irradiation of Interstellar Ice Analogues. *Nature* **2002**, *416*, 403–406.

(36) Meinert, C.; Myrgorodska, I.; de Marcellus, P.; Buhse, T.; Nahon, L.; Hoffmann, S. V.; d'Hendecourt, L. L. S.; Meierhenrich, U. J. Ribose and Related Sugars from Ultraviolet Irradiation of Interstellar Ice Analogs. *Science* **2016**, *352*, 208–212.

(37) Bredehöft, J. H.; Böhler, E.; Schmidt, F.; Borrmann, T.; Swiderek, P. Electron-Induced Synthesis of Formamide in Condensed Mixtures of Carbon Monoxide and Ammonia. *ACS Earth Space Chem.* **2017**, *1*, 50–59.

(38) Jorissen, A.; Cerf, C. Asymmetric Photoreactions as the Origin of Biomolecular Homochirality: A Critical Review. *Origins Life Evol. Biospheres* **2002**, *32*, 129–142.

(39) Nuevo, M.; Meierhenrich, U. J.; Muñoz Caro, G. M.; Dartois, E.; d'Hendecourt, L.; Deboffle, D.; Auger, G.; Blanot, D.; Bredehöft, J.-H.; Nahon, L. The Effects of Circularly Polarized Light on Amino Acid Enantiomers Produced by the UV Irradiation of Interstellar Ice Analogs. *Astron. Astrophys.* **2006**, *457*, 741–751.

(40) Rosenberg, R. A.; Mishra, D.; Naaman, R. Chiral Selective Chemistry Induced by Natural Selection of Spin-Polarized Electrons. *Angew. Chem.* **2015**, *127*, 7403–7406.

(41) Rosenberg, R. A. Electrochirogenesis: The Possible Role of Low-Energy Spin-Polarized Electrons in Creating Homochirality. *Symmetry* **2019**, *11*, 528.

(42) Rosenberg, R. A.; Rozhkova, E. A.; Novosad, V. Investigations into Spin- and Unpolarized Secondary Electron-Induced Reactions in Self-Assembled Monolayers of Cysteine. *Langmuir* **2021**, *37*, 2985–2992.

(43) Feldman, V. I.; Ryazantsev, S. V.; Saenko, E. V.; Kameneva, S. V.; Shiryaeva, E. S. Matrix Isolation Model Studies on the Radiation-Induced Transformations of Small Molecules of Astrochemical and Atmospheric Interest. *Radiat. Phys. Chem.* **2016**, *124*, 7–13.

(44) Zamirri, L.; Ugliengo, P.; Ceccarelli, C.; Rimola, A. Quantum Mechanical Investigations on the Formation of Complex Organic Molecules on Interstellar Ice Mantles. Review and Perspectives. *ACS Earth Space Chem.* **2019**, *3*, 1499–1523.

(45) Chuang, K.-J.; Fedoseev, G.; Qasim, D.; Ioppolo, S.; van Dishoeck, E. F.; Linnartz, H. Production of Complex Organic Molecules: H-Atom Addition versus UV Irradiation. *Mon. Not. R. Astron. Soc.* **2017**, *467*, 2552–2565.

(46) Arumainayagam, C. R.; Lee, H.-L.; Nelson, R. B.; Haines, D. R.; Gunawardane, R. P. Low-Energy Electron-Induced Reactions in Condensed Matter. *Surf. Sci. Rep.* **2010**, *65*, 1–44.

(47) Mason, N. J.; Nair, B.; Jheeta, S.; Szymańska, E. Electron Induced Chemistry: A New Frontier in Astrochemistry. *Faraday Discuss.* **2014**, *168*, 235–247.

(48) Boyer, M. C.; Rivas, N.; Tran, A. A.; Verish, C. A.; Arumainayagam, C. R. The Role of Low-Energy (≤ 20 eV) Electrons in Astrochemistry. *Surf. Sci.* **2016**, *652*, 26–32.

(49) Böhler, E.; Warneke, J.; Swiderek, P. Control of Chemical Reactions and Synthesis by Low-Energy Electrons. *Chem. Soc. Rev.* **2013**, *42*, 9219–9231.

(50) Balog, R.; Langer, J.; Gohlke, S.; Stano, M.; Abdoul-Carime, H.; Illenberger, E. Low Energy Electron Driven Reactions in Free and Bound Molecules: From Unimolecular Processes in the Gas Phase to Complex Reactions in a Condensed Environment. *Int. J. Mass Spectrom.* **2004**, *233*, 267–291.

(51) Warneke, J.; Wang, Z.; Swiderek, P.; Bredehöft, J. H. Electron-Induced Hydration of an Alkene: Alternative Reaction Pathways. *Angew. Chem., Int. Ed.* **2015**, *54*, 4397–4400.

(52) Hamann, T.; Böhler, E.; Swiderek, P. Low-Energy-Electron-Induced Hydroamination of an Alkene. *Angew. Chem., Int. Ed.* **2009**, *48*, 4643–4645.

(53) Böhler, E.; Bredehöft, J. H.; Swiderek, P. Low-Energy Electron-Induced Hydroamination Reactions between Different Amines and Olefins. *J. Phys. Chem. C* **2014**, *118*, 6922–6933.

(54) Swiderek, P.; Deschamps, M. C.; Michaud, M.; Sanche, L. Bond Formation in Reactions of Solid Cyclopropane Induced by Low-Energy Electrons. *J. Phys. Chem. B* **2003**, *107*, 563–567.

(55) Weeks, L. D.; Zhu, L. L.; Pellon, M.; Haines, D. R.; Arumainayagam, C. R. Low-Energy Electron-Induced Oligomerization of Condensed Carbon Tetrachloride. *J. Phys. Chem. C* **2007**, *111*, 4815–4822.

(56) Lias, S. G.; Rosenstock, H. M.; Draxl, K.; Steiner, B. W.; Herron, J. T.; Holmes, J. L.; Levin, R. D.; Liebman, J. F.; Kafafi, S. A. Ionization Energetics Data. In *NIST Chemistry WebBook*, NIST Standard Reference Database No. 69; Linstrom, P. J., Mallard, W. G., Eds.; National Institute of Standards and Technology: Gaithersburg, MD. http://webbook.nist.gov.

(57) Tronc, M.; Azria, R.; Arfa, M. B. Differential Cross Section for H^- and NH_2^- Ions in NH_3. *J. Phys. B: At., Mol. Opt. Phys.* **1988**, *21*, 2497–2506.

(58) Yuan, B.; Shin, J.-W; Bernstein, E. R. Dynamics and Fragmentation of van der Waals and Hydrogen Bonded Cluster Cations: $(NH_3)_n$ and $(NH_3BH_3)_n$ Ionized at 10.51 eV. *J. Chem. Phys.* **2016**, *144*, 144315.

(59) Sun, Y. M.; Sloan, D.; Ihm, H.; White, J. M. Electroninduced Surface Chemistry: Production and Characterization of NH_2 and NH Species on Pt(111). *J. Vac. Sci. Technol., A* **1996**, *14*, 1516–1521.

(60) Zheng, W.; Jewitt, D.; Osamura, Y.; Kaiser, R. I. Formation of Nitrogen and Hydrogen-bearing Molecules in Solid Ammonia and Implications for Solar System and Interstellar Ices. *Astrophys. J.* **2008**, *674*, 1242–1250.

(61) Borrmann, T. University of Bremen, Bremen, Germany. Personal communication, 2021.

(62) Bald, I.; Langer, J.; Tegeder, P.; Ingólfsson, O. From Isolated Molecules through Clusters and Condensates to the Building Blocks of Life. *Int. J. Mass Spectrom.* **2008**, *277*, 4–25.

(63) Ingólfsson, O.; Weik, F.; Illenberger, E. The Reactivity of Slow Electrons with Molecules at Different Degrees of Aggregation: Gas Phase, Clusters and Condensed Phase. *Int. J. Mass Spectrom. Ion Processes* **1996**, *155*, 1–68.

(64) Nag, P.; Nandi, D. Fragmentation Dynamics in Dissociative Electron Attachment to CO Probed by Velocity Slice Imaging. *Phys. Chem. Chem. Phys.* **2015**, *17*, 7130–7137.

(65) Gope, K.; Tadsare, V.; Prabhudesai, V. S.; Mason, N. J.; Krishnakumar, E. Negative Ion Resonances in Carbon Monoxide: Probing Dissociative Electron Attachment in CO by Velocity Slice Imaging. *Eur. Phys. J. D* **2016**, *70*, 134.

(66) Azria, R.; Parenteau, L.; Sanche, L. Mechanisms for O^- Electron Stimulated Desorption via Dissociative Attachment in Condensed CO. *J. Chem. Phys.* **1988**, *88*, 5166–5170.

(67) Itikawa, Y.; Mason, N. Cross Sections for Electron Collisions with Water Molecules. *J. Phys. Chem. Ref. Data* **2005**, *34*, 1–22.

(68) *Low-Energy Electrons: Fundamentals and Applications*, Ingólfsson, O., Ed.; Pan Stanford Publishing: Singapore, 2019.

(69) Illenberger, E. Formation and Evolution of Negative Ion Resonances at Surfaces. *Surf. Sci.* **2003**, *528*, 67–77.

(70) Lepage, M.; Michaud, M.; Sanche, L. Low-Energy Electron Scattering Cross Section for the Production of CO within Condensed Acetone. *J. Chem. Phys.* **2000**, *113*, 3602–3608.

(71) Yu, K. Y.; McMenamin, J. C.; Spicer, W. E. UPS Measurements of Molecular Energy Level of Condensed Gases. *Surf. Sci.* **1975**, *50*, 149–156.

(72) Wallace, W. E.; Mass Spectra. In *NIST Chemistry WebBook*; Linstrom, P. J., Mallard, W. G., Eds.; NIST Standard Reference Database Number 69; National Institute of Standards and Technology: Gaithersburg, MD, http://webbook.nist.gov.

(73) El-Shall, M. S.; Marks, C.; Sieck, L. W.; Meot-Ner, M. Reactions and Thermochemistry of Protonated Methanol Clusters Produced by Electron Impact Ionization. *J. Phys. Chem.* **1992**, *96*, 2045–2051.

(74) Lengyel, J.; Fedor, J.; Fárník, M. Ligand Stabilization and Charge Transfer in Dissociative Ionization of $Fe(CO)_5$ Aggregates. *J. Phys. Chem. C* **2016**, *120*, 17810–17816.

(75) Ramsier, R. D.; Yates, J. T. Electron-Stimulated Desorption: Principles and Applications. *Surf. Sci. Rep.* **1991**, *12*, 243–378.

(76) Burke, D. J.; Brown, W. A. Ice in Space: Surface Science Investigations of the Thermal Desorption of Model Interstellar Ices on Dust Grain Analogue Surfaces. *Phys. Chem. Chem. Phys.* **2010**, *12*, 5947–5969.

(77) Menzel, D.; Gomer, R. Desorption from Metal Surfaces by Low-Energy Electrons. *J. Chem. Phys.* **1964**, *41*, 3311–3328.

(78) Madey, T. E. History of Desorption Induced by Electronic Transitions. *Surf. Sci.* **1994**, *299–300*, 824–836.

(79) Menzel, D. Thirty Years of MGR: How It Came About, and What Came of It. *Nucl. Instrum. Methods Phys. Res., Sect. B* **1995**, *101*, 1–10.

(80) Redhead, P. A. The First 50 Years of Electron Stimulated Desorption (1918-1968). *Vacuum* **1997**, *48*, 585–596.

(81) Avouris, P.; Walkup, R. E. Fundamental Mechanisms Of Desorption And Fragmentation Induced By Electronic Transitions At Surfaces. *Annu. Rev. Phys. Chem.* **1989**, *40*, 173–206.

(82) Antoniewicz, P. R. Model for Electron- and Photon-Stimulated Desorption. *Phys. Rev. B* **1980**, *21*, 3811–3815.

(83) Knotek, M. L.; Feibelman, P. J. Ion Desorption by Core-Hole Auger Decay. *Phys. Rev. Lett.* **1978**, *40*, 964–967.

(84) Madey, T. E. Electron- and Photon-Stimulated Desorption: Probes of Structure and Bonding at Surfaces. *Science* **1986**, *234*, 316–322.

(85) Sambe, H.; Ramaker, D. E.; Parenteau, L.; Sanche, L. Image-Charge Effects in Electron-Stimulated Desorption: O^- from O_2 Condensed on Ar Films Grown on Pt. *Phys. Rev. Lett.* **1987**, *59*, 236–239.

(86) Rowntree, P.; Parenteau, L.; Sanche A, L. Electron Stimulated Desorption via Dissociative Attachment in Amorphous H_2O. *J. Chem. Phys.* **1991**, *94*, 8570–8576.

(87) Kimmel, G. A.; Orlando, T. M. Observation of Negative Ion Resonances in Amorphous Ice via Low-Energy (5–40 eV) Electron-Stimulated Production of Molecular Hydrogen. *Phys. Rev. Lett.* **1996**, *77*, 3983–3986.

(88) Kimmel, G. A.; Orlando, T. M. Low-Energy (5–120 eV) Electron Stimulated Dissociation of Amorphous D_2O Ice: $D(^2S)$, $O(^3P_{2,1,0})$, and $O(^1D_2)$ Yields and Velocity Distributions. **1995**, *75*, 2606–2609.

(89) Parenteau, L.; Jay-Gerin, J.-P.; Sanche, L. Electron-Stimulated Desorption of H^- Ions via Dissociative Electron Attachment in Condensed Methanol. *J. Phys. Chem.* **1994**, *98*, 10277–10281.

(90) Antic, D.; Parenteau, L.; Sanche, L. Electron-Stimulated Desorption of H^- from Condensed-Phase Deoxyribose Analogues: Dissociative Electron Attachment versus Resonance Decay into Dipolar Dissociation. *J. Phys. Chem. B* **2000**, *104*, 4711–4716.

(91) Orzol, M.; Martin, I.; Kocisek, J.; Dabkowska, I.; Langer, J.; Illenberger, E. Bond and Site Selectivity in Dissociative Electron Attachment to Gas Phase and Condensed Phase Ethanol and Trifluoroethanol. *Phys. Chem. Chem. Phys.* **2007**, *9*, 3424–3431.

(92) Warneke, J.; Swiderek, P. Electron-Induced Decomposition of Condensed Acetone Studied by Quantifying Desorption and Retention of Volatile Products. *J. Phys. Chem. C* **2015**, *119*, 8725–8735.

(93) King, D. A. Thermal Desorption from Metal Surfaces: A Review. *Surf. Sci.* **1975**, *47*, 384–402.

(94) Burean, E.; Ipolyi, I.; Hamann, T.; Swiderek, P. Thermal Desorption Spectrometry for Identification of Products Formed by Electron-Induced Reactions. *Int. J. Mass Spectrom.* **2008**, *277*, 215–219.

(95) Burean, E.; Swiderek, P. Thermal Desorption Measurement of Cross Section for Reactions in Condensed Acetaldehyde Induced by Low-Energy Electrons. *Surf. Sci.* **2008**, *602*, 3194–3198.

(96) King, D. A. Kinetics of Adsorption, Desorption, and Migration at Singlecrystal Metal Surfaces. *Crit. Rev. Solid State Mater. Sci.* **1978**, *7*, 167–208.

(97) de Jong, A. M.; Niemantsverdriet, J. W. Thermal Desorption Analysis: Comparative Test of Ten Commonly Applied Procedures. *Surf. Sci.* **1990**, *233*, 355–365.

(98) Nieskens, D. L. S.; van Bavel, A. P.; Niemantsverdriet, J. W. The Analysis of Temperature Programmed Desorption Experiments of Systems with Lateral Interactions; Implications of the Compensation Effect. *Surf. Sci.* **2003**, *546*, 159–169.

(99) Suhasaria, T.; Thrower, J. D.; Zacharias, H. Thermal Desorption of Ammonia from Crystalline Forsterite Surfaces. *Mon. Not. R. Astron. Soc.* **2015**, *454*, 3317–3327.

(100) Suhasaria, T.; Thrower, J. D.; Zacharias, H. Thermal Desorption of Astrophysically Relevant Molecules from Forsterite(010). *Mon. Not. R. Astron. Soc.* **2017**, *472*, 389–399.

(101) Thrower, J. D.; Collings, M. P.; Rutten, F. J. M.; McCoustra, M. R. S. Thermal Desorption of C_6H_6 from Surfaces of Astrophysical Relevance. *J. Chem. Phys.* **2009**, *131*, 244711.

(102) Zubkov, T.; Smith, R. S.; Engstrom, T. R.; Kay, B. D. Adsorption, Desorption, and Diffusion of Nitrogen in a Model Nanoporous Material. I. Surface Limited Desorption Kinetics in Amorphous Solid Water. *J. Chem. Phys.* **2007**, *127* (18).

(103) Dohnálek, Z.; Kim, J.; Bondarchuk, O.; Mike White, J.; Kay, B. D. Physisorption of N_2, O_2 and CO on Fully Oxidized TiO_2(110). *J. Phys. Chem. B* **2006**, *110*, 6229–6235.

(104) Ayotte, P.; Smith, R. S.; Stevenson, K. P.; Dohnálek, Z.; Kimmel, G. A.; Kay, B. D. Effect of Porosity on the Adsorption, Desorption, Trapping, and Release of Volatile Gases by Amorphous Solid Water. *J. Geophys. Res.: Planets* **2001**, *106*, 33387–33392.

(105) May, R. A.; Smith, R. S.; Kay, B. D. The Release of Trapped Gases from Amorphous Solid Water Films. I. "Top-down" Crystallization-Induced Crack Propagation Probed Using the Molecular Volcano. *J. Chem. Phys.* **2013**, *138* (10).

(106) Alan May, R.; Scott Smith, R.; Kay, B. D. The Release of Trapped Gases from Amorphous Solid Water Films. II. "Bottom-up" Induced Desorption Pathways. *J. Chem. Phys.* **2013**, *138*, 104502.

(107) Burke, D. J.; Brown, W. A. The Effects of Methanol on the Trapping of Volatile Ice Components. *Mon. Not. R. Astron. Soc.* **2015**, *448*, 1807–1815.

(108) Salter, T. L.; Wootton, L.; Brown, W. A. Thermal Processing and Interactions of Ethyl Formate in Model Astrophysical Ices Containing Water and Ethanol. *ACS Earth Space Chem.* **2019**, *3*, 1524–1536.

(109) Simon, A.; Öberg, K. I.; Rajappan, M.; Maksiutenko, P. Entrapment of CO in CO_2 Ice. *Astrophys. J.* **2019**, *883*, 21.

(110) Burke, D. J.; Puletti, F.; Woods, P. M.; Viti, S.; Slater, B.; Brown, W. A. Trapping and Desorption of Complex Organic Molecules in Water at 20 K. *J. Chem. Phys.* **2015**, *143*, 164704.

(111) Tzvetkov, G.; Koller, G.; Netzer, F. P. Interactions between Glycine and Amorphous Solid Water Nanoscale Films. *Surf. Sci.* **2012**, *606*, 1879–1885.

(112) Chaabouni, H.; Diana, S.; Nguyen, T.; Dulieu, F. Thermal Desorption of Formamide and Methylamine from Graphite and Amorphous Water Ice Surfaces. *Astron. Astrophys.* **2018**, *612*, A47.

(113) Kim, Y.-K.; Irikura, K. K.; Rudd, M. E.; Ali, M. A.; Stone, P. M.; Chang, J.; Coursey, J. S.; Dragoset, R. A.; Kishore, A. R.; Olsen, K. J.; et al., *Electron-Impact Cross Sections for Ionization and Excitation Database (version 3.0)*. National Institute of Standards and Technology, Gaithersburg, MD, 2004, http://physics.nist.gov/ionxsec.

(114) Kim, Y.-K.; Rudd, M. E. Binary-Encounter-Dipole Model for Electron-Impact Ionization. *Phys. Rev. A: At., Mol., Opt. Phys.* **1994**, *50*, 3954–3967.

(115) Hwang, W.; Kim, Y.-K.; Rudd, M. E. New Model for Electron-Impact Ionization Cross Sections of Molecules. *J. Chem. Phys.* **1996**, *104*, 2956–2966.

(116) Ibănescu, B. C.; May, O.; Monney, A.; Allan, M. Electron-Induced Chemistry of Alcohols. *Phys. Chem. Chem. Phys.* **2007**, *9*, 3163–3173.

(117) Rempt, R. D. Electron-Impact Excitation of Carbon Monoxide Near Threshold in the 1.5- to 3-eV Incident Energy Range. *Phys. Rev. Lett.* **1969**, *22*, 1034–1036.

(118) Thynne, J. C. J.; MacNeil, K. A. G. Negative Ion Formation by Ethylene and 1,1-Difluoroethylene. *J. Phys. Chem.* **1971**, *75*, 2584–2591.

(119) Trepka, L. v.; Neuert, H. Über Die Entstehung von Negativen Ionen Aus Einigen Kohlenwasserstoffen Und Alkoholen Durch Elektronenstoß. *Z. Naturforsch.* A: Phys. Sci. **1963**, *18* , 1295–1303.

(120) Walker, I. C.; Stamatovic, A.; Wong, S. F. Vibrational Excitation of Ethylene by Electron Impact: 1–11 eV. *J. Chem. Phys.* **1978**, *69*, 5532–5537.

(121) Szymańska, E.; Mason, N. J.; Krishnakumar, E.; Matias, C.; Mauracher, A.; Scheier, P.; Denifl, S. Dissociative Electron Attachment and Dipolar Dissociation in Ethylene. *Int. J. Mass Spectrom.* **2014**, *365–366*, 356–364.

(122) Butscher, T.; Duvernay, F.; Rimola, A.; Segado-Centellas, M.; Chiavassa, T. Radical Recombination in Interstellar Ices, a Not so Simple Mechanism. *Phys. Chem. Chem. Phys.* **2017**, *19*, 2857–2866.

(123) Enrique-Romero, J.; Rimola, A.; Ceccarelli, C.; Ugliengo, P.; Balucani, N.; Skouteris, D. Reactivity of HCO with CH_3 and NH_2 on Water Ice Surfaces. A Comprehensive Accurate Quantum Chemistry Study. *ACS Earth Space Chem.* **2019**, *3*, 2158–2170.

(124) Enrique-Romero, J.; Rimola, A.; Ceccarelli, C.; Balucani, N. The (Impossible?) Formation of Acetaldehyde on the Grain Surfaces: Insights from Quantum Chemical Calculations. *Mon. Not. R. Astron. Soc.: Lett.* **2016**, *459*, L6–L10.

(125) Rimola, A.; Skouteris, D.; Balucani, N.; Ceccarelli, C.; Enrique-Romero, J.; Taquet, V.; Ugliengo, P. Can Formamide Be Formed on Interstellar Ice? An Atomistic Perspective. *ACS Earth Space Chem.* **2018**, *2*, 720–734.

(126) Zhu, C.; Frigge, R.; Bergantini, A.; Fortenberry, R. C.; Kaiser, R. I. Untangling the Formation of Methoxymethanol (CH_3OCH_2OH) and Dimethyl Peroxide (CH_3OOCH_3) in Star-Forming Regions. *Astrophys. J.* **2019**, *881*, 156.

(127) Garrod, R. T.; Weaver, S. L. W.; Herbst, E. Complex Chemistry in Star-Forming Regions: An Expanded Gas-Grain Warum-Up Chemical Model. *Astrophys. J.* **2008**, *682*, 283–302.

(128) Wang, D.; Astruc, D. The Golden Age of Transfer Hydrogenation. *Chem. Rev.* **2015**, *115*, 6621–6686.

(129) Birch, A. J. 117. Reduction by Dissolving Metals. Part I. *J. Chem. Soc.* **1944**, 430–436.

(130) Birch, A. J. The Birch Reduction in Organic Synthesis. *Pure Appl. Chem.* **1996**, *68*, 553–556.

(131) Peters, B. K.; Rodriguez, K. X.; Reisberg, S. H.; Beil, S. B.; Hickey, D. P.; Kawamata, Y.; Collins, M.; Starr, J.; Chen, L.; Udyavara, S.; Klunder, K.; Gorey, T. J.; Anderson, S. L.; Neurock, M.; Minteer, S. D.; Baran, P. S. Scalable and Safe Synthetic Organic Electroreduction Inspired by Li-Ion Battery Chemistry. *Science* **2019**, *363*, 838–845.

(132) Glaser, F.; Kerzig, C.; Wenger, O. S. Multi-Photon Excitation in Photoredox Catalysis: Concepts, Applications, Methods. *Angew. Chem., Int. Ed.* **2020**, *59*, 10266–10284.

(133) Brauman, J. I.; Biairlb, L. K. Gas-Phase Acidities of Alcohols. *J. Am. Chem. Soc.* **1970**, *92*, 5986–5992.

(134) Mackay, G. I.; Bohme, D. K. Bridging the Gap between the Gas Phase and Solution: Transition in the Relative Acidity of Water and Methanol at 296 ± 2 K. *J. Am. Chem. Soc.* **1978**, *100*, 327–329.

(135) Jorgensen, W. L.; Ibrahim, M. Ab Initio Studies of $RO^-\cdots HOR'$ Complexes. Solvent Effects on the Relative Acidities of Water and Methanol. *J. Comput. Chem.* **1981**, *2*, 7–11.

(136) Saenko, E. V.; Laikov, D. N.; Baranova, I. A.; Feldman, V. I. Communication: Stabilization of Radical Anions with Weakly Bound Electron in Condensed Media: A Case Study of Diacetonyl Radical Anion. *J. Chem. Phys.* **2011**, *135, 101103.*

(137) Melton, C. E. Cross Sections and Interpretation of Dissociative Attachment Reactions Producing OH^-, O^- , and H^- in H_2O. **1972**, *57*, 4218–4225.

(138) Kühn, A.; Fenzlaff, H.-P.; Illenberger, E. Formation and Dissociation of Negative Ion Resonances in Methanol and Allylalcohol. *J. Chem. Phys.* **1988**, *88*, 7453–7458.

(139) Yamamoto, S.; Beniya, A.; Mukai, K.; Yamashita, Y.; Yoshinobu, J. Low-Energy Electron-Stimulated Chemical Reactions of CO in Water Ice. *Chem. Phys. Lett.* **2004**, *388*, 384–388.

(140) Petrik, N. G.; Monckton, R. J.; Koehler, S. P. K.; Kimmel, G. A. Electron-Stimulated Reactions in Layered CO/H_2O Films: Hydrogen Atom Diffusion and the Sequential Hydrogenation of CO to Methanol. *J. Chem. Phys.* **2014**, *140*, 204710.

(141) Harb, T.; Kedzierski, W.; McConkey, J. W. Production of Ground State OH Following Electron Impact on H_2O. *J. Chem. Phys.* **2001**, *115*, 5507–5512.

(142) Varela, K.; Hargreaves, L. R.; Ralphs, K.; Khakoo, M. A.; Winstead, C.; McKoy, V.; Rescigno, T. N.; Orel, A. E. Excitation of the 4 Lowest Electronic Transitions in Methanol by Low-Energy Electrons. *J. Phys. B: At., Mol. Opt. Phys.* **2015**, *48*, 115208.

(143) Michaud, M.; Fraser, M.-J.; Sanche, L. Low-Energy Electron-Energy-Loss Spectroscopy of Solid Methanol: Vibrational and Electronic Excitations. *J. Chim. Phys.* **1994**, *91*, 1223–1227.

(144) Curtis, M. G.; Walker, I. C. Dissociative Electron Attachment in Water and Methanol (5-14 eV). *J. Chem. Soc., Faraday Trans.* **1992**, *88*, 2805–2810.

(145) Rohdenburg, M.; Martinović, P.; Ahlenhoff, K.; Koch, S.; Emmrich, D.; Gölzhäuser, A.; Swiderek, P. Cisplatin as a Potential Platinum Focused Electron Beam Induced Deposition Precursor: NH_3 Ligands Enhance the Electron-Induced Removal of Chlorine. *J. Phys. Chem. C* **2019**, *123*, 21774–21787.

(146) Rohdenburg, M.; Boeckers, H.; Brewer, C. R.; McElwee-White, L.; Swiderek, P. Efficient NH_3-Based Process to Remove Chlorine from Electron Beam Deposited Ruthenium Produced from $(\eta^3\text{-}C_3H_5)Ru(CO)_3Cl$. *Sci. Rep.* **2020**, *10*, 10901.

(147) Lee, J.; Grabowski, J. J. Reactions of the Atomic Oxygen Radical Anion and the Synthesis of Organic Reactive Intermediates. *Chem. Rev.* **1992**, *92*, 1611–1647.

(148) Neese, F. The ORCA Program System. *Wiley Interdiscip. Rev.: Comput. Mol. Sci.* **2012**, *2*, 73–78.

(149) Neese, F.; Wennmohs, F.; Becker, U.; Riplinger, C. The ORCA Quantum Chemistry Program. *J. Chem. Phys.* **2020**, *152*, 224108.

(150) Kamarchik, E.; Rodrigo, C.; Bowman, J. M.; Reisler, H.; Krylov, A. I. Overtone-Induced Dissociation and Isomerization Dynamics of the Hydroxymethyl Radical (CH_2OH and CD_2OH). I. A Theoretical Study. *J. Chem. Phys.* **2012**, *136*, 084304.

(151) Wang, B.; Hou, H.; Gu, Y. Ab Initio/Density Functional Theory and Multichannel RRKM Calculations for the CH_3O + CO Reaction. *J. Phys. Chem. A* **1999**, *103*, 8021–8029.

(152) McMahon, R. J. Chemical Reactions Involving Quantum Tunneling. *Science* **2003**, *299*, 833–834.

(153) Sirjean, B.; Dames, E.; Wang, H.; Tsang, W. Tunneling in Hydrogen-Transfer Isomerization of n-Alkyl Radicals. *J. Phys. Chem. A* **2012**, *116*, 319–332.

(154) Shannon, R. J.; Blitz, M. A.; Goddard, A.; Heard, D. E. Accelerated Chemistry in the Reaction between the Hydroxyl Radical and Methanol at Interstellar Temperatures Facilitated by Tunnelling. *Nat. Chem.* **2013**, *5*, 745–749.

(155) Meisner, J.; Kästner, J. Atom Tunneling in Chemistry. *Angew. Chem., Int. Ed.* **2016**, *55*, 5400–5413.

(156) Jaglan, R.; Mandal, D. The Role of Potential Energy Surface in Quantum Mechanical Tunneling: A Computational Perspective. *Comput. Theor. Chem.* **2020**, *1187*, 112920.

(157) Klinman, J. P.; Kohen, A. Hydrogen Tunneling Links Protein Dynamics to Enzyme Catalysis. *Annu. Rev. Biochem.* **2013**, *82*, 471–496.

(158) Schreiner, P. R. Tunneling Control of Chemical Reactions: The Third Reactivity Paradigm. *J. Am. Chem. Soc.* **2017**, *139*, 15276–15283.

(159) Greer, E. M.; Kwon, K.; Greer, A.; Doubleday, C. Thermally Activated Tunneling in Organic Reactions. *Tetrahedron* **2016**, *72* (47), 7357–7373.

(160) Bennett, C. J.; Hama, T.; Kim, Y. S.; Kawasaki, M.; Kaiser, R. I. Laboratory Studies on the Formation of Formic Acid (HCOOH) in Interstellar and Cometary Ices. *Astrophys. J.* **2011**, *727*, 27.

(161) McCunn, L. R.; Lau, K.-C.; Krisch, M. J.; Butler, L. J.; Tsung, J.-W.; Lin, J. J. Unimolecular Dissociation of the CH_3OCO Radical: An Intermediate in the CH_3O + CO Reaction. *J. Phys. Chem. A* **2006**, *110*, 1625–1634.

(162) Nguyen, T. L.; Xue, B. C.; Weston, R. E.; Barker, J. R.; Stanton, J. F. Reaction of HO with CO: Tunneling Is Indeed Important. *J. Phys. Chem. Lett.* **2012**, *3*, 1549–1553.

(163) Tachikawa, H.; Kawabata, H. Effects of a Single Water Molecule on the Reaction Barrier of Interstellar CO_2 formation Reaction. *J. Phys. Chem. A* **2016**, *120*, 6596–6603.

(164) Zhang, L.; Yang, L.; Zhao, Y.; Zhang, J.; Feng, D.; Sun, S. Effects of Water Molecule on CO Oxidation by OH: Reaction Pathways, Kinetic Barriers, and Rate Constants. *J. Phys. Chem. A* **2017**, *121*, 4868–4880.

(165) Ruscic, B.; Feller, D.; Dixon, D. A.; Peterson, K. A.; Harding, L. B.; Asher, R. L.; Wagner, A. F. Evidence for a Lower Enthalpy of Formation of Hydroxyl Radical and a Lower Gas-Phase Bond Dissociation Energy of Water. *J. Phys. Chem. A* **2001**, *105*, 1–4.

(166) Belić, D. S.; Landau, M.; Hall, R. I. Energy and Angular Dependence of $H^-(D^-)$ Ions Produced by Dissociative Electron Attachment to $H_2O(D_2O)$. *J. Phys. B: At., Mol. Opt. Phys.* **1981**, *14*, 175–190.

(167) Johnson, C. J.; Continetti, R. E. Dissociative Photodetachment Studies of Cooled $HOCO^-$ Anions Revealing Dissociation below the Barrier to H + CO_2. *J. Phys. Chem. Lett.* **2010**, *1*, 1895–1899.

(168) Arasa, C.; van Hemert, M. C.; van Dishoeck, E. F.; Kroes, G. J. Molecular Dynamics Simulations of CO_2 Formation in Interstellar Ices. *J. Phys. Chem. A* **2013**, *117*, 7064–7074.

(169) Ryazantsev, S. V.; Feldman, V. I.; Khriachtchev, L. Conformational Switching of HOCO Radical: Selective Vibrational Excitation and Hydrogen-Atom Tunneling. *J. Am. Chem. Soc.* **2017**, *139*, 9551–9557.

(170) Oyama, T.; Nakajima, M.; Sumiyoshi, Y.; Endo, Y. Pure Rotational Spectroscopy of the H_2O trans-HOCO Complex. *J. Chem. Phys.* **2013**, *138* (20).

(171) Marushkevich, K.; Khriachtchev, L.; Räsänen, M. Hydrogen Bonding between Formic Acid and Water: Complete Stabilization of the Intrinsically Unstable Conformer. *J. Phys. Chem. A* **2007**, *111*, 2040–2042.

(172) Klyachko, D.; Rowntree, P.; Sanche, L. Oxidation of Hydrogen-Passivated Silicon Surfaces Induced by Dissociative Electron Attachment to Physisorbed H_2O. *Surf. Sci.* **1996**, *346*, L49–L54.

(173) Simpson, W. C.; Sieger, M. T.; Orlando, T. M.; Parenteau, L.; Nagesha, K.; Sanche, L. Dissociative Electron Attachment in Nanoscale Ice Films: Temperature and Morphology Effects. *J. Chem. Phys.* **1997**, *107*, 8668–8677.

(174) Lane, C. D.; Orlando, T. M. Inelastic Electron Scattering and Energy-Selective Negative Ion Reactions in Molecular Films on Silicon Surfaces. *Appl. Surf. Sci.* **2007**, *253*, 6646–6656.

(175) Degirmenci, I.; Coote, M. L. Comparison of Thiyl, Alkoxyl, and Alkyl Radical Addition to Double Bonds: The Unusual Contrasting Behavior of Sulfur and Oxygen Radical Chemistry. *J. Phys. Chem. A* **2016**, *120*, 1750–1755.

(176) McConkey, J. W.; Malone, C. P.; Johnson, P. V.; Winstead, C.; McKoy, V.; Kanik, I. Electron Impact Dissociation of Oxygen-Containing Molecules–A Critical Review. *Phys. Rep.* **2008**, *466*, 1–103.

(177) Lengyel, J.; Papp, P.; Matejčík, Š.; Kočišek, J.; Fárník, M.; Fedor, J. Suppression of Low-Energy Dissociative Electron Attachment in $Fe(CO)_5$ upon Clustering. *Beilstein J. Nanotechnol.* **2017**, *8*, 2200–2207.

(178) Jensen, E. T.; Sanche, L. Electron Transfer Reactions for Image and Image-Derived States in Dielectric Thin Films. *J. Chem. Phys.* **2008**, *129*, 074703.

(179) Bartolucci, F.; Franchy, R. EELS of Negative-Ion Resonances: N_2 Films on Ag(110) at 15 K. *Surf. Sci.* **1996**, *368*, 27–37.

(180) Gadzuk, J. W. Shape Resonances, Overtones, and Electron Energy Loss Spectroscopy of Gas Phase and Physisorbed Diatomic Molecules. *J. Chem. Phys.* **1983**, *79*, 3982–3987.

(181) Afeefy, H. Y.; Liebman, J. F.; Stein, S. E.; Burgess, D. R., Jr. Neutral Thermochemical Data In *NIST Chemistry WebBook*; Linstrom, P. J., Mallard, W. G., Eds.; NIST Standard Reference Database Number 69; National Institute of Standards and Technology: Gaithersburg, MD, http://webbook.nist.gov.

(182) Meister, E. C.; Willeke, M.; Angst, W.; Togni, A.; Walde, P. Confusing Quantitative Descriptions of Brønsted-Lowry Acid-Base Equilibria in Chemistry Textbooks – A Critical Review and Clarifications for Chemical Educators. *Helv. Chim. Acta* **2014**, *97*, 1–31.

Appendix

Appendix 1 Formation of Formic Acid, Formaldehyde, and Carbon Dioxide by Electron-Induced Chemistry in Ices of Water and Carbon Monoxide (Publication I)

Appendix 2 Electron-Induced Processing of Methanol Ice (Publication II)

Appendix 3 Electron-Induced Formation of Ethyl Methyl Ether in Condensed Mixtures of Methanol and Ethylene (Publication III)

Appendix 4 Mechanisms of Methyl Formate Production During Electron-Induced Processing of Methanol-Carbon Monoxide Ices (Publication IV)

Publications I–IV are not reprinted due to copyright reasons. The online versions of the articles are accessible via the links on page v.